TECHNISCHE UNIVERSITÄT WIEN
Vienna University of Technology

Diploma Thesis

Spirocyclic Monomers for Hot Lithography Technology

Performed at the

Institute of Applied Synthetic Chemistry

IAS
TU Wien

under the supervision of

Univ. Prof. Dipl.-Ing. Dr. techn. Robert Liska

Univ.Ass. Dr. techn. Katharina Ehrmann, M.Sc.

Senior Scientist Dipl.-Ing. Dr.techn. Patrick Knaack

Dipl.-Ing. Dr.techn. Yazgan Diren Mete

by

Danijela Kojic, B.Sc.

01425175

December, 2021

Danijela Kojic, B.Sc.

Danksagung

An dieser Stelle möchte ich herzlichst Prof. Liska danken, der mir ermöglichte, meine Diplomarbeit in so einem spannenden Fachgebiet zu schreiben und Neues zu erlernen. Danke für deine tolle Unterstützung und deinen Input, der mir immer weitergeholfen hat. Vielen Dank, dass du so ein wunderbares Klima in unserer Arbeitsgruppe geschaffen hast.

Mein besonderer Dank gilt auch Dr. Katharina Ehrmann, die mich stets während meiner Arbeit unterstützte und immer ein offenes Ohr für mich hatte. Dr. Patrick Knaack möchte ich auch herzlichst danken, du hast mir vor allem am Anfang meiner Arbeit viel wichtigen Input gegeben. Ebenso danke ich Dr. Yazgan Mete für Ihre tolle Unterstützung und Hilfe während meiner Arbeit. Danke, dass du mich so gut in das Thema eingeführt hast.

Ich möchte mich besonders beim ganzen FBMC-Team für die wunderschöne Zeit bedanken und freue mich auf die nächsten Jahre! Besonders danke ich den Bois, Ponte, Markus, Flo P. und Michi, mit denen ich meine gesamte Studienzeit sehr genossen habe. Danke auch an die Mädels Larissa, Anna, Babsi und Lisa, die immer ein offenes Ohr für mich hatten und mich so gut in die Arbeitsgruppe aufgenommen haben. Natürlich danke ich auch Roli, Bettina, Lukas, Philip, David, Oskar, Ricky, Sarah, Anna Z., Stefan und besonders meinen Laborkollegen Stephan und Ralle für die wunderbare gemeinsame Zeit. Großen Dank will ich auch an Tina, Toni, Flo M., Klausi, Carola und Jakob aussprechen. Danke dass ihr immer für mich da wart und immer mit guten Rat zur Seite gestanden seid.

Besonders danke ich dir, Mico, für deine Unterstützung während der vielen Jahre meines Studiums. Ich freue mich sehr, auf das was kommt. Na kraju naravno zelim da zahvalim mojim roditeljima Mihajlu i Mariji za njihovu neizmjernu podrsku tokom svih ovih godina. Hvala sto ste me uvjek u svakom smislu podrzavali, bez vas, ovo ne bi bilo moguce. Hvala mojoj sestri Leli i bratu Milutinu za njihovu podrsku i za prelijepo zajednicko vrijeme.

Danke!

Abstract

Additive manufacturing is raising great interest as a manufacturing technique for polymeric materials since it enables rapid production of complex geometries. Stereolithography, a widely used light-based 3D-printing method combines high resolution and excellent surface quality with short printing times. Layers of the desired object are cured sequentially by a light source, which is focused on a liquid photopolymer resin. Within the field of stereolithography, Hot Lithography is a new technique that can utilize solid and highly viscous resins at room temperature through elevating the operating temperature up to 120 °C. Methacrylates and epoxides are the most common monomers in 3D-printing processes but their thermomechanical properties are often insufficient. Specifically, shrinkage upon polymerization results in crack formation and lowers surface quality.

Expanding monomers like spiro-orthoesters (SOE) and spiro-orthocarbonates (SOC), on the other hand, polymerize *via* a cationic (double) ring-opening process, thereby exhibiting low shrinkage. Herein, the applicability of spiro-orthoesters and spiro-orthocarbonates for Hot Lithography systems is investigated. Hence, spirocyclic monomers were synthesized and investigated with regard to their photopolymerization efficiency at different temperatures. Material properties of the resulting poly(ether)-esters were examined.

Photo-DSC analysis gave information about the reactivity of the synthesized spirocyclic compounds and monomer conversions were calculated from NMR-spectra. Gel permeation chromatography (GPC) provided the molecular weight of the obtained polymers. The impact of the monomer ring size on the polymerization modes was examined. Spiro-orthoesters proved to be the better monomer class in terms of reactivity and polymerization mode. Therefore, a difunctional monomer was synthesized containing the spiro-orthoester motif and investigated in analogy to the monofunctional compounds. The most promising monofunctional SOE was polymerized with a difunctional SOE and with a difunctional epoxide. Finally, the resulting polymers were tested with thermomechanical methods and light-exposure tests were performed as a proof of concept for additive manufacturing.

Kurzzusammenfassung

Additive Fertigung weckt immer mehr Interesse als Verfahren zur Herstellung von Polymeren, da sie schnelle Herstellung komplexer Geometrien ermöglicht. Stereolithographie ist ein weit verbreitetes, lichtbasiertes 3D-Druckverfahren, welches hohe Auflösung und ausgezeichnete Oberflächenqualität mit kurzen Druckgeschwindigkeiten kombiniert. Dabei werden einzelne Schichten des gewünschten Objekts nacheinander mit einem UV-Laser gehärtet, der auf ein flüssiges Photopolymer fokussiert wird. Hot Lithography ist ein Stereolithographie-basiertes Verfahren, welches die Verarbeitung von festen und hochviskosen Harzen bei Raumtemperatur durch hohe Arbeitstemperaturen ermöglicht. Herkömmliche Monomere in der 3D-Drucktechnologie wie Methacrylate weißen eine Schrumpfung während der Polymerisation auf, welche zu Rissbildungen im Material führt und die Oberflächenqualität erheblich vermindert.

Expandierende Monomere wie Spiro-orthoester (SOE) und Spiro-orthocarbonate (SOC) polymerisieren hingegen über kationische Ringöffnung und weisen dadurch nur einen geringen Schrumpf auf. In dieser Arbeit wird die Anwendbarkeit von Spiro-Othoestern und Spiro-Orthocarbonaten für die Hot-Lithography untersucht. Dazu wurden spirozyklische Verbindungen synthetisiert und ihre Photoreaktivität bei verschiedenen Temperaturen untersucht. Die Materialeigenschaften der resultierenden Poly(ether)-Ester wurden mit thermomechanischen Methoden analysiert.

Die Reaktivität der synthetisierten spirozyklischen Verbindungen wurde mittels Photo-DSC-Analyse ermittelt und Monomer-Umsätze wurden aus NMR-Spektren berechnet. Das Molekulargewicht der Polymere wurde mit der GPC-Analyse bestimmt. Der Einfluss der Monomer-ringgröße auf die Polymerisationsmodi wurde untersucht. Spiro-Orthoester erwiesen sich als die bessere Monomerklasse in Bezug auf die Reaktivität und den Polymerisationsmodus. Ein difunktionelles Spiro- Orthoesterderivat wurde analog zu den monofunktionellen Verbindungen synthetisiert und untersucht. Der am besten geeignete monofunktionelle SOE wurde zunächst mit dem difunktionellen SOE und darüber hinaus mit einem difunktionellen Epoxid polymerisiert. Schließlich wurden die Materialeigenschaften mit thermomechanischen Tests ermittelt und ein Belichtungstest wurde als Machbarkeitsnachweis für den 3D-Druck durchgeführt.

Table of contents

Introduction

1 Additive Manufacturing

Additive manufacturing (AM), also known as 3D-printing or rapid prototyping, was invented in the early 1980s and quickly developed into a significant polymer manufacturing method. In well-known manufacturing processes like injection molding and extrusion, the cured, thermoplastic material is processed by heating in appropriate tools and shaping them into the desired form. Additive manufacturing utilizes a different approach, where three-dimensional objects are formed layer by layer. This strategy allows the production of geometrically highly complex and customer-oriented products with low costs per unit. The printed parts are constructed by computer-aided design (CAD), which makes all shape geometries accessible by slicing them into layers.[1]

Additive manufacturing technologies are widely used in the health sector in combination with biocompatible materials, where patient-matched implants with geometric flexibility are required. AM-technology is also applied in combination with biodegradable materials for drug delivery applications. Furthermore, 3D-printing is suitable for electronics, photonics, and microfluidics.[1,2]

Generally, 3D-printing methods are divided into:[1]

- Methods for processing thermoplastic materials (thermo-processing)
  - Selective Laser Sintering (SLS)
    Herein, a powder is irradiated with a high-power laser whereby the produced heat sinters the powder on the surface of the powder bed. Afterwards, the powder bed is lowered by the defined layer thickness and the process repeats.
  - Fused-Deposition modeling (FDM)
    A polymer filament is extruded through a heated nozzle in layer-by-layer fashion. The molten material fuses with the underlying structure and solidifies immediately upon cooling.

1

- Methods for processing liquid, light sensitive resins
  - Direct-Writing (DW)

    The principle is similar to FDM (extrusion-based method) but the printed object requires a thermal or UV-cure process to solidify.
  - Stereolithography (SLA)

    A laser is focused on the surface of a liquid photopolymer, which solidifies due to its photosensitivity. Laser exposure occurs only in the focus point of the laser.
  - Digital Light Processing (DLP)

    A whole layer of the light sensitive resin is irradiated from the bottom with a conventional light source, while the build platform is pulled out of the resin tank.

Stereolithography

Stereolithography is a vat photopolymerization process, which results in parts with outstanding precision and resolution. Herein, the liquid photopolymer resin is cured layer by layer with a UV laser beam. SLA-printers are comprised of a tank, which is filled with the photopolymer, a building platform, and a laser-scanning system (Figure 1).
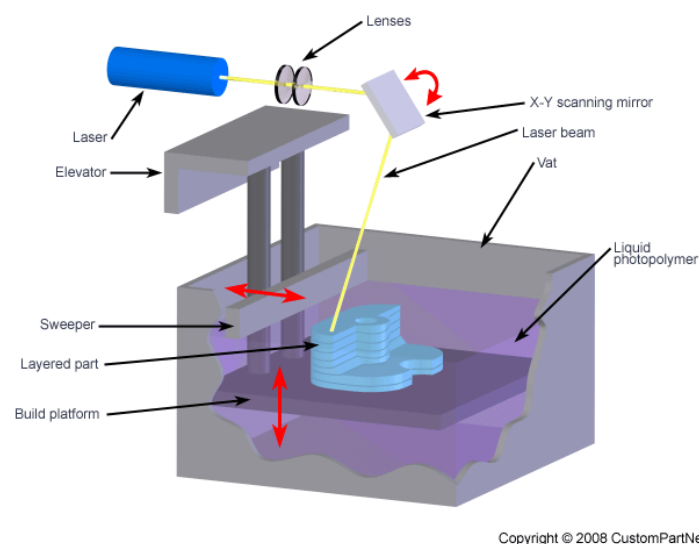
Figure 1: Setup of an SLA-printer

2

A CAD-model of the desired part is created, and the CAD data is sliced into thin layers. The data is transferred to the SLA-system and the building platform is placed in the liquid resin tank. The laser beam is focused onto the surface with an X-Y scanning mirror and cures the first photopolymerized layer. Once a layer is cured, the building platform is lowered by a distance equal to the layer thickness. The surface is recoated with the liquid resin and the process repeats until the final object is formed. Residual resin is removed from the printed part and optionally the object can be post-cured with UV light.[1]

The described process refers to a top-down SLA printer, where the laser beam is placed above the tank. The build platform is placed at the top of the resin and is layered during the process. Inverted SLA, known as bottom-up SLA enables printing with less resin and smaller machines. Smoother surfaces can be achieved within lower printing times. Thereby, the laser is placed below the resin tank and cures the photopolymer through a transparent floor. Once the layer is cured, the building platform with the adhered part is lifted and printing continues (Figure 2).[3]
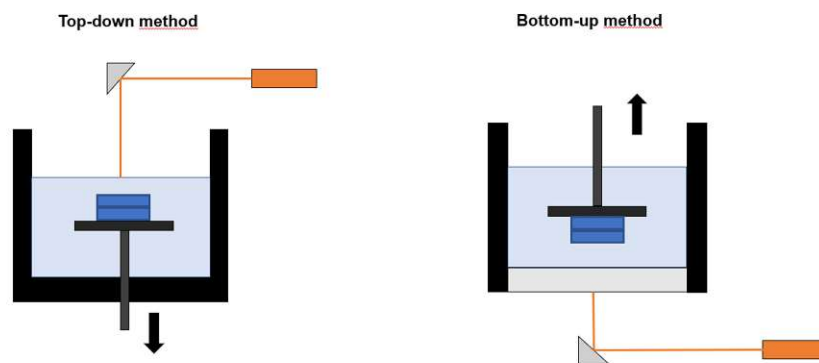
Figure 2: Different SLA-setups

Stereolithography requires fast photopolymerization reactions to print the desired parts in a short time. Therefore, highly reactive monomers like acrylates are commonly used and cured *via* radical photopolymerization. The main drawback of acrylate monomers is their relatively high shrinkage upon polymerization and the oxygen sensitivity of the radical polymerization process. These limitations can be tackled with the application of cationic polymerizable monomers like epoxides and vinyl ethers. However, longer reaction times and the sensitivity towards moisture must be considered.[1]

3

Additionally, fine-tuned viscosity is crucial for the process and essential for smooth surfaces and fast coating. Reduction of the viscosity can be achieved by application of reactive diluents and solvents. Moreover, increased operating temperatures can be applied to decrease viscosity, as it is done in Hot Lithography.[1,3]

Hot Lithography

Hot Lithography is a newly developed additive manufacturing process based on SLA and DLP, which is characterized by its outstanding precision and material properties. Stereolithography provides good surface qualities and high resolution but there are limitations to the materials that can be used in the process. Hot Lithography offers the same advantages as conventional SLA with the added benefit that formulations can be cured at higher temperatures due to a heated building platform and vat. This widens the range of formulations that can be processed with respect to viscosity and reactivity. For the first time, highly viscous and less reactive monomers are processable due to high operating temperatures.[4]

During the process, the printable formulation is placed in the heated vat and the building platform is preheated to the operating temperature. The laser/light engine is located below the transparent vat and cures the material layer by layer (Figure 3). Thereby, the wavelength is set to 375 or 405 nm and high precision is provided by a spot size of 10 µm.[4]
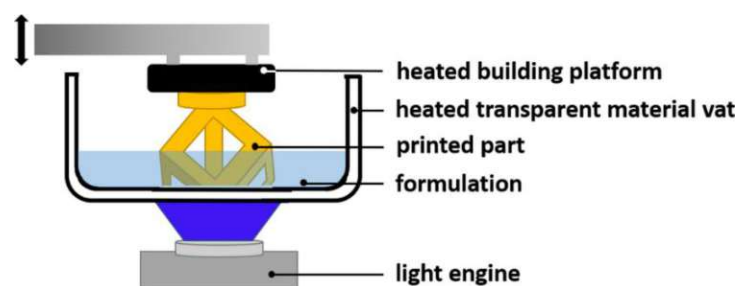
Figure 3: Setup of a Hot Lithography printer

Elevated operating temperatures improve not only the processability of the resins but also the material properties. High printing temperatures increase double-bond conversion, tensile strength, and modulus of dimethylacrylate-based photopolymers.[5] Besides acrylates, cationic monomers can also be processed with the Hot Lithography

technology.[6] The majority of cationically polymerizable monomers are polarized heterocyclic monomers prone to cationic ring opening polymerization.

2 Photopolymerization

Photopolymerization was established in early 1980s and is the underlying basic concept for lithographic additive manufacturing technologies. Unlike thermal curing processes, photopolymerization requires initiation by light instead of heat, which is highly beneficial.[7]

A photocurable system is comprised of the following components:[8]

- A photoinitiator, which absorbs the light and provides the reactive species *via* photolysis
- A photopolymerizable multifunctional monomer or oligomer capable of network formation
- A monofunctional monomer (reactive diluent), which decreases the viscosity of the formulation

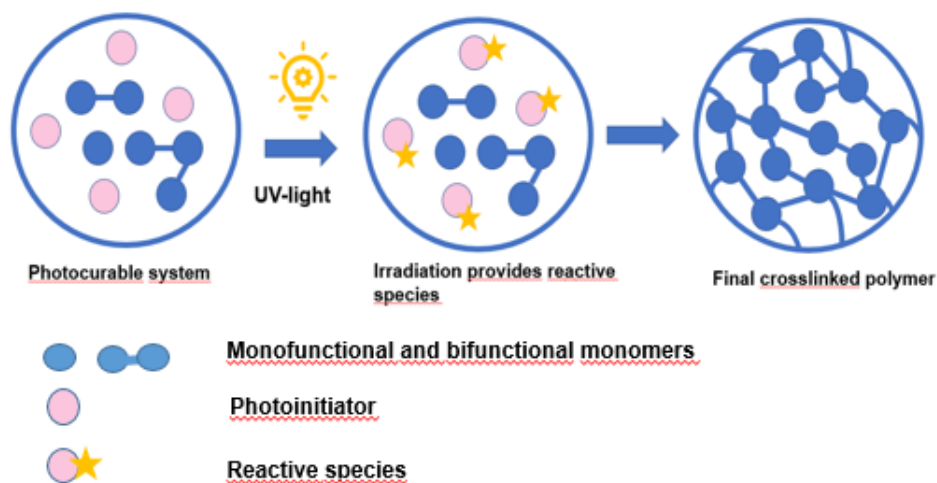Figure 4 depicts a schematic photopolymerization reaction.

Figure 4: Representation of a photopolymerization process

The significant step in photoinduced polymerizations is the light-induced generation of an active species, which initiates the chain-growth reaction. Depending on the photopolymerization mechanism, the active species can either be a radical or an ion.

First, electromagnetic radiation raises the electrons of the photoinitiator molecule from the ground state to the excited state. Afterwards, the activated photoinitiator decomposes and generates the reactive species (radical or ion). Consequently, the formed active species reacts with the monomer and initiates the photopolymerization.[7]

High polymerization rates are beneficial for efficient polymerizations and strongly depend on the photoinitiator. Therefore, two factors should be considered before the component is chosen, namely the quantum yield of initiation ϕ_i and the quantum yield for polymerization ϕ_m. They express the amount of the generated active species and of polymerized monomer units per number of photons absorbed. Equation I describes the relationship between the quantum yield for initiation (ϕ_i) and the polymerization rate (R_p).[9]

$$R_p = K_p[M](\frac{\Phi_i I_a}{K_t})^{1/2} \tag{I}$$

Herein, I_a is the light intensity, [M] the concentration of the functional groups, K_p the propagation rate coefficient, and K_t the termination rate coefficient.[7,10]

Depending on the propagating species generated via photolysis of the photoinitiator, a distinction can be made between radical, cationic and anionic photopolymerization. Radical photoinduced photopolymerization has been investigated for a long time as the first and major photopolymerization mechanism. However, cationic photopolymerization received later more attention since new, promising cationic photoinitiators were developed. Additionally, it brought the benefit of a broad monomer variety and oxygen-insensitive polymerization. Anionic photopolymerization is by far not that common as radical or cationic photopolymerization. This is due to the required strict conditions such as absence of impurities and absence of compounds sensitive to nucleophiles.[7,11]

Monomers for 3D-Printing

The first monomers used for light-based additive manufacturing were acrylates and methacrylates (Figure 5), which still are used in state-of-the-art applications. They exhibit high reactivity, good storage stability and hardness. Additionally they are compatible with different types of commercially available 3D-printers.[12]
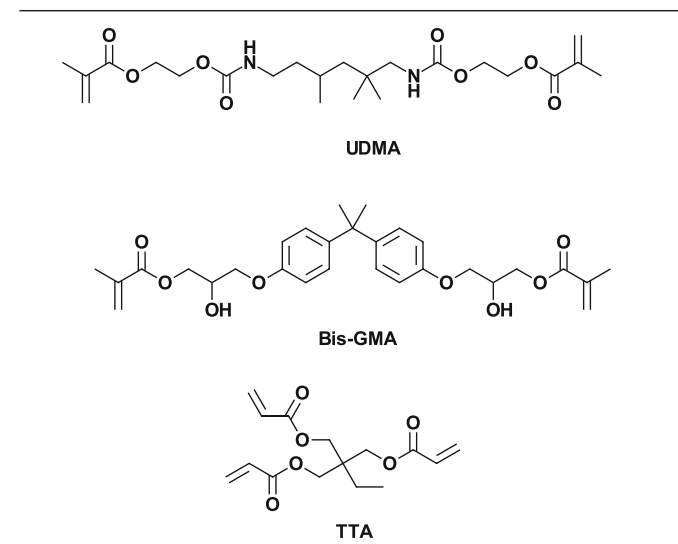
Figure 5: (Meth)acrylate monomers used in 3D photopolymerization[13]

Beside the above-mentioned advantages, acrylate-based systems also have several drawbacks that limit their application in AM-techniques. Oxygen inhibition is one of them and is unavoidable when light induced radical polymerizations are performed in air. Oxygen inhibition can be reduced by the addition of oxygen scavengers such as tertiary amines but the additives tend to discolor the material.[13]

Another significant drawback of acrylate-based monomers is their polymerization shrinkage. This term is defined as the dimensional shrinkage formed during the solidification of the liquid resin.[14] During the polymerization, the bonds of the monomers are shortened from a Van der Waals distance to a covalent bond distance (Figure 6).[15]

Figure 6: Bond changes upon the polymerization of methacrylate[15]

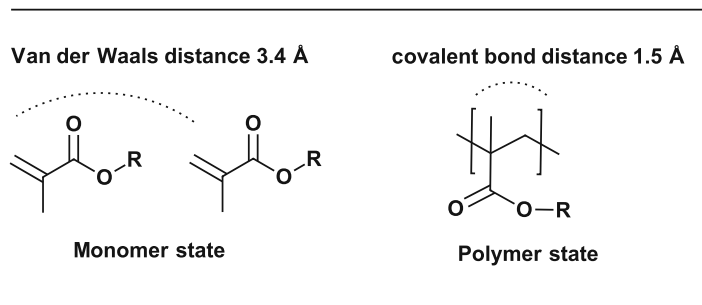Volumetric shrinkage is unavoidable during the polymerization of acrylates and varies between 5 and 12%.[16] Cyclic and aromatic acrylate monomers tend to show lower shrinkage stress (e.g. Bis-GMA: 5%) but consequences like structural deformations and curling during the 3D-fabrication are still significant.[13,16]

Furthermore, the radical chain growth polymerization of (meth)acrylates leads to inhomogeneous crosslinking due to the occurrence of various chain transfer and termination reactions. They take place because of the high reactivity of the formed radicals and lack of control over the reactions. The irregular polymer architecture and high crosslinking density of the materials lead to brittle and glassy behavior. Cracks can propagate more easily and stress cannot be dissipated well. Several techniques for the toughening of (meth)acrylate polymers are necessary to overcome this.[17]

On the other hand, cationically polymerizable monomers represent an important monomer class in 3D-photopolymerization. Commonly used monomers are epoxides like 3,4-(epoxycyclohexane)methyl-3,4-epoxycyclohexylcarboxylate (CE), bisphenol A diglycidyl ether (BADGE), vinyl ethers like 1,4-cyclohexane dimethanol divinyl ether (CDVE) and disubstituted oxetanes like bis(3-ethyl-3-oxetanylmethyl) ether (DSO) (Figure 7).[13]
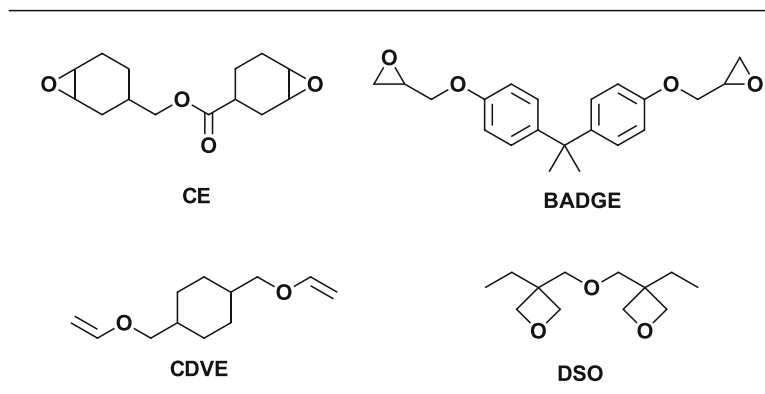
Figure 7: Cationic monomers used in 3D-photopolymerization[13]

Cationically polymerizable monomers are characterized by their good mechanical strength, as well as low shrinkage upon polymerization and excellent thermal and electrical properties. Epoxides show high reactivity, which can additionally be tuned *via* the monomer structure. Clycloaliphatic epoxides have high polymerization rates, while monomers with nucleophilic moieties, like CE, show reduced reactivity. Epoxide monomers show lower shrinkage than methacrylates due to their ring-opening polymerization. However, they polymerize slower than methacrylates and are therefore used in combination with more reactive vinyl ethers and oxetanes. Cationic polymerizations proceed *via* chain-growth mechanism. High number of crosslinking points are thereby aligned along the polymer backbone, which results in brittle materials. Toughness can be increased by the addition of chain-transfer agents or with toughening additives.[16,18]

Generally, classical photopolymers, especially acrylates are brittle, but though and thermoplast-like properties of the materials are desired for industrial applications. Therefore, the crosslinking density of the network must be decreased and intermolecular non-covalent interactions should be increased through the introduction of functional groups. These requirements lead to high molecular weight, high viscosity resins, which are difficult to process with SLA-technologies. One important strategy is the processing of these resins at elevated temperatures. Elevated temperatures additionally bring the advantage of increased reactivity. Hot Lithography, a heated SLA or DLP process, offers both benefits.[19]

3   Cationic Photopolymerization

Cationic photopolymerization was first discovered in the 1970s. It has the same advantages as free radical photopolymerization, but due to its polymerization mechanism (Figure 8) it also has the potential to overcome the previously discussed disadvantages of radical-mediated photopolymerization.[20]

Initiation:

Propagation:
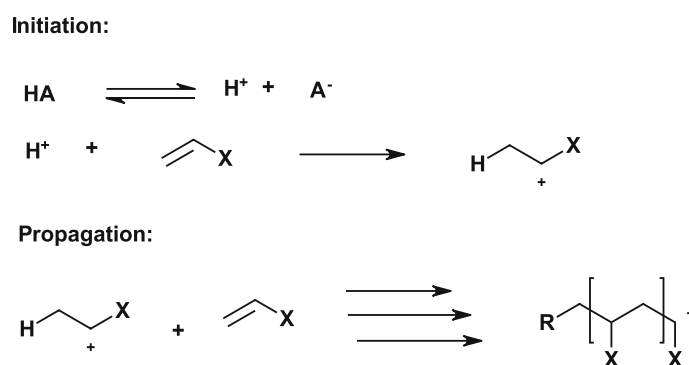
Figure 8: General mechanism of cationic polymerization

Generally, cationic polymerization is initiated by Brønsted acids or Lewis acids. The formed cationic species reacts with monomers such as olefins with electron-donating groups and heterocycles. Propagation takes place by the addition of further monomer molecules, and a 'living' cationic chain end is generated (Figure 8). Unlike in radical polymerizations, termination does not take place by recombination of two propagating chains. Instead, termination can occur by ion pair rearrangement, whereby the anionic species reacts with the cationic chain end (Figure 9).[21] Chain transfer may occur by hydrogen abstraction from the cationic chain end to the counterion. This results in the formation of a double bound and in regeneration of the initiator (Figure 9).[21]

Termination:

Chain Transfer:

Figure 9: Termination and chain transfer in cationic polymerization[21]

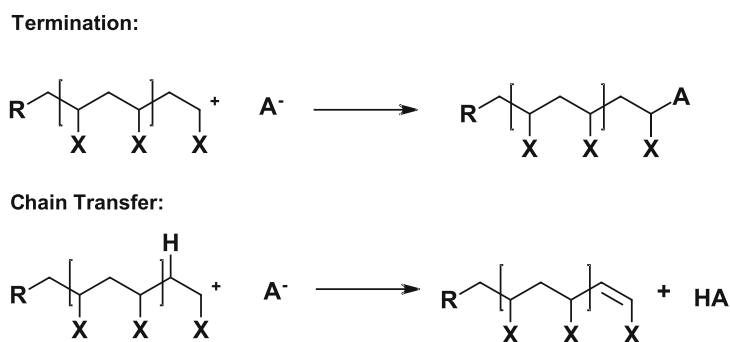Several monomer types can be used in cationic polymerization. These monomers may be olefins with electron-donating side groups. Electron-donating substituents increase the nucleophilicity of the olefin, thereby making the reaction with the electrophilic initiator possible. Additionally, heterocycles containing nitrogen, oxygen and sulfur can be polymerized cationically. Most frequently used monomers in cationic polymerization are epoxides, oxetanes and vinyl ethers (Figure 10). Oxetanes and epoxides show lower volumetric shrinkage due to their ring-opening and are less toxic than acrylate monomers.[8]
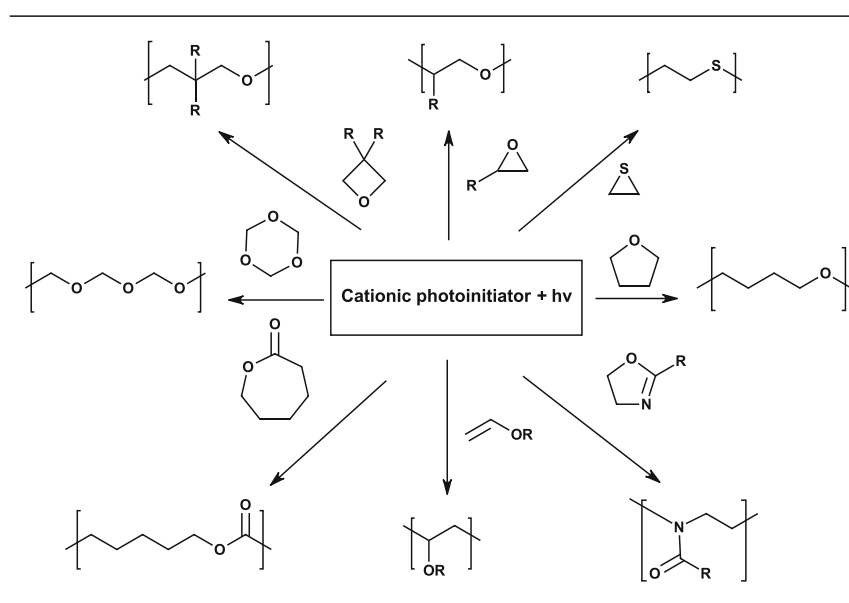
Figure 10: Cationically polymerizable monomers[8]

The mechanism of cationic photopolymerization differs from conventional cationic polymerization only in the formation of the initiating species. Hereby, cationic photoinitiators called photoacid generators (PAGs) generate a super-acid, or photoacid, upon irradiation, which then initiates the polymerization.[22]

Photoinitiators for Cationic Photopolymerization

Photoacid generators (PAGs) need to fulfill the following requirements:[23]

- High photoinitiation efficiency
- High thermal and photochemical stability
- Good solubility in monomers
- Release of non-toxic compounds upon decomposition

PAGs are comprised of an organic cation and an inorganic anion. Photochemical properties like the molar extinction coefficient, quantum yield of initiation, and thermal stability are predefined by the organic cation of the salt. In turn, the anion determines the acidity of the generated photoacid. Thereby it determines the efficiency of polymerization and the propagation rate constant.[18]

Diaryliodonium and triphenylsulfonium salts are the most popular PAGs, which find regular use in industry applications (Figure 11).[16] The latter regularly show better thermal stabilities and can be easily sensitized for photopolymerizations up to 400 nm. Non-nucleophilic anions such as SbF_6^-, AsF_6^-, PF_6^- and BF_4^- are appropriate to make the initiator highly reactive.[16]
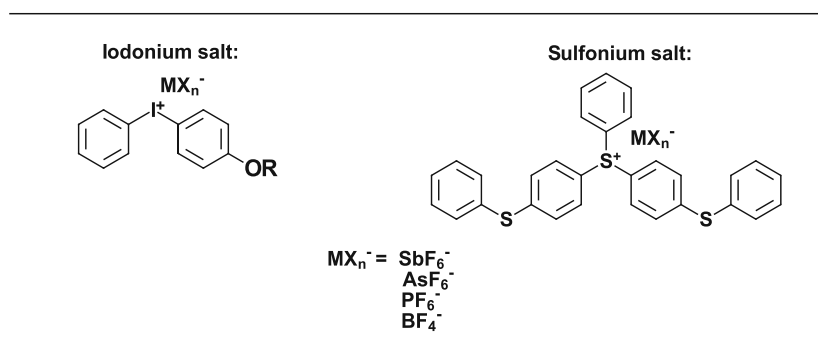
Figure 11: Representative iodonium and sulfonium salts[16]

The formation of the initiating species, the photoacid, is a quite complex process. After irradiation of the salt and excitement to the singlet state, homolytic and heterolytic cleavage of Ar-I bonds follow. By that, cations as well as cation radicals are generated (Scheme 1). The formed compounds are unstable and subsequently react with a proton-donating species in the reaction mixture. The initiating species, a Brønsted acid, is generated in this last step. The more detailed mechanism considers intersystem crossing to the triplet state and the solvent-induced cage recombination and cage escape of the formed fragments.[20]
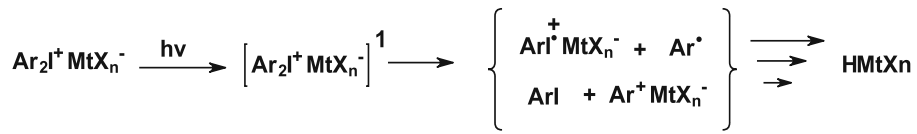
Scheme 1: Simplified mechanism for the formation of the photoacid[20]

Once the active species is generated by irradiation of the PAG, cationic photopolymerization proceeds as shown in Scheme 2.
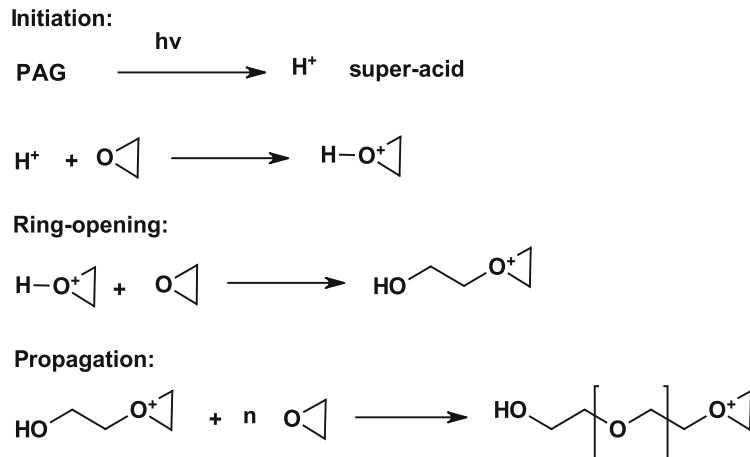
Scheme 2: Cationic photopolymerization of an epoxy monomer[22]

The super-acid protonates the epoxy group of the monomer. Subsequently, the protonated epoxy groups react with another monomer and ring-opening follows. The positive charge is thereby transferred to the new epoxy group. The propagation continues until all monomers are consumed. Generally, the propagation step in cationic ring-opening polymerization competes with back-biting and ring elimination reactions. By that, cyclic oligomeric products are formed instead of linear polymer chains.[24,25]

Figure 12: Back-biting and ring elimination as side reactions in cationic (ring-opening) polymerization[24]
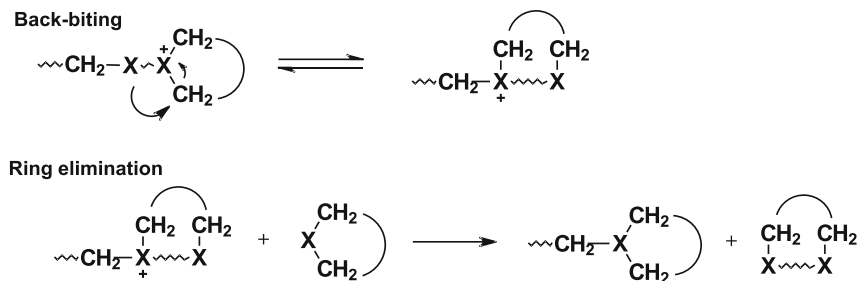
13

Ideally, termination reactions are absent and may only arise from recombination with the anion of the PAG salt or in presence of basic impurities. Furthermore, the polymerization is not inhibited by oxygen.

Since cationic polymerization proceeds with less termination and chain-transfer reactions then radical polymerization, well-defined structures of the polymers can be achieved. Materials derived from cationic photopolymerization have therefore the potential to perform better thermomechanically, compared to radical networks. Once initiated, cationic polymerization can proceed without further irradiation, which is termed as 'dark cure reaction'. The long-living character of the formed protonic species enables this process.[18,26] Due to the above-mentioned advantages, cationically polymerizable monomers are also used in 3D-printing.

Cationic Ring-Opening Polymerization

Ring-opening polymerization (ROP) provides many commercially important polymers. According to the polymerization mechanism, ROP can be divided into radical ROP (RROP), cationic ROP (CROP), anionic ROP (AROP), and ring-opening metathesis polymerization (ROMP).[27] Ring-opening polymerizations result in low polymerization shrinkage, as ring-opening counterbalances the contraction during polymerization.[28]

Cationic ring opening polymerization (CROP) is a chain growth polymerization of heterocyclic monomers (Figure 13) and proceeds *via* a cationic intermediate.[28]
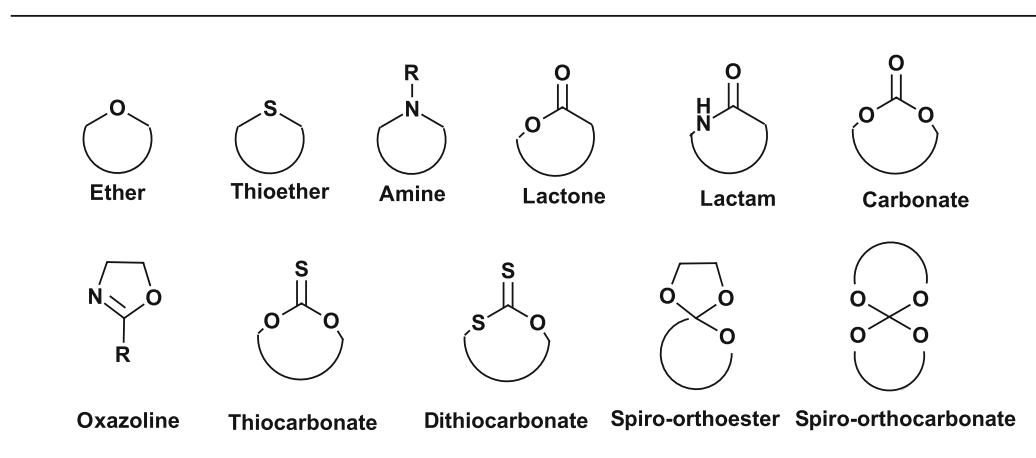
Figure 13: Common monomers in cationic ring-opening polymerization[28]

14

Typically, cyclic monomers readily undergo CROP since greater degrees of rotational freedom are achieved in their linear chains. The driving force for the polymerization is the release of the ring-strain energy, which makes the process highly dependent on the ring-size of the monomers.[24]

Two different CROP mechanisms are postulated in literature, which differ in the location of the cationic active species. In both, the cationic intermediate is formed after an electrophilic attack by the initiator. The general, active chain end mechanism (ACE) comprises a cationic center at the chain end, which reacts with a monomer *via* an S_N1 or S_N2 mechanism (Scheme 3).[24]
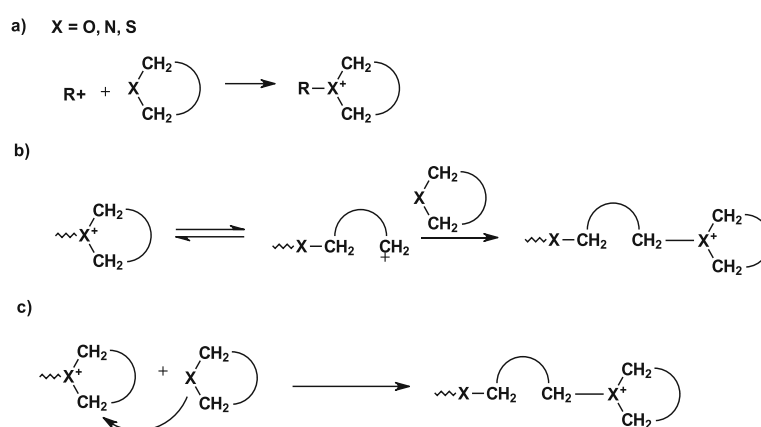
Scheme 3: Active chain-end mechanism (ACE) in CROP: a) Initiation of CROP b) propagation *via* S_N1-mechanism c) propagation *via* S_N2-mechanism[24]

The second mechanism is called activated monomer mechanism (AM) and usually occurs during the polymerization of cyclic carbonates (Scheme 4). Herein, the cationic species is the activated monomer instead of the growing chain end of the polymer. This mechanism requires an activator in addition to the electrophile, which is usually an alcohol.[28]
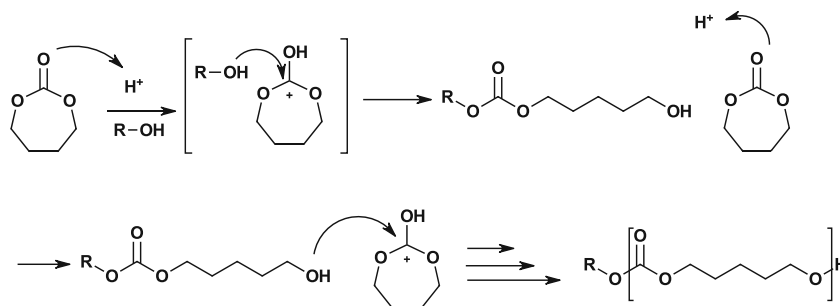
Scheme 4: Activated monomer mechanism (AM)[28]

While common termination reactions by recombination of chain ends is impossible in cationic polymerizations, back-biting and ring elimination reactions may take place as side reactions during cationic ring-opening polymerizations (Scheme 9).
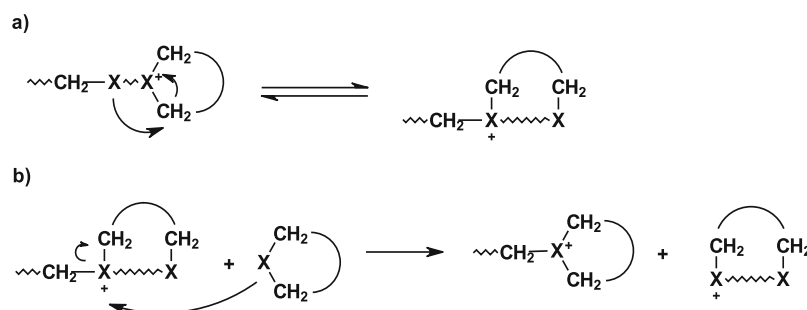
Scheme 5:Side reactions in CROP: a) back-biting b) ring-elimination

CROP can also be accompanied by an isomerization process during the polymerization of oxazolines, thiocarbonates, dithiocarbonates, and spiro-orthoesters. Thereby, the functional group isomerizes during the polymerization into a more stable form. Scheme 6 illustrates the stepwise double ring opening polymerization of a seven-membered spiro-orthoester. Thereby, the second ring-opening proceeds with an isomerization process, leading to a linear polyester.[28]
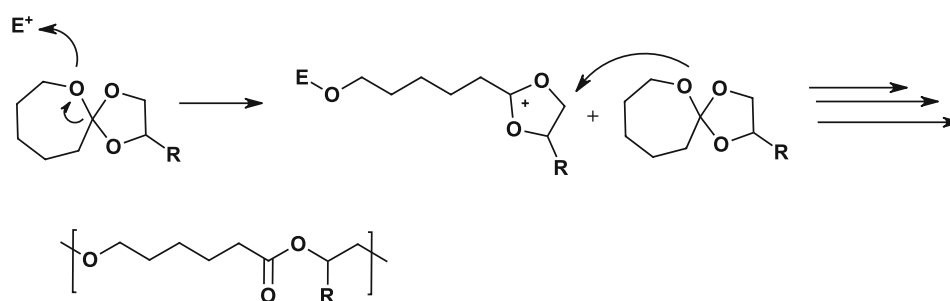
Scheme 6: Double ring opening polymerization of spiro-orthoesters with isomerization process into linear polymers[28]

As mentioned previously, cyclic monomers undergoing ring-opening, or even double ring-opening polymerization, counteract volumetric shrinkage. Therefore, these monomers are called low shrinkage or expanding monomers. They are generally comprised of cyclic structural motifs, of which the most prominent ones are the cationic polymerizable spiro-orthoesters (SOE) (Figure 14,a) and spiro-orthocarbonates (SOC) (Figure 14,b).[29,30]

16
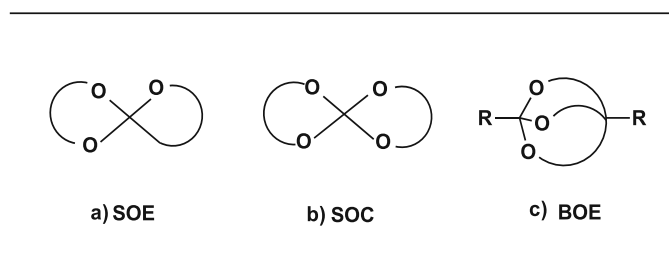
Figure 14: Structures of expanding monomers: a) spiro-orthoester, b) spiro-orthocarbonate, c) bicycle orthoester

The double ring-opening of spiro-orthoesters and spiro-orthocarbonates leads to reduced polymerization shrinkage or even volume expansion. The contraction caused by the formation of new covalent bonds is thereby counterbalanced by the double ring-opening (Scheme 7). During ring-opening of the monomers, two bonds move from a covalent distance to a near van der Waals distance. This process cancels out the shrinkage caused by the shortening of one van der Waals distance to a covalent distance.[31]

c... covalent bond

v... van der Waals distance

nv... near van der Waals distance
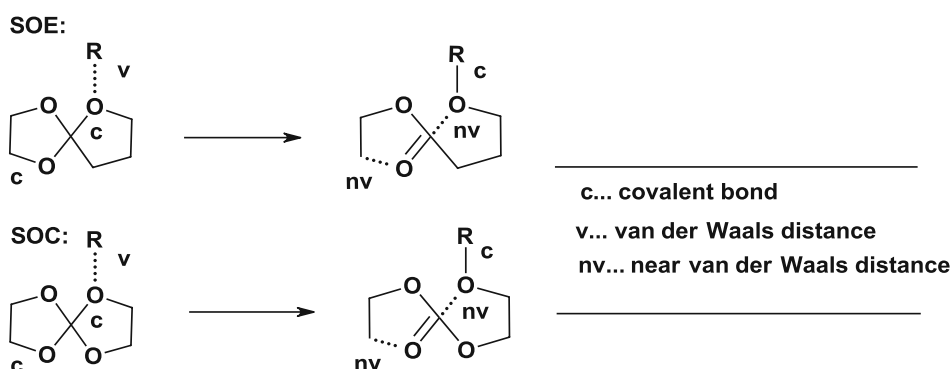
Scheme 7: Ring opening of expanding monomers[31]

SOEs and SOCs polymerize *via* a cationic ring opening process, initiated by protic or Lewis acids. Their polymerization mechanism depends on the monomer class and the ring-size. Polymerization temperature is another significant factor since low temperatures contribute to single ring-opening reactions. Temperatures above 100 °C are required for the double ring-opening of spiro-orthoesters.[31] The polymerization mechanism of spiro-orthoesters is depicted in Scheme 12, while Scheme 13 illustrates the double ring-opening of spiro-orthocarbonates.

Die approbierte gedruckte Originalversion dieser Diplomarbeit ist an der TU Wien Bibliothek verfügbar

The approved original version of this thesis is available in print at TU Wien Bibliothek.
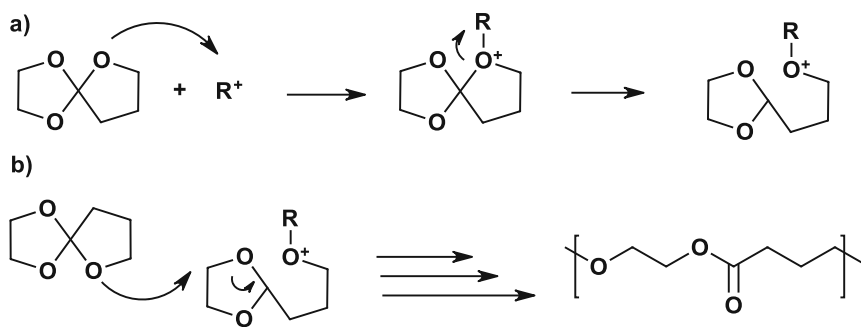
Scheme 8: Ring-opening of spiro orthoesters: a) single ring-opening, b) double ring-opening[29]
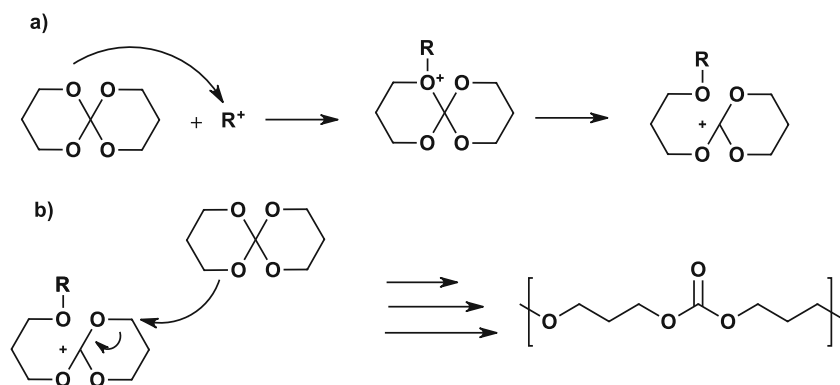
Scheme 9: Ring-opening of spiro orthocarbonates: a) single ring-opening, b) double ring-opening[29]

Objective

In recent years, lithography-based additive manufacturing technologies have gained a lot of interest. They enable fast fabrication of complex parts with very high precision and good surface qualities. However, these technologies require better photopolymerizable monomers leading to improved material properties. Currently, they are mostly based on radical photopolymerization, using conventional acrylates and methacrylates as monomers. Due to the polymerization mechanism and the monomer properties, the systems suffer from oxygen inhibition, high volumetric shrinkage and poor biocompatibility.

To avoid these drawbacks, cationic ring-opening photopolymerization can be implemented as an oxygen insensitive reaction with low shrinkage and high conversions. Thereby crack formations and surface deformations can be avoided. However, cationic ring-opening polymerizations are temperature-dependent and proceed at low temperatures with low reaction rates. This can be improved with the newly developed Hot Lithography technology where elevated temperatures are used during the printing-process leading to a significant increase of the reactivity.

The aim was hereby to evaluate the applicability of two cationically curable expanding monomer classes, spiro-orthocarbonates and spiro-orthoesters, for the Hot Lithography technology. Therefore, the reactivity towards photopolymerization of these monomers should be investigated as a first step. Based on these results and the polymerization modes of the specific monomers, the more suitable monomer class will be identified and a bifunctional expanding crosslinker is designed based on these results to achieve crosslinked networks by the photopolymerization of these monomers. Since material properties are decisive for the application of the monomers, the materials obtained from varying monomer compositions will be characterized thermomechanically.

Lastly, light exposure tests for the Hot Lithography process should be carried out. On the basis of these, the suitability for 3D-printing with Hot Lithography is to be determined.

19

State of the Art

1 Expanding Monomers

Many scientists investigated the effects of polymerization shrinkage and searched for solutions. One of the most successful investigators was Professor William J. Bailey who saw the ring-opening effect as a possible strategy for shrinkage reduction.[32] He observed a lower shrinkage during the polymerization of ethylene oxide and THF, after which he started to develop the concept of expanding monomers. According to his theoretical considerations, bicyclic compounds would be the most suitable. They should fulfill following requirements:[32]

- The bicyclic rings are fused
- Each ring contains an element other than carbon, i.e. an oxygen
- The ring opening does not proceed in a symmetrical manner, i.e. one oxygen may form a carbonyl group, the other an ether group

Monomers meeting these requirements, among others, were spiro-orthocarbonates and spiro-orthoesters. Spiro-orthocarbontates were first described by Bailey and coworkers in 1972. Their synthesis is more challenging and was primarily carried out using trimethylene glycol and carbon disulfide with tin catalysts (Scheme 10).[33]
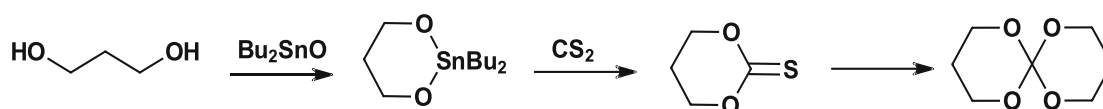
Scheme 10: Synthesis of spiro-orthocarbonates catalyzed by organo-tin compounds[33]

Due to the highly toxic and flammable CS_2, alternative synthetic routes were investigated by many scientists. A new, nowadays used approach to spiro- orthocarbonates was reported by Mues *et al.* in March 1990 (Scheme 10).[34]
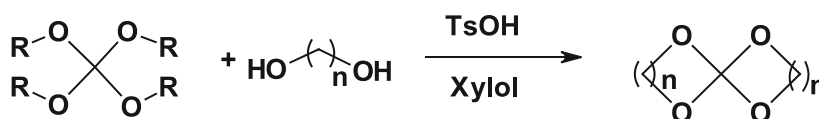
Scheme 11: Synthesis of spiro-orthocarbonates from tetraalkoxymethanes[34]

20

The first spiro-orthoester derivatives were synthesized by Bodenbenner *et al.* in 1959, where the reaction of cyclic esters and epoxides was catalyzed with BF$_3$·Et$_2$O. This well-established method is used nowadays and is represented in Scheme 12.[35]
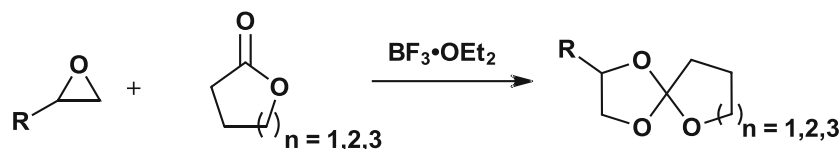
Scheme 12: Synthesis of spiro-orthoesters[35]

1.1 Cationic (Photo)Polymerization of Spiro-Orthocarbonates

After the development of the concept of expanding monomers, interest in spiro-orthocarbonates also increased rapidly. Several spiro-orthocarbonates were synthesized and subjected to cationic polymerization, most of them comprised of aromatic substituents. Endo *et al.* reported 1987 the synthesis and polymerization of 3,9-dibenzyl-l,5,7,ll-tetraoxaspiro[5.5]undecane (Scheme 13). Like other spiro-orthocarbonates, it polymerized *via* ring-opening to poly(ether carbonate).[36]
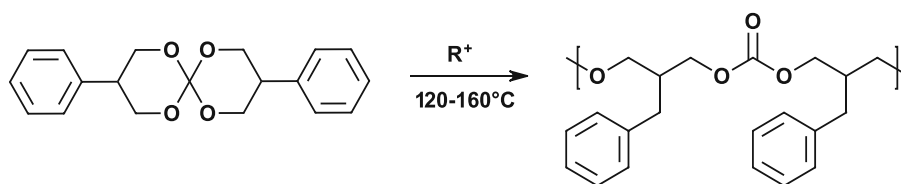
Scheme 13: Polymerization of aromatic spiro-orthocarbonate

Takata and Endo revealed that the polymerization of spiro-orthocarbonates proceeds *via* the single ring-opening process. An unsymmetrical SOC, prepared from 2,2- dichlorobenzodiaxole (Figure 15) was thereby reacted with BF$_3$·Et$_2$O at room temperature and the polymerization was followed by careful NMR analysis. In the initial stage of the polymerization, the single ring-opening adduct was obtained first (Scheme 17 a) and subsequently converted into poly(ether carbonate) (Scheme 17 b).[29]
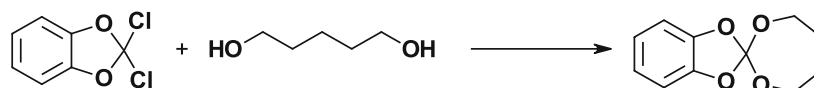
Figure 15: Synthesis of the unsymmetrical aromatic SOC
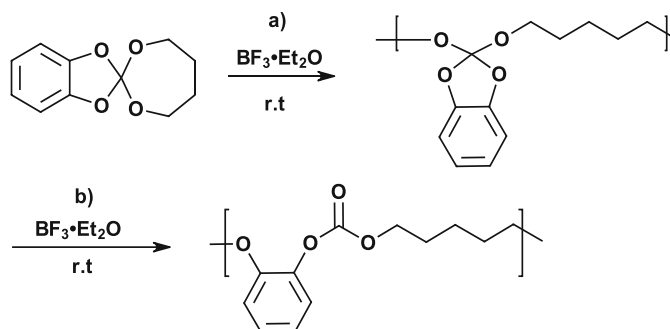
Scheme 14: Cationic polymerization of aromatic SOC: a) single ring-opening adduct, b) double ring-opening adduct[29]

In 2010 Oritz *et al.* synthesized glycerol-based spiro-orthocarbonates and used them as anti-shrinkage derivatives for the photopolymerization of epoxides. The desired spiro-orthocarbonates were obtained by the reaction of tetraethyl orthocarbonate with glycerol and used as a mixture without further separation (Figure 16).[37]
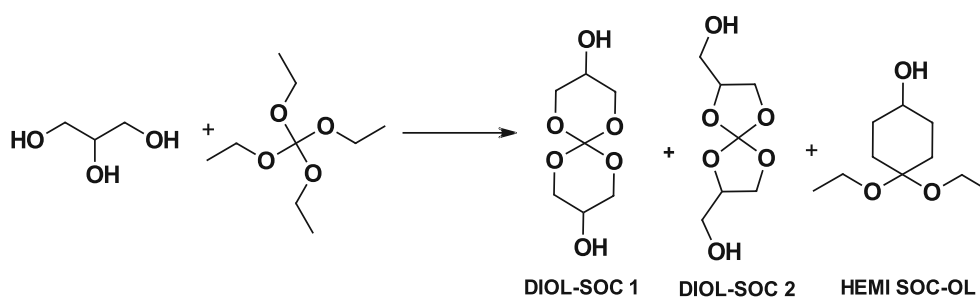
Figure 16: Preparation of SOC-diols used as anti-shrinkage additives[37]

Formulations containing 0, 5, 10 and 20 mol% of DIOL-SOC (as a mixture of DIOL-SOC 1 and DIOL-SOC 2), the commercial epoxide 3,4-epoxycyclohexylmethyl-3',4'-epoxycyclohexane carboxylate (CE), and 1 mol% of the onium photoinitiator bis(4-dodecylphenyl)iodonium hexaflurorantimonate (DDPI) were subjected to photopolymerization. Already low contents of the spiro-orthocarbonates (5 mol%) increase the photopolymerization rate and the conversion due to the occurrence of the activated monomer mechanism, which takes place in the polymerization of epoxides with alcohols as co-initiators. The glass-transition temperature of the obtained polymers was determined with dynamic mechanical analysis (DMA). The material obtained after the photopolymerization of the pure epoxide exhibited a T_g of 105 °C, which was lowered to 81 °C with 20 mol% of DIOL-SOC. Generally, a trend was observed where the T_g decreased with increasing SOC- content. Finally, the

researchers determined the polymerization shrinkage, which could be reduced by 45% at 20 mol% DIOL-SOC content compared to the SOC-free polymer.[37]

Tetrafunctional spiro-orthocarbonates, which were used as anti-shrinkage additives in the polymerization of CE, were also investigated (Figure 17).[38]
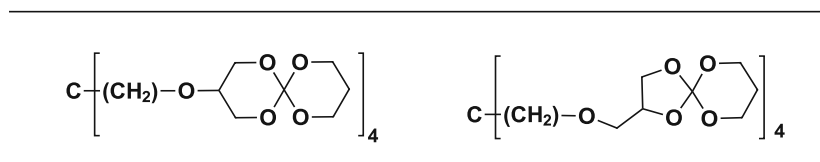
Figure 17: Tetra spiro-orthocarbonates (tetra-SOC) used as anti-shrinkage additives

The tetrafunctional spiro-orthocarbonates were synthesized from tetraethyl orthocarbonate in a three-step reaction.[38]
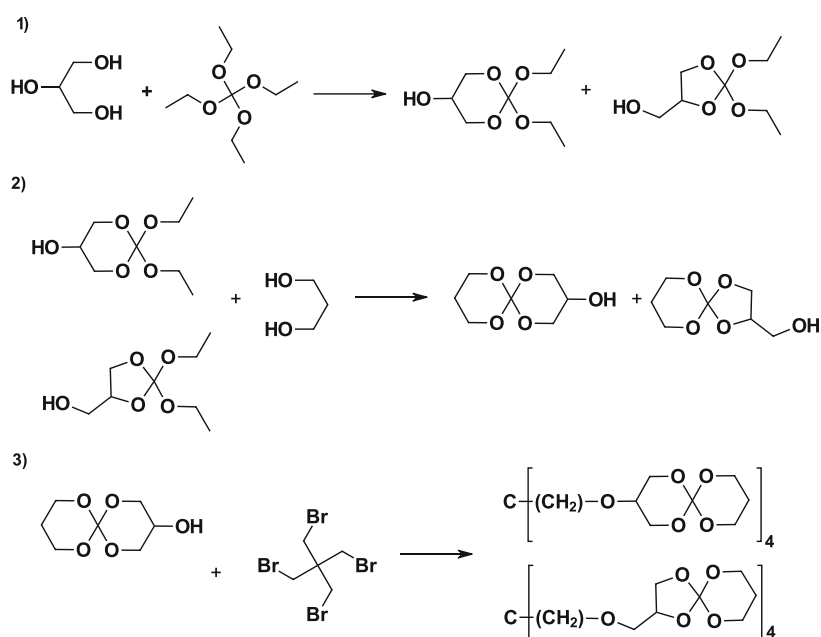
Figure 18: Synthesis of tetra-SOC[38]

Only low amounts of the synthesized additives were used in the photopolymerization of the epoxide CE. The content ranged between 2.5 and 7 mol% tetra-SOC. As expected, the T_g was lowered with increasing amounts of the tetra-SOC additive. Furthermore, a low concentration of 7 mol% of the tetra-SOC resulted in an expansion of 2.18%, confirming thereby the efficiency of spiro-orthocarbonates as anti-shrinkage additives.[38]

In 2013, a bulky aromatic spiro-orthocarbonate FSOC was synthesized by Oritz *et al.* to investigate the efficiency of the aromatic spiro-orthocarbonate as anti-shrinkage additive. The spiro-orthocarbonate was used in the photopolymerization of bis-glycidyl ether of bisphenol A (BADGE). The monomer was synthesized by the well-established condensation reaction of tetraethyl orthocarbonate and 9H-flourene-9,9-dimethanol (FDiOH) (Scheme 15).[39]
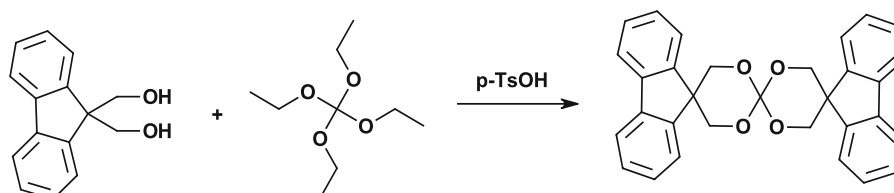
Scheme 15: Synthesis of the fluorene spiro-orthocarbonate FSOC[39]

The formulations contained 2.5 – 10 mol% FSOC and as expected, the shrinkage decreased with increasing content of FSOC: Furthermore, a slight expansion (0.19%) during the polymerization of the mixture containing 10 mol% FSOC was achieved.[39]

In 2019, Min et al. investigated a six-membered spiro-orthocarbonate as an anti-shrinkage additive for ultraviolet nanoimprint lithography. The polymerization shrinkage was reduced gradually and high-fidelity pattern replication was possible. Without the spiro-orthocarbonate, a volumetric shrinkage of 7.86% was observed, whereby the incorporation of 50 wt% of the spiro-orthocarbonate reduced the shrinkage to 1.86 %.[40]

1.2 Cationic (Photo)Polymerization of Spiro-Orthoesters

Soon after the synthesis of spiro-orthoesters, their cationic polymerization was studied in detail. Takata *et al.* reported a very interesting polymer structure, which was obtained after the reaction of a spiro-orthoester with aluminium acetylacetonate $Al(acac)_3$ at room temperature.[29] Acetal groups remained in the polymer chain and the structure was considered to be a poly(cyclic orthoester) (Scheme 16). The polymer structure indicated a single ring-opening polymerization and was also obtained when spiro- orthoesters were polymerized with the cationic initiator $SnCl_4$ at low temperatures.[29]
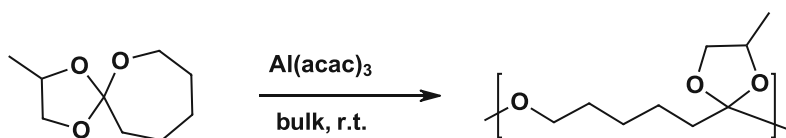
Scheme 16: Single ring-opening polymerization of spiro-orthoester with Al(acac)₃[29]

Chikaoka *et al.* continued the study and investigated the polymer structures, polymerization mechanisms and the temperature-dependence of the cationic polymerization of spiro-orthoesters. He revealed a temperature dependent polymerization, whereby an increasing amount of poly(ether-ester) was obtained at elevated temperatures (Scheme 17). It is considered that the initially formed poly(cyclic orthoester) isomerizes to a poly (ether ester), whereby double-ring opening takes place *via* an isomerization polymerization as described in a previous chapter (**Cationic ring-opening polymerization**).[31]
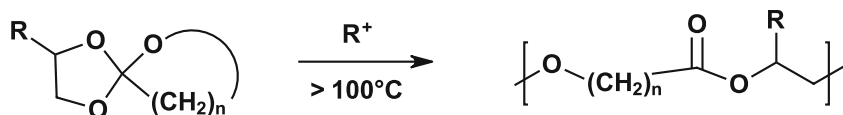
Scheme 17: Double ring-opening process of spiro-orthoesters[31]

Besides the polymer structure and the mechanism, Chikaoka also investigated the volume changes during the single ring-opening and double ring-opening process. According to Baileys theory, a volume shrinkage of 2.6% was observed during the single ring-opening. On the other hand, double ring-opening polymerization causes smaller shrinkage of 1.0 % and proves to be the significant factor for shrinkage reduction. For every bond that goes from the Van der Waals distance in the monomer to the covalent distance in the polymer, two bonds go from a covalent distance to a Van der Waals distance.[31]

Not long after cationic polymerization of spiro-orthoesters, their photopolymerization was studied. Elisabeth Klemm reported the photoinduced copolymerization of spiro- orthoesters and epoxides in 1984.[41] Two years later, a patent was published by Ludwig Haase and Elisabeth Klemm, where the photopolymerization of spiro-orthoesters using high pressure Hg-lamps was described.[42] The research group

continued their investigations and published the preparation of photocurable mixtures containing spiro-orthoesters and fillers.[43]

Hsu and Wan investigated and compared the cationic polymerization and of a five-membered spiro-orthoester bearing a cycloaliphatic ring with its photopolymerization in 2009.[44] They could confirm that a mixture of the single ring-opened and the double ring-opened polymer was obtained (Scheme 18). This is according to previous findings, since complete double ring-opening processes require high temperature. Hsu and Wan conducted the photopolymerizations at room temperature with 1 wt% of the photoinitiator diphenyliodoniumhexylfluorophosphate (DPI). They could show that conventional cationic polymerization requires long reaction times, whereas the efficient photoinitiator provides a fast cationic photopolymerization.[44]
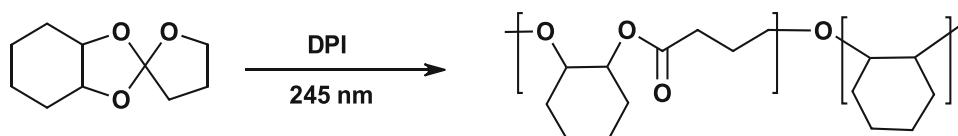
Scheme 18: Photopolymerization of the aliphatic spiro-orthoester[44]

It was found that conventional cationic catalysts attack the cyclic ether oxygen, whereas the superacid, generated from cationic photoinitiators, is reactive enough to attack the cyclic ether and the acetal oxygen simultaneously.[44]

Some years later, spiro-orthoesters were used as additives in commercial polymerizations to reduce volumetric shrinkage. [45,30] Marx *et al.* investigated the effect of spiro-orthoesters as anti-shrinkage additives in thiol-ene reactions in 2019.[45] Thereby, a dual-cure system consisting of a trifunctional thiol, a bisfunctional allyl-bisphenol A compound, and a spiro-orthoester was polymerized with visible light (Figure 19). In a dual-cure system, radical photopolymerization and cationic photopolymerization take place simultaneously. A radical photoinitiator, as well as a cationic photoinitiator and a sensitizer were necessary to utilize the dual-cure mechanism. Formulations with different spiro-orthoester contents, ranging from 0 to 30 wt%, were cured whereby volumetric expansions up to 1.70% could be achieved.[45]
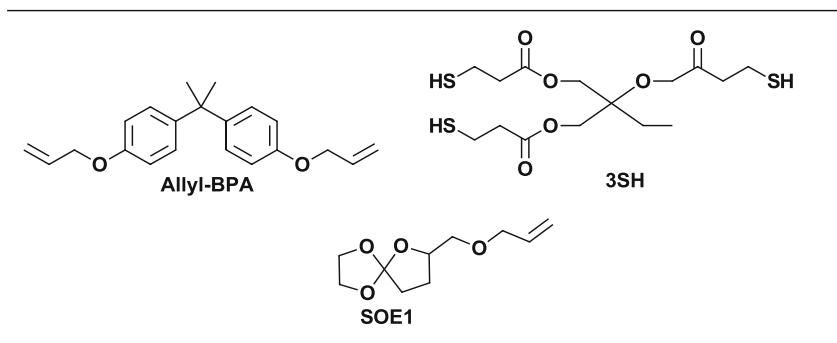
Figure 19: Monomers used for the investigation of applicability of spiro-orthoesters as anti-shrinkage additives

The first 3D-printing with spiro-orthoesters was conducted in the same research group in 2019 utilizing the same dual curing mechanism as published previously. The mixtures were comprised of tri(ethyleneglyol) divinyl ether, a tetrafunctional thiol crosslinker, and a spiro-orthoester. The content of the spiro-orthoester in the formulations ranged between 0 and 50 wt%, which were printed on a DLP printer with a LED light source with 405 nm.[46]

Compared to the resins without the additive, Marx *et al.* could demonstrate the reduction of the polymerization shrinkage up to 39 % with the use of the spiro- orthoester. Furthermore, it was shown that the incorporation of the spiro- orthoester did not alter the storage modulus and the glass-transition temperature of the resins. The formulations were printed successfully, whereas the formulations without spiro-orthoesters show rapid gelation and a rather low resolution of 200 µm. Through the addition of the spiro-orthoester, the shrinkage was reduced and therefore better resolution was achieved. The formulation with 30 wt% of spiro-orthoester resulted in a resolution of 50 µm (Figure 20).[46]
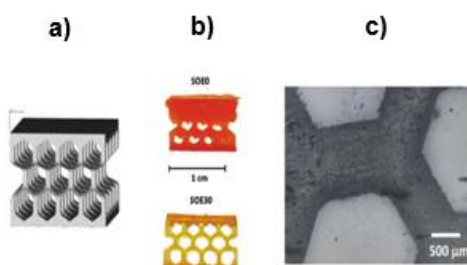
Figure 20: a) CAD-model of the desired structure to be printed b) 3D-printed structure containing 0 wt% SOE and 30 wt% SOE c) Light microscopic photography of the specimen with 30 wt% SOE[46]

27

Results and Discussion

1 Evaluation of Spiro-Orthocarbonates and Spiro-Orthoesters

A crucial step in this work was the detailed investigation of the suitability of expanding monomers spiro-orthocarbonates and spiro-orthoesters for 3D-printing. To define the more suitable monomer class, various derivatives of both monomer classes with different ring sizes were synthesized as described in the following chapter. An overview of all investigated monomers is given here (Figure 21).
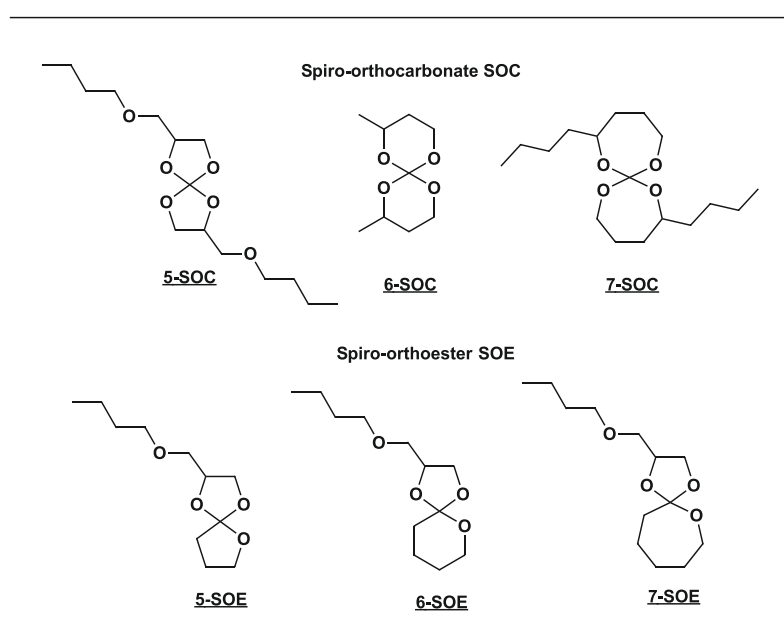
Figure 21: Overview of synthesized SOE and SOC monomers

In the consecutive chapters, photopolymerization of these monomers was investigated. Fast polymerization rates are essential in additive manufacturing technologies. Therefore, the photoreactivity of the compounds was tested carefully. Furthermore, the photopolymerization should proceed as a near-ideal double ring-opening process without interfering byproducts. To ensure this, the polymerization modes of the monomer classes were deduced from NMR-analysis.

1.1 Monofunctional Spiro-orthocarbonates

1.1.1 Synthesis of Monofunctional Spiro-Orthocarbonates

In order to better compare spiro-orthocarbonates with spiro-orthoesters, synthesis of unsymmetrical SOCs was implemented first. Thereby, equimolecular amounts of 1,3- propanediol were reacted with tetraethyl orthocarbonate, to obtain the monocyclic intermediate in a yield of 48% (Figure 22).[47]
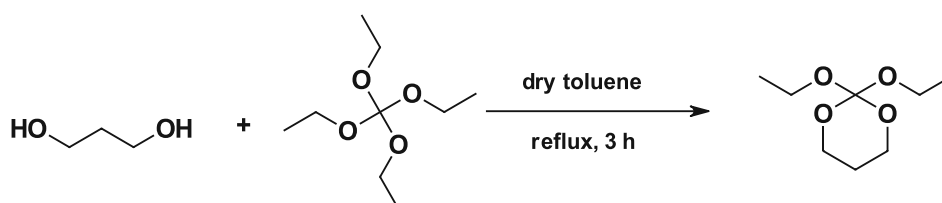
Figure 22: Synthesis towards the monocyclic SOC intermediate

The obtained intermediate was subsequently reacted with one equivalent of 3-butoxy-1,2-propanediol to obtain the corresponding unsymmetrical SOC (Figure 23).
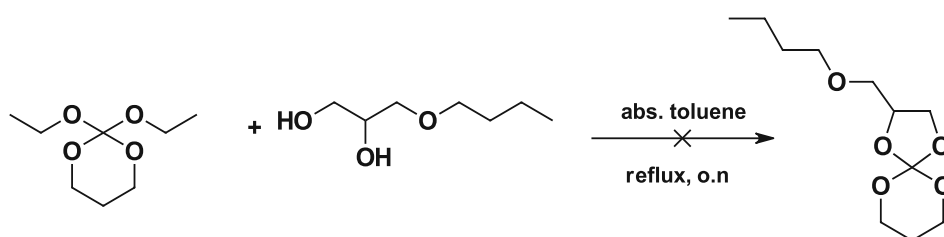
Figure 23: Synthesis towards the unsymmetrical SOC

Although the reaction times were followed closely, the symmetrical SOC was obtained as the main product after column chromatography, which was confirmed by NMR-analysis (Figure 24).
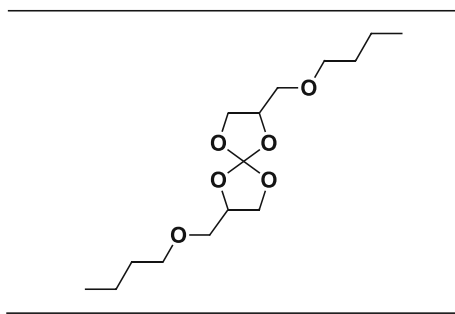
Figure 24: Obtained five-membered, symmetric SOC

After these findings, the synthesis of symmetrical spiro-orthocarbonates (SOC) was carried out based on the general approach by Mues *et al* (Scheme 19).[34]
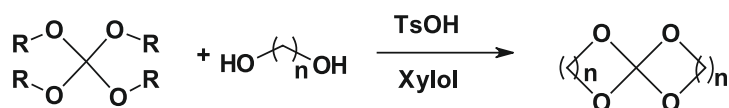
Scheme 19: Synthesis of spiro-orthocarbonates by Mues et al[34]

Three monomers differing in their ring size were synthesized by the reaction of tetraethyl orthocarbonate (TEOC) with the corresponding alcohols (n = 2 - 4). The synthesis of the five-membered SOC proceeded as a two-step reaction (Scheme 20).
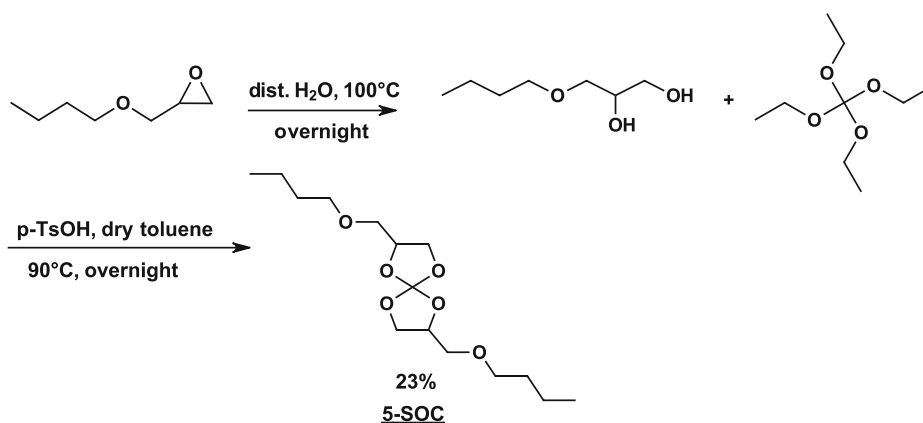
Scheme 20: Synthesis of the five-membered SOC (5-SOC)

The desired alcohol was thereby first obtained after hydrolysis of 2-(butoxymethyl)oxirane. The ring-opening step of the epoxide was conducted following a literature procedure with hot water as reactant.[48] Subsequently, the second step was conducted following a literature procedure.[36] The condensation reaction between the obtained diol and TEOC was catalyzed by p-toluenesulfonic acid p-tsOH. To shift the

30

equilibrium towards the spiro-orthocarbonate, the formed ethanol was continuously removed as an azeotropic mixture with toluene. Since spiro-orthocarbonates are prone to ring-opening under acidic conditions, column chromatography was carried out using neutral alumina-oxide as stationary phase instead of silica. As the monocyclic compound can be formed and other side reactions take place, a moderate yield of 23% of the desired compound were obtained as colorless liquid as confirmed by ^{1}H- and ^{13}C-NMR.

Unlike the synthesis of 5-SOC, the synthesis of the six-membered SOC was performed as one-step reaction, since the starting material was commercially available. The reaction was performed following the same procedure as for the 5-SOC (Scheme 21).[36] Due to their symmetry, six-membered rings are more stable and are preferably formed. Therefore, 44% of the desired SOC were obtained as a colorless liquid after purification as identified with ^{1}H- and ^{13}C-NMR.
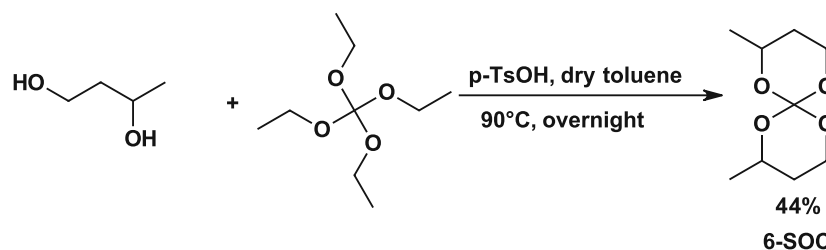
Scheme 21: Synthesis of the six-membered SOC (6-SOC)

The synthesis of the seven-membered SOC also proceeded in two steps as for the 5- SOC. Therefore, the corresponding lactone was reduced to 1,4-Octanediol following a literature procedure (Scheme 22).[49]

According to literature, catalytic amounts of NaOMe stabilize monomethoxyborohydride (NaBH$_3$OMe), which is the formed intermediate responsible for the reduction of esters at room temperature. Through the stabilization effect, the catalyst prevents solvent-induced loss of hydride.[49]

The colorless diol obtained as crude material was used for the further step without purification. Following the literature procedure,[36] 11% of a colorless liquid were obtained as desired material, which was confirmed with ^{1}H- and ^{13}C-NMR.

31
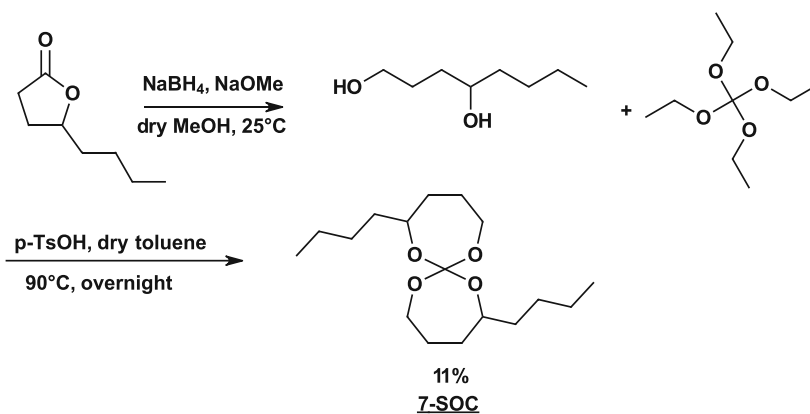
Scheme 22: Synthesis of the seven-membered SOC (7-SOC)

1.1.2 Photoreactivity by Photo-DSC

The reactivity of the spiro-orthocarbonates during cationic photopolymerization was investigated with photo-DSC analysis. The extension of classical calorimetry to photo- DSC allows the determination of enthalpy changes during the photopolymerization of light sensitive compounds. Before irradiation, the sample and the reference are conditioned in an isothermal phase at the selected temperature. Afterwards, the samples are irradiated twice and the heat evolution is detected simultaneously. Parameters relevant for the assessment of the photopolymerization were obtained after the evaluation of the measurements. These parameters are the heat of polymerization (curve area), which is calculated from the difference between the second exposure phase and the first exposure phase. Additionally, the time until a peak maximum is reached (t_{max}), the peak height (h) which correspondents to the rate of polymerization, and t_{95}, time at which 95% of the polymerization enthalpy are obtained after evaluation.

The measurements were conducted at 25, 70, 90, and 110° C to gain information about the temperature-dependence of the polymerization process. Formulations containing the corresponding monomer and the photoinitiator *tert*.-butyldiphenyliodonium tetrakis(perfluoro-t-butyloxy) aluminate (tBuI-Al, 1 mol%, Figure 25) were prepared and irradiated with a Hg broadband lamp (320-500 nm).
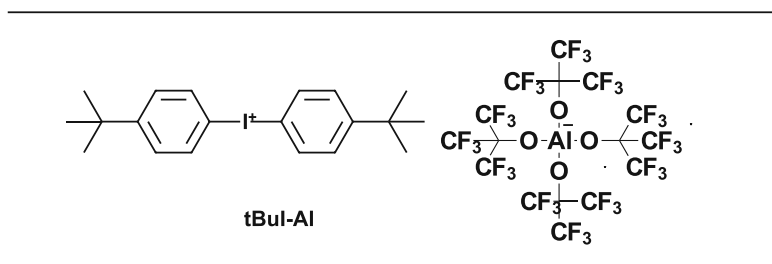
Figure 25: Photoacid generator (PAG) *tert.*-butyldiphenyliodonium tetrakis(perfluoro-t-butyloxy) aluminate (tBuI-Al) used for photoreactivity studies

Materials obtained from the photopolymerization by photo-DSC were additionally analyzed with NMR and GPC to provide information about the monomer conversion and the molecular weight of the polymers (Table 1). Generally, the conversion increased with increasing temperature as expected. Therefore, the highest temperature of 110 °C was most suitable for the photopolymerization. For a better overview, only the results obtained at 110 °C are shown in Figure 26.

Table 1: Results obtained from the photoreactivity study of spiro-orthocarbonates (SOC) of different ring sizes (5-7) at 110°C: yield; polymerization enthalphy (area); time at maximum heat development t_{max}; time at 95% of heat development t_{95}: molecular weight M_n; degree of polymerization P_n; conversion C

| Monomer | Yield [%] | Photo-DSC | | | GPC | | NMR |
		Area [J g^{-1}]	t_{max} [s]	t_{95} [s]	M_n [Da]	P_n [-]	C [%]
5-SOC	23	130	42	98	1 300	4	95
6-SOC	44	87	73	84	2 050	11	88
7-SOC	11	-	-	-	650	2	100
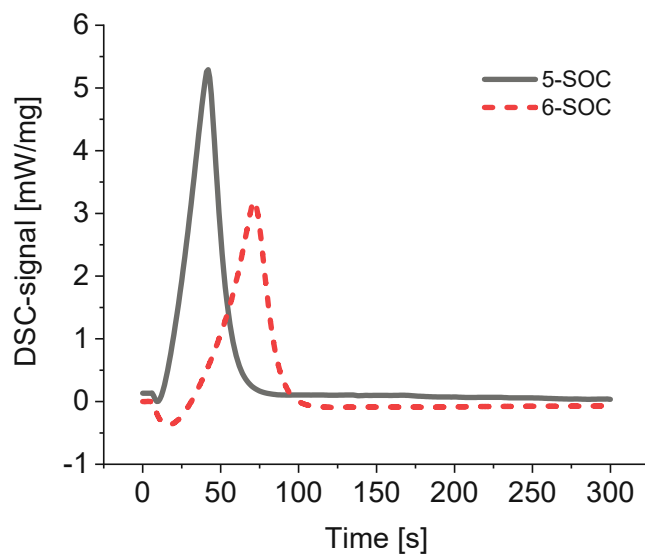
Figure 26: Photo-DSC plot of 5-SOC (black, solid line) and 6-SOC (red, dashed line) at 110 °C

A higher peak height was obtained for 5-SOC, which is related to the rate of polymerization. According to these values 5-SOC is more reactive than 6-SOC (Table 1). The polymerization enthalpy is related to the peak area and is also higher for 5-SOC (Table 1). Additionally, polymerization of the 5-SOC starts earlier as it can be seen in Figure 21. NMR and GPC data are in accordance with the photo-DSC analysis. As assumed, the 5-SOC achieved higher monomer conversions than 6-SOC.

The polymerization of 7-SOC started already before irradiation of the sample in the isothermal phase of the measurement. The reason for this is assumed to be the instability of the fused 7-membered rings and the thermal instability of the initiator. As the initiator was not soluble in the monomer, the formulation needed to be heated up to 110° C to obtain a homogenous solution. Most likely, the initiator decayed at the high temperature. Due to these facts, the polymerization process could not be evaluated by photo-DSC measurement. On the other hand, no residual monomer was detected in the NMR-spectra after the polymerization of 7-SOC. However, a low degree of polymerization was obtained.

Influence of Temperature on Photoreactivity

As already mentioned in chapter 1.1.2, photo-DSC measurements were conducted at different temperatures to study the temperature-dependence of the photopolymerization. Two different system, 5-SOC and 6-SOC are shown below, 7- SOC is excluded due to early polymerization at 110°C.
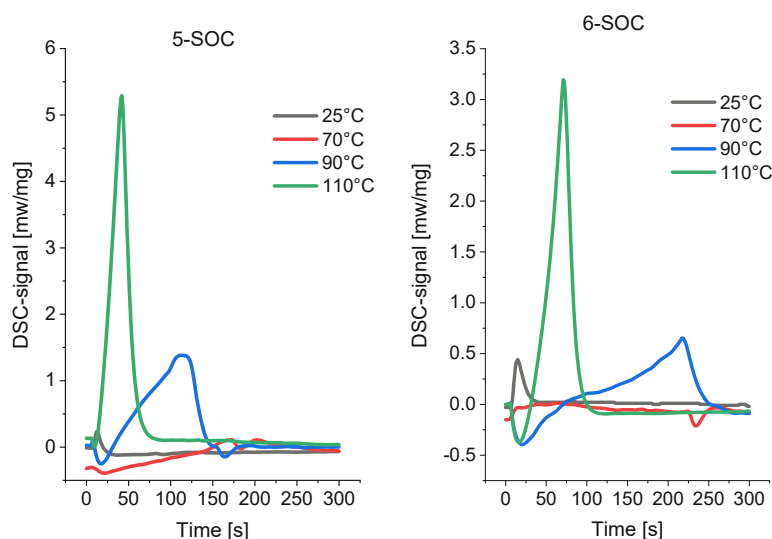
Figure 27: Left: photo-DSC plot of 5-SOC at different temperatures; Right: photo-DSC plot of 6-SOC at different temperatures, both with 1mol% tBuI-Al as photoiniitator

Table 2: Results obtained from the photoreactivity study of 5-SOC and 6-SOC at different temperatures: polymerization enthalphy (area); time at maximum heat development t_{max}; time at 95% of heat development t_{95}: molecular weight M_n; conversion C

5-SOC					
T [°C]	Area [J g^{-1}]	t_{max} [s]	t_{95} [s]	M_n [Da]	C [%]
25	-1.70	13	270	492	12
70	13.17	169	266	884	86
90	85.81	127	141	1 127	88
110	129.57	42	98	1 313	95
6-SOC					
25	14.03	15	224	787	4
70	11.00	128	187	2 940	48
90	66.31	216	234	2 238	88
110	86.69	73	84	2 056	88

Figure 27 clearly demonstrates the influence of the polymerization temperature on the reactivity of the monomers. Both of them have low reactivities at 25 °C, which is also proven by NMR-analysis, where 5-SOC reaches a conversion of 12% and 6-SOC a lower conversion of 4% (Table 2). With increasing temperature (70 °C and 90 °C), polymerization enthalpy as well as monomer conversion increase. The best values were obtained for both systems at 110°C (Figure 27, Table 2). Based on these results, 3D-printing processes utilizing cationic ring-opening monomers should be performed at elevated temperatures.

1.1.3 Polymerization Modes

To ensure efficient polymerization processes, the polymerization modes of spiro-orthocarbonates, were studied in detail with ^{1}H- and ^{13}C NMR-spectra. In literature it is described that the polymerization of spiro-orthocarbonates strongly depends on the monomer ring size. The following polymerization pathways of SOCs were reported by Okada *et al.*(Scheme 23):[50]
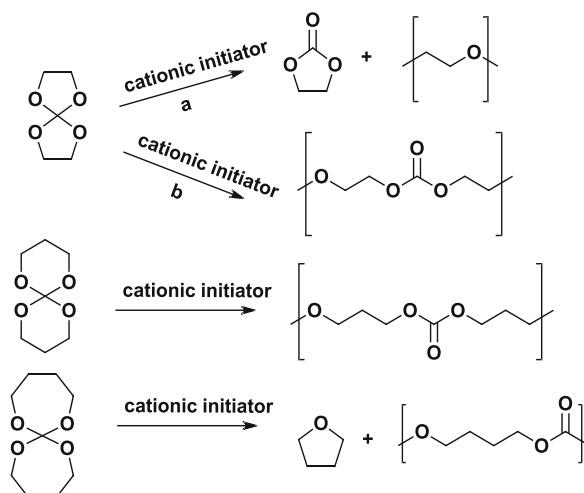
Scheme 23: Polymerization modes of spiro-orthocarbonates[50]

According to literature, only six-membered spiro-orthocarbonates polymerize *via* a complete double ring-opening process. Five-membered SOCs may form poly(ether)carbonates but are more likely to form poly-ethers and eliminate cyclic carbonates during their polymerization. Seven-membered SOCs polymerize with the elimination of THF-derivatives.[50]

36

Polymerization mode of 5-SOC:

Having a closer look at the spectra these were coherent with findings in literature: The presence of the corresponding ethylene carbonate and poly(ether) could be proven with ^{1}H- and ^{13}C-APT-NMR analysis (Figure 28 and Figure 29). Pyridine signals can be detected in every ^{13}C-APT spectra, since it was used to quench the polymerization immediately after the photo-DSC analysis. No double ring-opening polymerization could be observed.
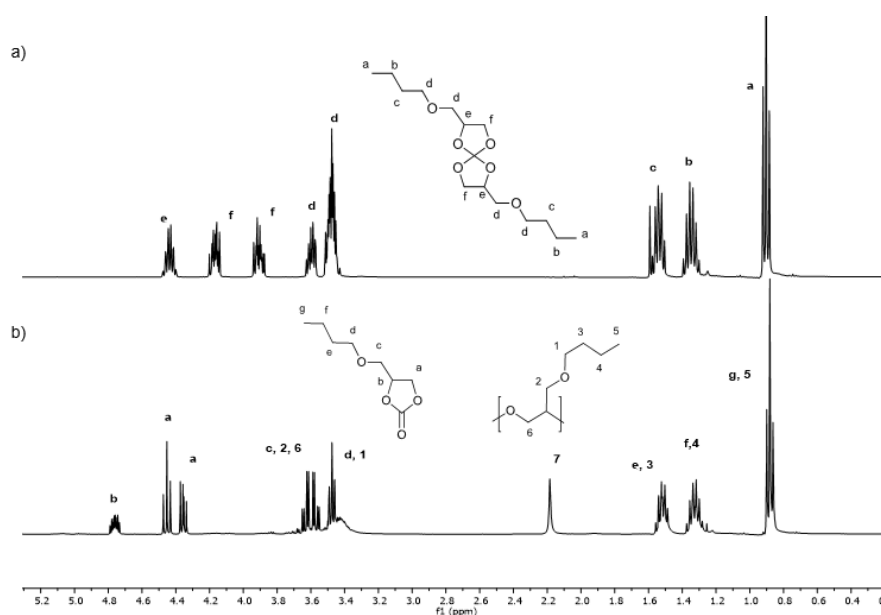
Figure 28: a) ^{1}H-NMR spectra of monomer 5-SOC, b) ^{1}H-NMR spectra after photopolymerization of 5- SOC at 110 °C
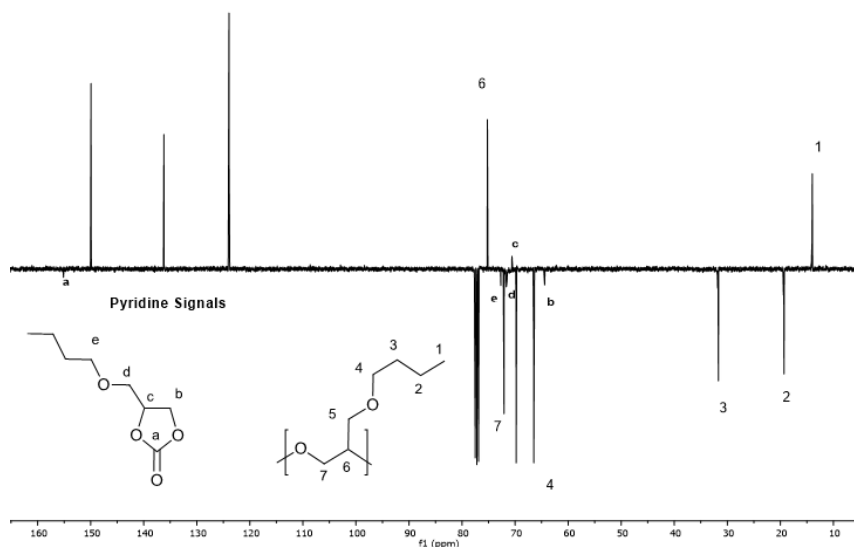
Figure 29: Relevant part of ¹³C-APT-NMR spectra after photopolymerization of 5-SOC at 110° C which shows the signals of the cyclic carbonate and the poly(ether)

The polymerization for 5-SOC therefore proceeded as follows (Scheme 24):
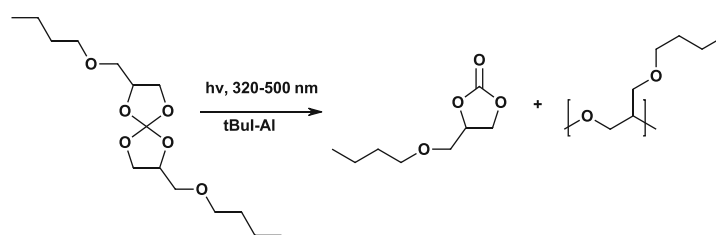
Scheme 24: Polymerization mode of 5-SOC

Polymerization mode of 6-SOC:

NMR-analysis of 6-SOC proved the occurrence of single ring- and double ring-opening polymerization. ¹³C APT-NMR proved the formation of the poly(ether)-carbonate polymer structures at 90 °C, where the quaternary carbon was detected at 154 ppm. Additionally, the multiplet obtained at 4.9 ppm in ¹H-NMR spectra after photopolymerization proves this structure again (Figure 30). Below this temperature (at 70° C), predominantly single ring opening (SRO) took place, which was confirmed by ¹H- and ¹³C-APT NMR (Figure 31). This result is in agreement with the literature, since double ring-opening polymerizations (DRO) are known to require high temperatures.

38
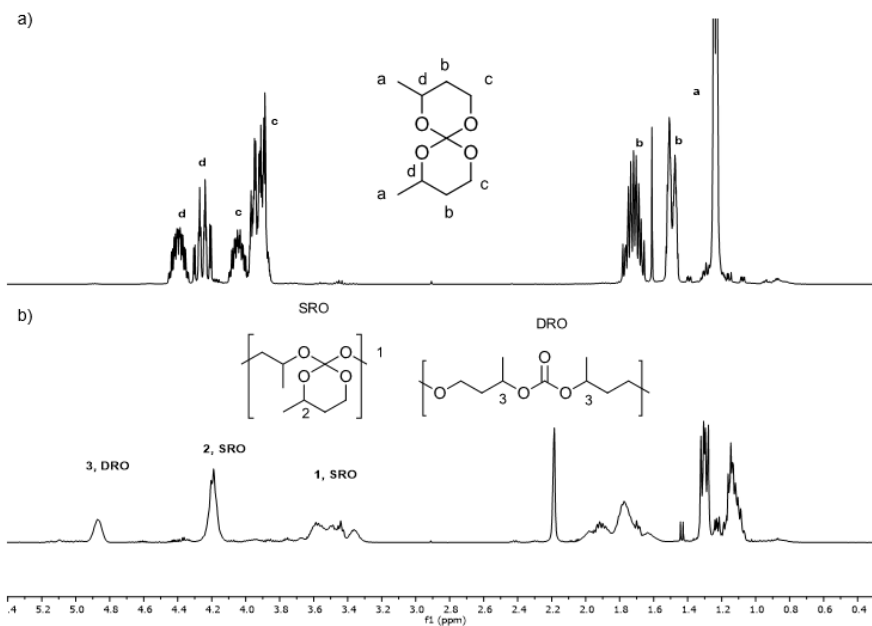
Figure 30: a) ^{1}H-NMR spectra of monomer 6-SOC, b) ^{1}H-NMR spectra after photopolymerization of 6-SOC at 90° C
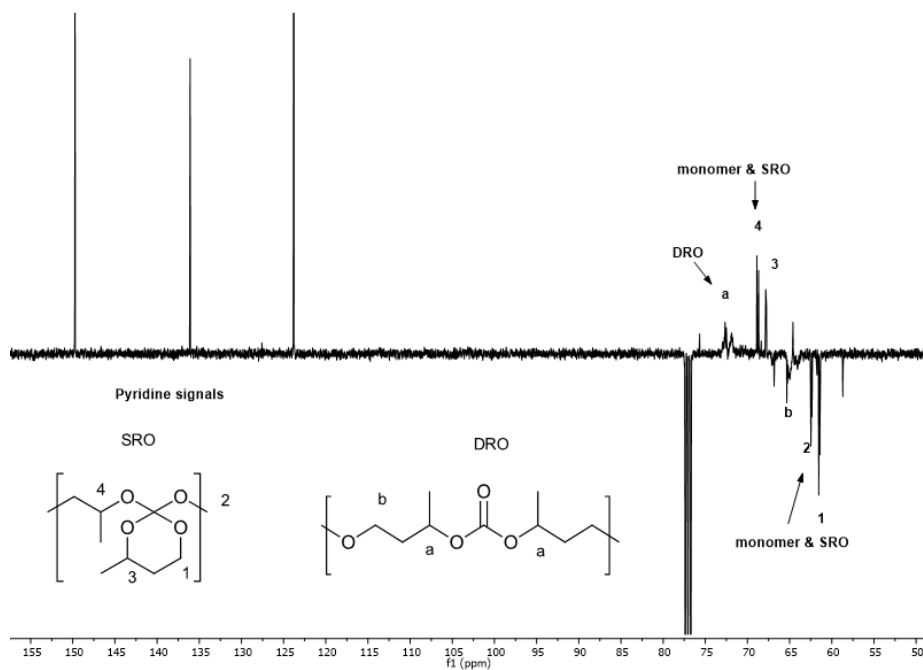
Figure 31: Relevant part of ^{13}C-APT-NMR spectra after photopolymerization of 6-SOC at 70° C which proves the occurrence of both polymerization modes

As expected and predicted by literature, the polymerization proceeded without elimination of by-products (Scheme 25).[50]
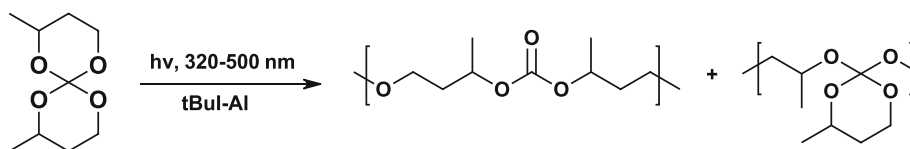
Scheme 25: Polymerization modes of 6-SOC

Polymerization mode of 7-SOC:

Takata *et al.* reported two possilble polymerization modes of seven-membered spiro-orthocarbonates, depending on their substitution. Polymerization of the seven-membered spiro-orthocarbonate can lead to the poly(ether)carbonate but is more likely to result in the formation of a polycarbonate with the elimination of a THF-derivative.[51]

^{1}H-NMR and ^{13}C-APT-NMR spectra of photopolymerized 7-SOC confirmed the presence of the THF derivative and the poly(carbonate) (Figure 32 and Figure 33).
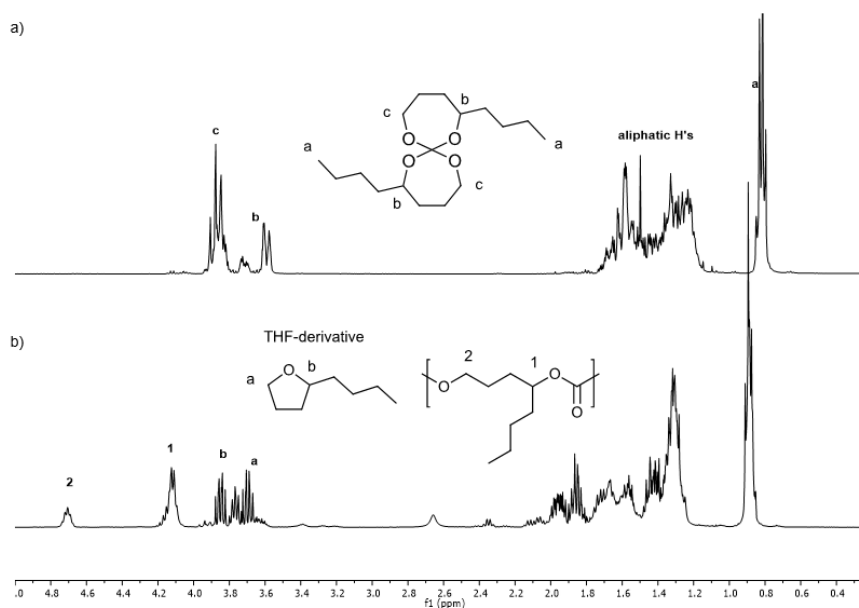
Figure 32: a) ^{1}H-NMR spectra of monomer 7-SOC, b) ^{1}H-NMR spectra after photopolymerization of 7-SOC at 90° C
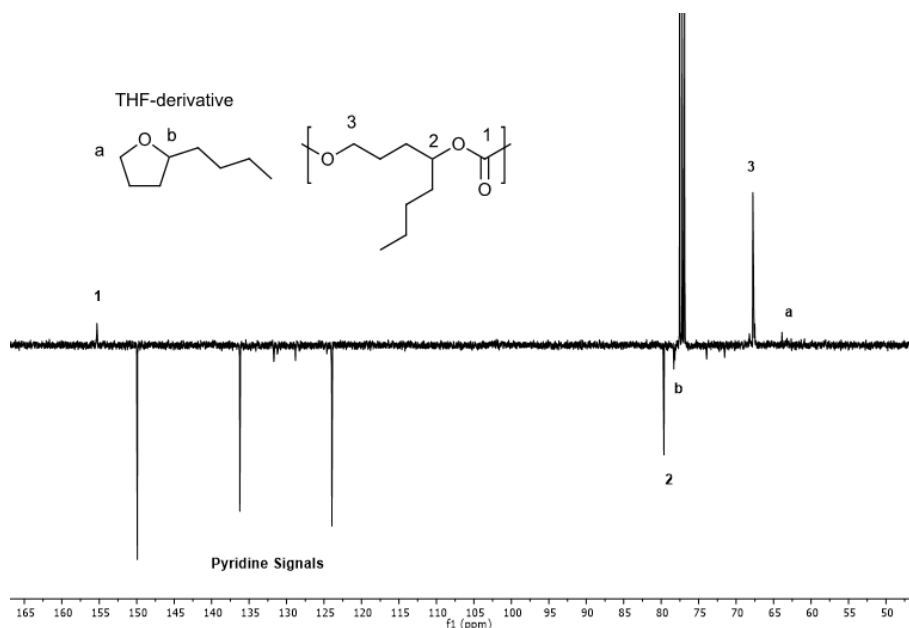
Figure 33: Relevant part of ^{13}C-APT-NMR spectra after photopolymerization of 6-SOC at 90° C which proves the presence of the poly(carbonate) and THF-derivative

The results are therefore in agreement with literature and elimination of the by-product took place (Scheme 26).[50]
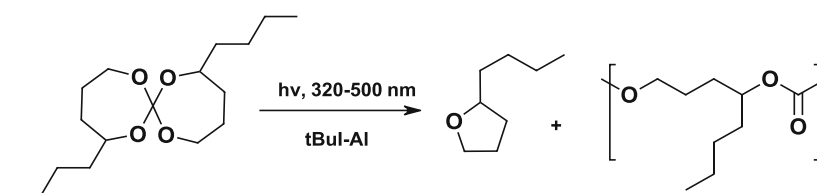
Scheme 26: Polymerization mode of 7-SOC

Based on the results obtained, the polymerization mechamisms of the carbonates were found to be very complex. Only one monomer, 6-SOC, polymerizes *via* an efficient double ring-opening process. Eliminations of by-products during polymerization limit the application of 5-SOC and 7-SOC for 3D printing. Therefore, spiro-orthoesters were synthesized as more promising monomer candidates and investigated with regard to their photoreactivity and polymerization mechanism.

41

1.2 Monofunctional Spiro-Orthoesters

1.2.1 Synthesis of Monofunctional Spiro-Orthoesters

Syntheses of spiro-orthoesters (SOE) were carried out with epoxides and the corresponding lactones based on the procedure of K. Bodenbenner (Scheme 27).[35] The reaction was catalyzed by boron trifluoride diethyl etherate $BF_3 \cdot Et_2O$. Low reaction temperatures (0 °C) were necessary to suppress side reactions such as polymerization of the epoxide and the copolymerization of the epoxide and the freshly formed spiro-orthoester.[52]
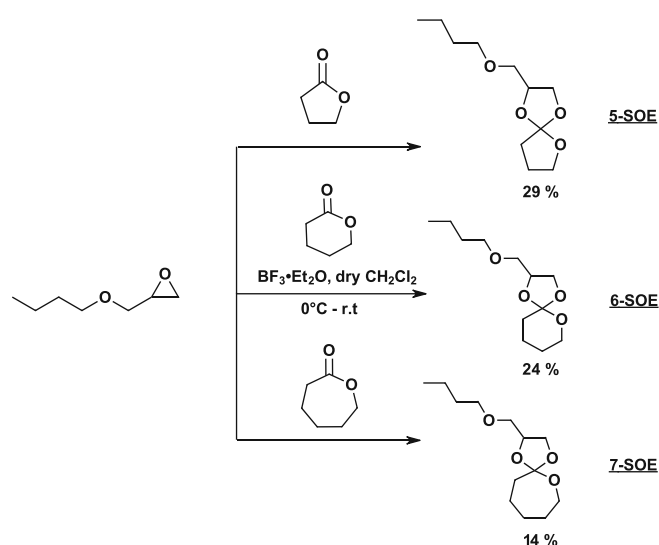
Scheme 27: Synthesis of spiro-orthoesters (SOE) of different ring sizes (5-7)

The five-membered spiro-orthoester, 5-SOE was obtained from the catalyzed reaction of γ-butyrolactone and butyl-glycidyl ether (BGE) in dry dichloromethane.[53] Through slow addition of BGE homopolymerization and loss of the reactant BGE should be reduced. Following the literature procedure[53], 29% of the desired SOE were obtained as colorless liquid after distillation in *vacuo*. The product was identified by ^{1}H- and ^{13}C- NMR.

The six-membered spiro-orthoeseter 6-SOE was synthesized from BGE and δ- valerolactone following the same literature procedure as before.[53] The reaction was carried out as for the 5-SOE and the workup remained unchanged. Following this

approach, 24% of a colorless liquid were obtained and identified as the targeted compound by ^{1}H- and ^{13}C-NMR.

To obtain the seven membered spiro-orthoester, ε-caprolactone was reacted with BGE, whereby the procedure was as for the other SOEs. Thereby, 14% of the desired compound could be isolated and identified by ^{1}H- and ^{13}C-NMR.

To investigate the influence of the SOE-structure on reactivity, an aromatic SOE was synthesized in analogy to the aliphatic monomers following the procedure from Nishida *et al* (Scheme 28). [53] The colorless crystalline solid with a melting point of 73 °C was obtained in a yield of 33%.
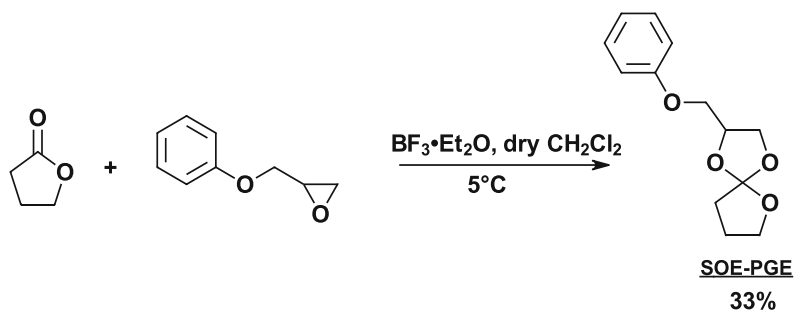
Scheme 28: Synthesis of the aromatic spiro-orthoester (SOE-PGE)

1.2.2 Photoreactivity by Photo-DSC
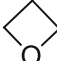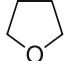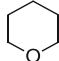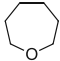
As with the spiro-orthocarbonates, the photoreactivity of the spiro-orthoesters was determined with photo-DSC analysis. The photopolymerization was conducted at 25, 70, 90 and 110 °C. The same trend in reactivities was obtained as for the SOC, namely that the reactivity increases with increasing temperature. Therefore, only photo-DSC plots of spiro-orthoesters at 110 °C are shown below (Figure 34).
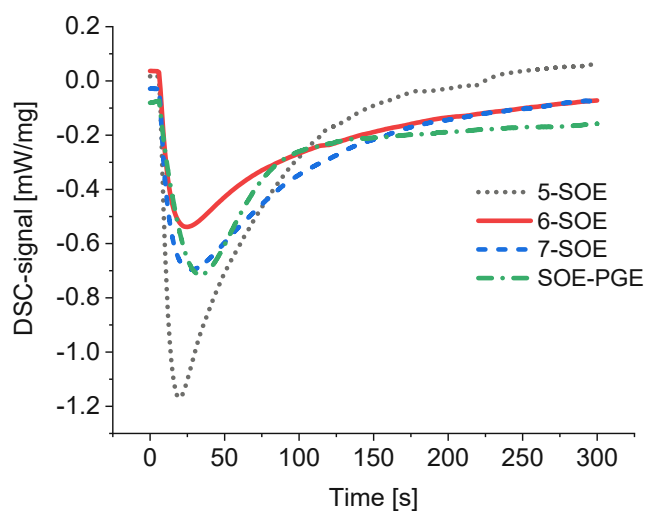
Figure 34: Photo-DSC plots of spiro-orthoesters (SOE) of different ring sizes (5-7) at 110 °C, 5-SOE (black, dotted line), 6-SOE (red, solid line), 7-SOE (blue, dashed line) and SOE-PGE (green, dash dot line)

In contrast to the SOC results, however, negative peak areas were obtained for SOEs (Figure 26). As explained previously, the peak area is calculated from the difference between the second exposure phase and the first exposure phase. This means that no exothermic behavior was observed during the photopolymerizations and therefore calorimetric information could not be obtained. As established previously, the driving force for ring-opening polymerizations is the ring strain. Generally, polymerization of heterocyclic monomers is exothermic due to the release of ring strain. This ring strain is mainly caused by angle and bond deformations and is therefore highest for three- and four membered rings. Five- and six membered cycles, however, are less strained due to their geometry, which explains their lower reactivity. Seven-membered monomers, show a rather low ring-strain which is similar to five- and six-membered rings. The ring strain increases for 8-13 membered rings and decreases again for larger cyclic monomers. The phenomenon of the ring-size is demonstrated using the example of cyclic ethers (Table 3).[54,55,25]

Table 3: ring strains of cyclic ethers[54]

Cyclic ether				
Strain [kJ/mol]	-114	-107	-23	-5	-33

44

Because of the low ring-strain of five-, six- and seven-membered spiro-orthoesters, their polymerization enthalpy cannot be detected with photo-DSC. In literature it is described that ring strain also increases with transannular strain. Transannular interactions arise from the repulsion of ring substituents across the ring.[54] Due to the repulsion of the additional oxygen in spiro-orthocarbonates, their ring strain is higher than that of SOEs. For this reason, detection of the exothermic behavior of spiro-orthocarbonates is possible (Figure 26).

Nevertheless, information about the time until a peak maximum is reached (t_{max}), the peak height (h) and time at which 95% of the polymerization enthalpy was obtained (t_{95}), could be determined (Table 3). Additionally, monomer conversions and molecular weights were obtained by NMR and GPC-analysis after the photopolymerization (Table 4). The results agree with the findings about the monomer ring-size. Monomer conversions of 5- and 7-SOE are quite similar while 6-SOE is unreactive with a conversion of 14%. Additionally, it gives the highest t_{95} values. This outcome confirms the low reactivity of six-membered rings caused by their symmetry. The five-membered, aromatic SOE-PGE gives the highest monomer conversion, but also low molecular weights. An explanation for that could be the occurrence of a backbiting-reaction, a side-reaction which takes place in cationic polymerization. However, the obtained t_{95} value is similar to others and t_{max} is slightly higher (Table 4).

Table 4: Results obtained from the photoreactivity study of spiro-orthoesters (SOE) of different ring sizes and structure (5-7 and SOE-PGE): yield; polymerization enthalphy (area); time at maximum heat development t_{max}; time at 95% of heat development t_{95}: molecular weight M_n; degree of polymerization P_n; conversion C

| Monomer | Yield [%] | Photo-DSC | | | GPC | | NMR |
		Area [$J\ g^{-1}$]	t_{max} [s]	t_{95} [s]	M_n [Da]	P_n [-]	C [%]
5-SOE	29	-	20	190	930	4	62
6-SOE	24	-	23	215	2 400	10	14
7-SOE	14	-	26	197	1 500	6	65
SOE-PGE	33	-	36	193	486	2	83

Influence of Temperature on Photoreactivity

As with spiro-orthocarbonates, the temperature-dependence of the photopolymerization was also investigated with spiro-orthoesters (Figure 35, Table 5).
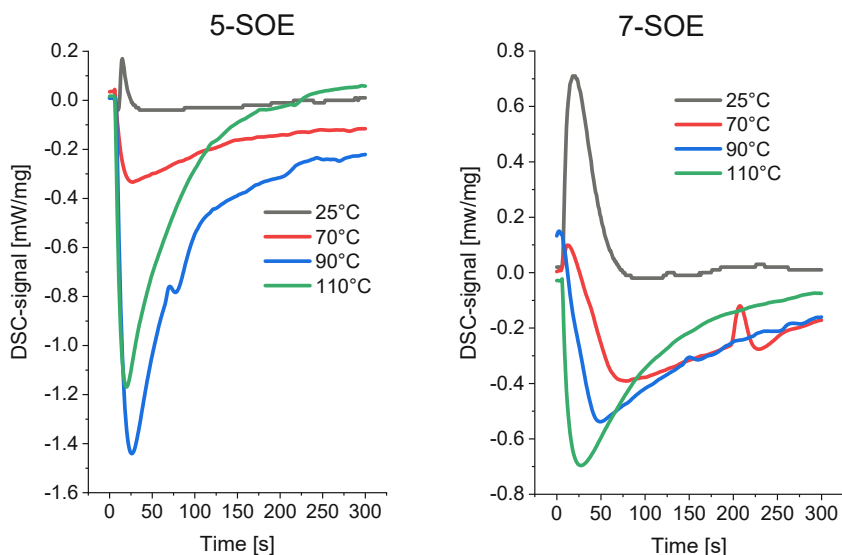
Figure 35: Figure 36: Left: photo-DSC plot of 5-SOE at different temperatures; Right: photo-DSC plot of 7- SOE at different temperatures, both with 1 mol% tBuI-Al as photoinitiator

Table 5: Results obtained from the photoreactivity study of 5-SOE and 7-SOE at different temperatures: polymerization enthalphy (area); time at maximum heat development t_{max}; time at 95% of heat development t_{95}: molecular weight M_n; conversion C

5-SOE					
T [°C]	Area [J g^{-1}]	t_{max} [s]	t_{95} [s]	M_n [Da]	C [%]
25	2.45	15	235	688	12
70	-	14	190	703	48
90	-	25	210	557	56
110	-	20	161	564	61
7-SOE					
25	20.68	19.0	41	832	34
70	-	82	254	1091	44
90	-	56	224	1202	51
110	-	26.2	197	1506	65

46

Due to the symmetry of 6-SOE and the low ring strain, no relevant changes of the photopolymerization process were observed with increased temperature. The results are therefore shown for 5-SOE and 7-SOE.

Figure 35 represents a similar photopolymerization behavior of 5-SOE and 7-SOE. No exothermic heat could be detected the photopolymerization, despite of the polymerization of 7-SOE and 5-SOE at 25 °C. Thereby, low peak heights of were observed. The exothermic heat is probably derived from the single ring-opening polymerization, which predominantly takes place at 25 °C for both compounds (Table 5). Thereby, 7-SOE is more reactive than 5-SOE and reaches a conversion of 34% at 25 °C, while 5-SOE reaches a conversion of only 12%. At higher temperatures, both monomers reach similar conversions, but 5-SOE reaches better t_{max} and t_{95} values than 7-SOE. With the obtained results, the temperature-dependence of cationic ring-opening polymerization was again proven (Table 5).

1.2.2.1 Polymerization Modes

Spiro-orthoesters are known to polymerize *via* double ring-opening polymerization at elevated temperatures.[31] At room temperature, single ring-opening polymerization also takes place.[56] To verify the polymerization mechanisms, NMR spectra were recorded and investigated after the photopolymerizations.

The five-membered SOE (5-SOE) polymerized at 70 °C *via* double ring-opening, the quaternary carbonyl peak could be detected in ^{13}C-APT-spectra at 173 ppm and the corresponding protons were detected in ^{1}H-spectra (Figure 37 and Figure 38). Additionally, a signal at 122 ppm proved the presence of the single ring-opening adduct (Figure 38). At 110 °C, double ring-opening predominantly took place. Since full conversion of the monomer was not achieved, its signals could also be detected in the ^{13}C-APT-NMR (Figure 39).

47
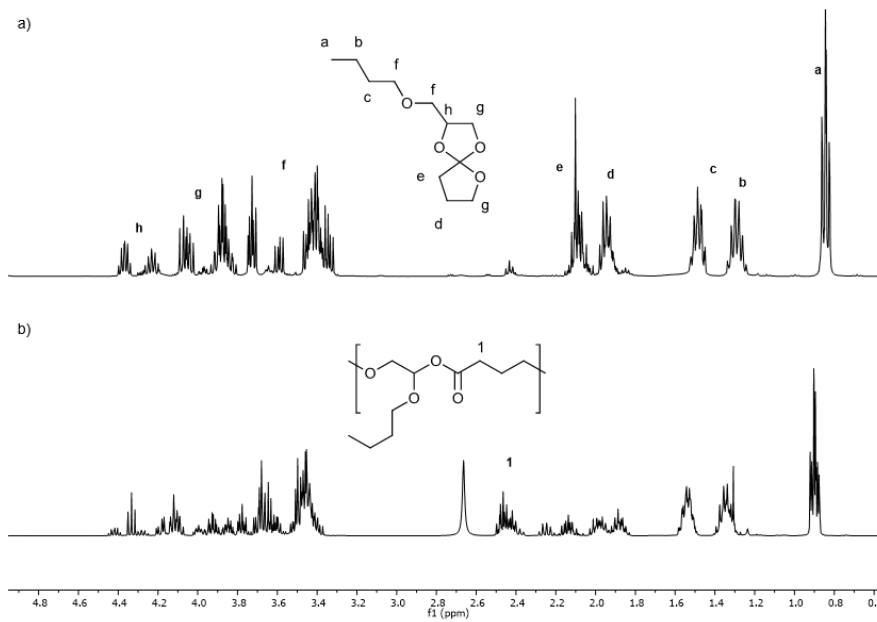
Figure 37: a) ¹H-NMR spectra of monomer 5-SOE, b) ¹H-NMR spectra after photopolymerization of 5-SOE at 70° C
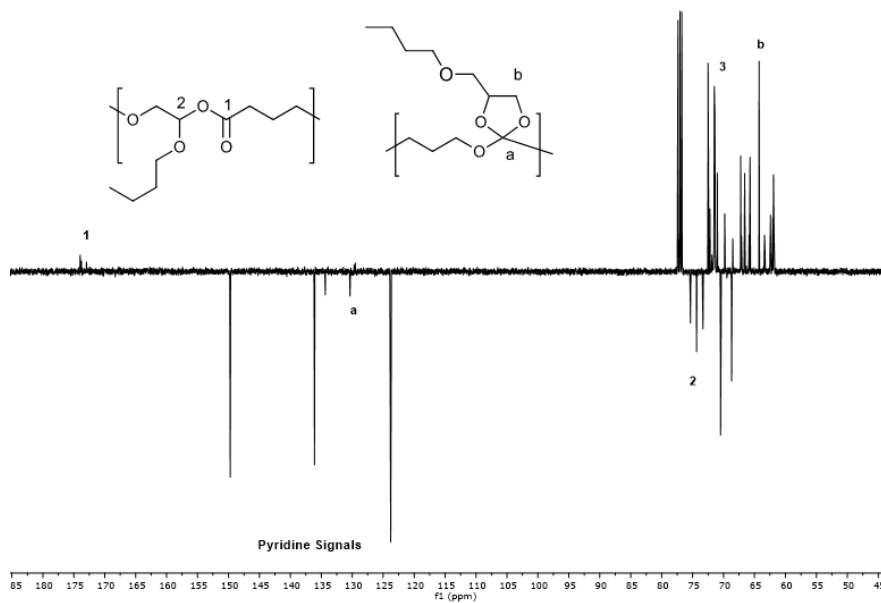
Figure 38: Relevant part of ¹³C-APT-NMR spectra after photopolymerization of 5-SOE at 70° C which proves the occurrence of both polymerization modes
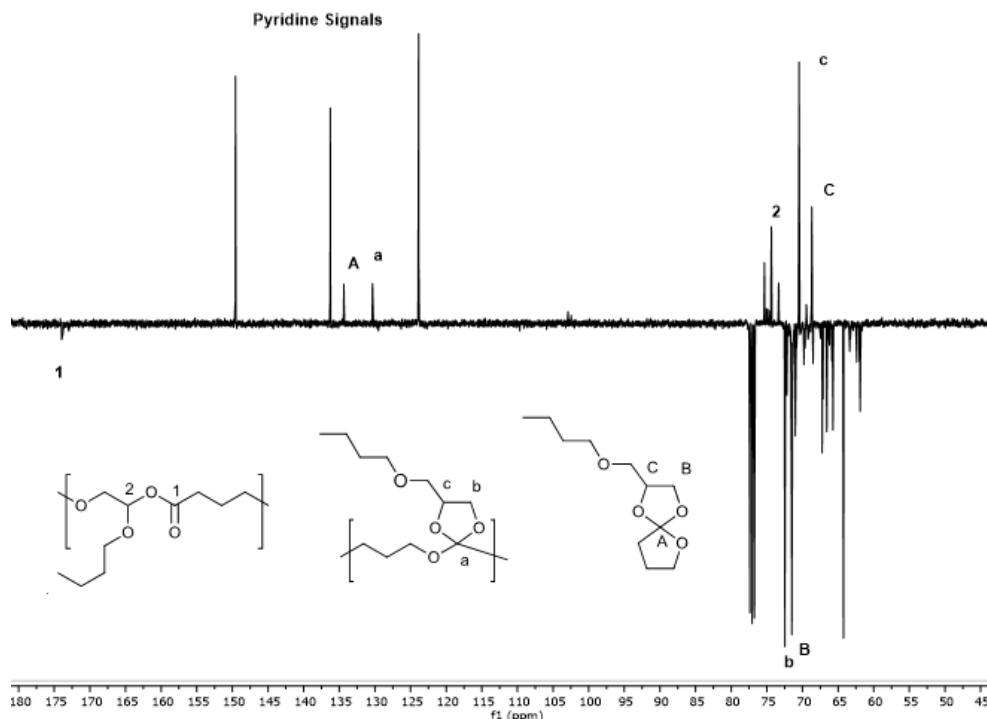
Figure 39: Relevant part of ^{13}C-APT-NMR spectra after photopolymerization of 5-SOE at 110° C which proves the occurrence of both polymerization modes and the presence of the monomer

The found polymerization mode of 5-SOE is shown in Scheme 29.
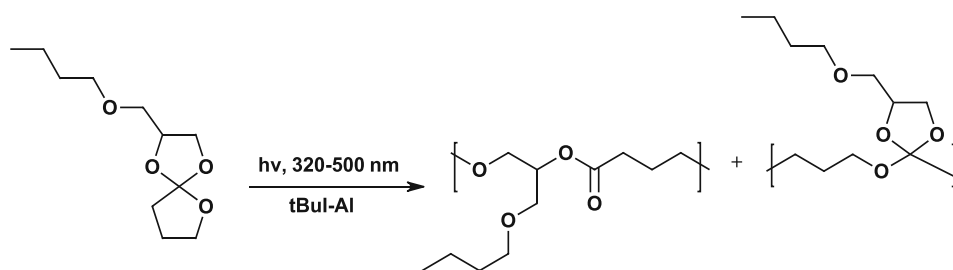
Scheme 29: Polymerization modes of 5-SOE

The least reactive monomer, the six-membered SOE (6-SOE), reached a conversion of 14% at 110 °C. Residual monomer peaks were observed after photopolymerization in ^{1}H-spectra (Figure 40). ^{13}C-APT-spectra revealed that at 110 °C no double-ring opening took place (Figure 41). The corresponding carbonyl peak was absent and additionally, monomer carbon signals could be detected. Moderate amounts of single ring-opening polymerization (SRO) took place (Scheme 30).

49
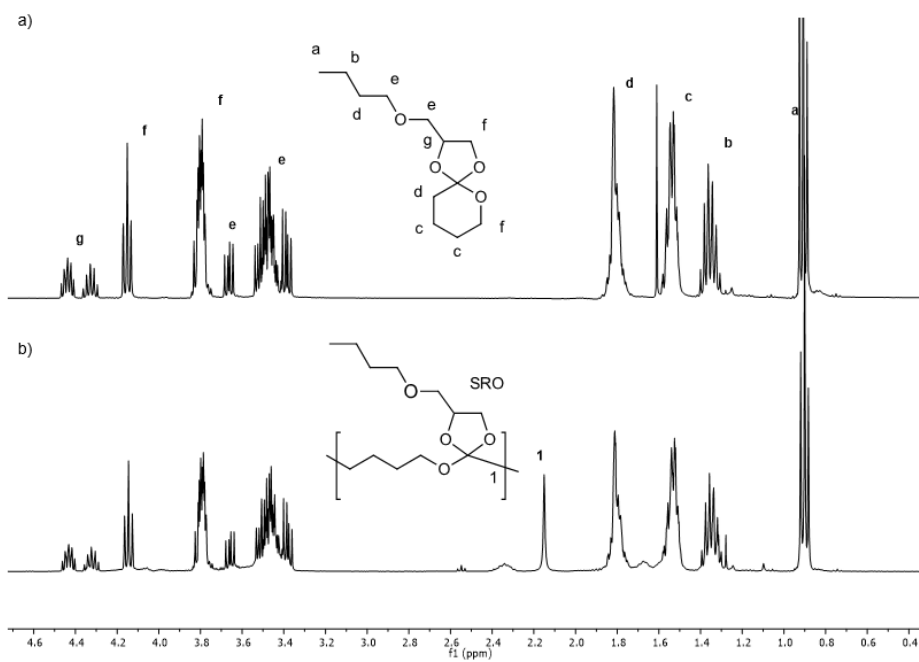
Figure 40: a) ^{1}H-NMR spectra of monomer 6-SOE, b) ^{1}H-NMR spectra after photopolymerization of 6-SOE at 110° C
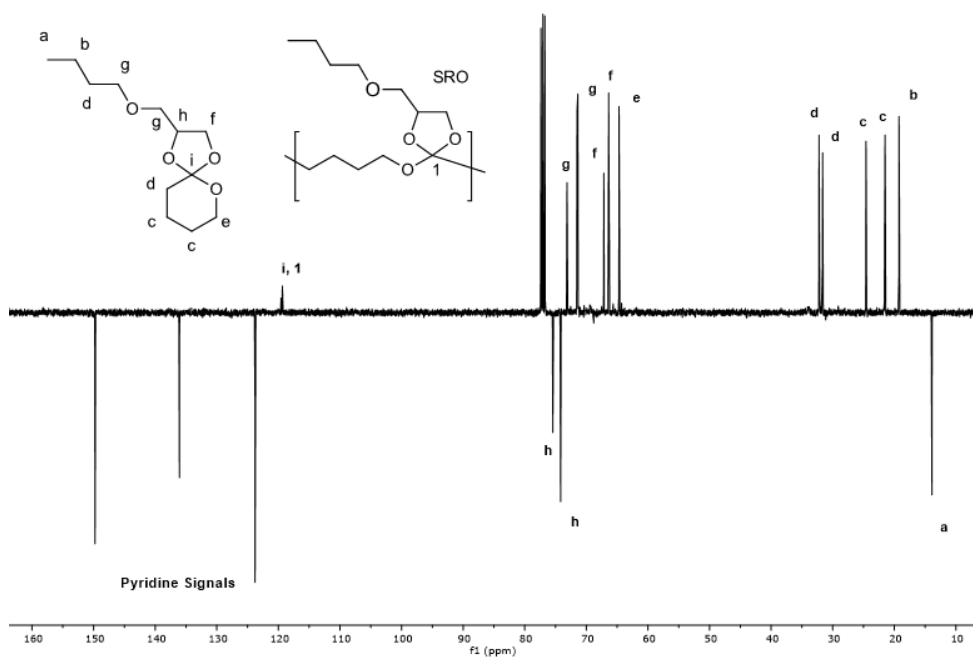
Figure 41: ^{13}C-APT-NMR spectra after photopolymerization of 6-SOE at 110° C with moderate amounts of SRO
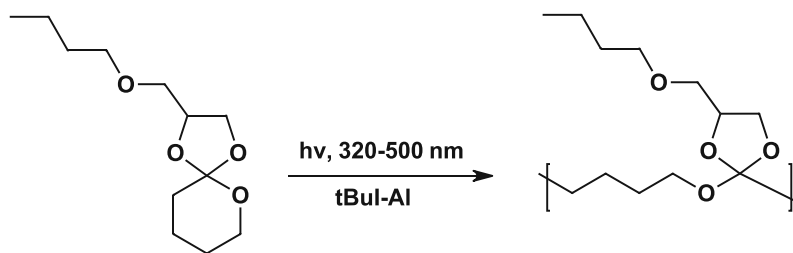
Scheme 30: Polymerization mode of 6-SOE

The seven-membered spiro-orthoester (7-SOE), polymerized *via* double ring opening already at 25 °C. A carbonyl signal could be detected in ^{13}C-APT-NMR. This is linked to the higher ring strain and the resulting reactivity of seven-membered SOEs. However, residual monomer was detected in [1]H-spectra after photopolymerization at 110° C (Figure 42). Accompanying single ring-opening polymerization took place below 90 °C, which was proven by ^{13}C-APT NMR (Figure 43, Scheme 34).
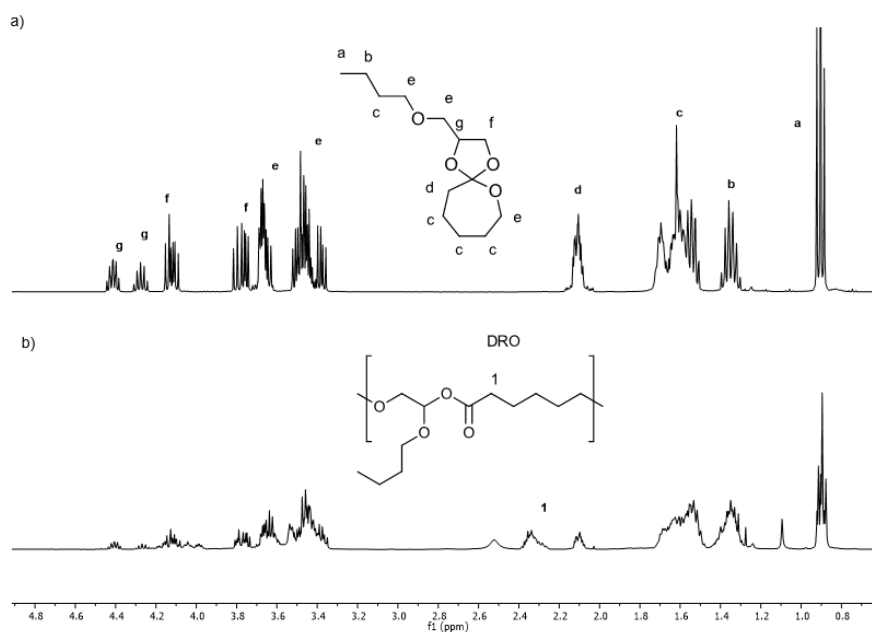
Figure 42: a) ^{1}H-NMR spectra of monomer 7-SOE, b) ^{1}H-NMR spectra after photopolymerization of 7-SOE at 110° C
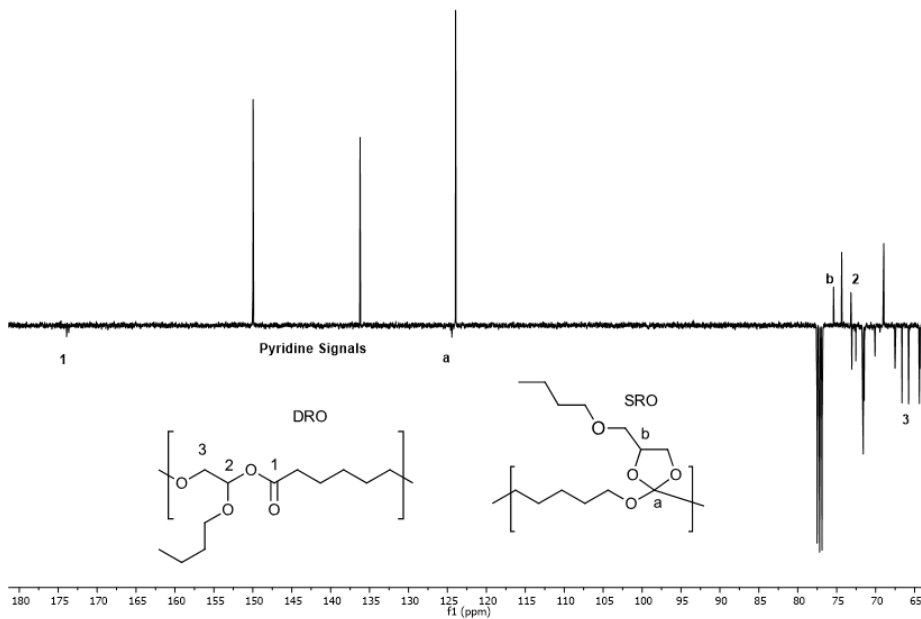
Figure 43: Relevant part of ^{13}C-APT-NMR spectra which confirms both polymerization modes during photopolymerization of 6-SOE at 90° C
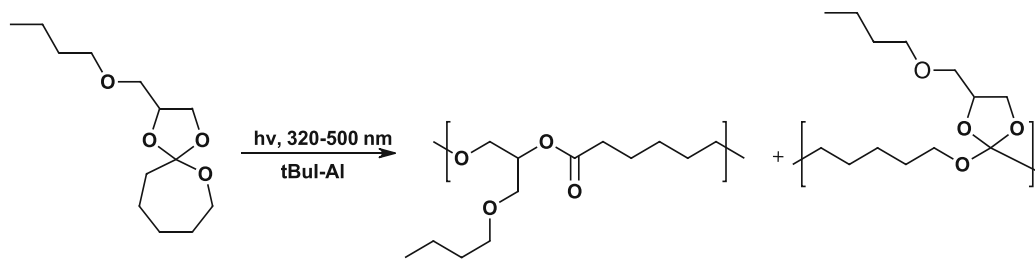
Scheme 31: Polymerization mode of 7-SOE

In summary, spiro-orthocarbonates show higher reactivities than spiro-orthoesters because of the greater ring strain. However, due to their polymerization, which proceeds with elimination of byproducts, they do not form polymeric products. Spiro- orthoesters, on the other hand, polymerize efficiently *via* single and/or double ring-opening processes. Additionally, the synthesis of spiro-orthoesters is more straightforward. Considering these findings, spiro-orthoesters were found to be the more suitable monomer class for bulk polymerization purposes and eventually Hot Lithography.

Die approbierte gedruckte Originalversion dieser Diplomarbeit ist an der TU Wien Bibliothek verfügbar
The approved original version of this thesis is available in print at TU Wien Bibliothek.

TU Bibliothek Your knowledge hub WIEN

1.3 Synthesis and Reactivity Study of Bifunctional Monomer

1.3.1 Synthesis of Bifunctional Spiro-Orthoester

Once the better monomer class had been defined, a bifunctional monomer serving as a crosslinker in bulk polymerization was synthesized from this class. To increase the rigidity in the desired spiro-orthoesters, an aromatic bifunctional SOE was chosen and synthesized. Crystalline monomers reported in literature were based on the epoxide BADGE and exhibit high melting points, which are above the operating temperatures of the Hot Lithography device (120 °C). To lower the melting point of the crosslinker, resorcinol diglycidyl ether was used as starting material instead of BADGE, which introduces more flexibility into the monomer. The synthesis was carried out following a literature procedure (Figure 55).[57] 25% of the desired crystalline compound could be obtained after recrystallization from methanol and a melting point of 105 °C was achieved, which lies within the range of Hot Lithography.
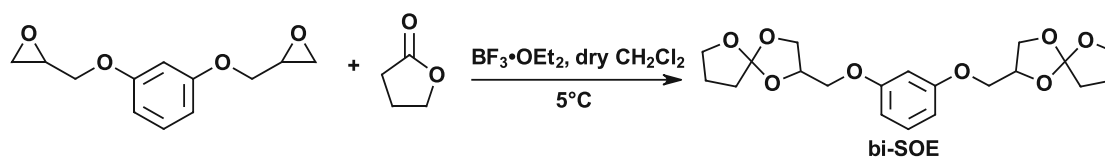
Scheme 32: Synthesis of the aromatic bifunctional spiro-orthoester (bi-SOE)

1.3.2 Photoreactivity by Photo-DSC

The photoreactivity of the synthesized bifunctional monomer was investigated with photo-DSC in analogy to the monofunctional monomers. The photo-DSC analysis was performed at 110 °C. Again, no polymerization heat could be detected during the irradiation of the bifunctional spiro-orthoester as already observed for monofunctional spiro-orthoesters: A negative peak area was obtained after evaluation of the measurement (Figure 44). Nevertheless, the peak height, t_{max} and t_{95} values could be determined to provide additional information about the polymerization process (Table 6).
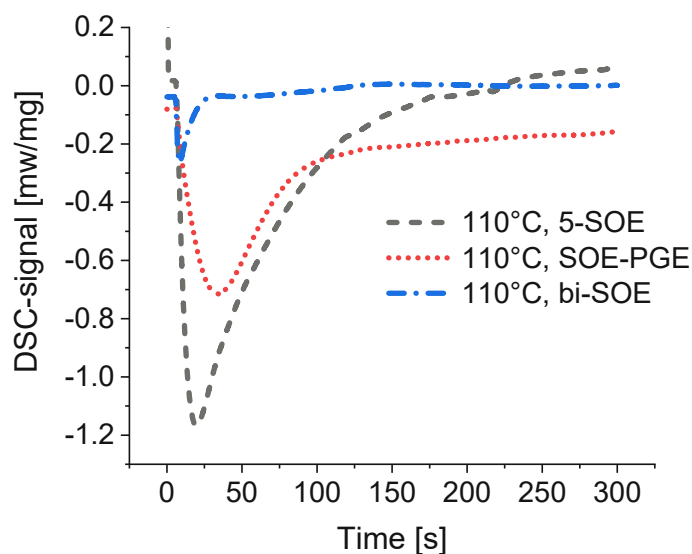
Figure 44: Photo-DSC plots of the bifunctional SOE (blue, dash-dotted line), 5-SOE (black, dashed line) and SOE-PGE (red, dotted line) at 110 °C

Table 6: Results obtained from the photo-DSC measurement of bifunctional SOE; polymerization enthalphy (area); peak height h; time at maximum heat development t_{max}; time at 95% of heat development t_{95}

	Area [J g^{-1}]	h [mW mg^{-1}]	$t_{max.}$ [s]	t_{95} [s]
bi-SOE	-	0.27	9.5	150
5-SOE	-	0.11	14	279
SOE-PGE	-	0.61	36	193

The bifunctional SOE is more reactive than its monofunctional analog, which is demonstrated by lower t_{max} and t_{95} values. Since an insoluble polymer network was formed, NMR- and GPC-analysis were not performed.

2   Bulk-Photopolymerization of Spiro-Orthoesters

After the synthesis of the bifunctional spiro-orthoester, the photopolymerization of the spiro-orthoesters and the (thermo)mechanical properties of the resulting poly(ether)-esters were investigated in detail. This allows conclusions to be drawn as to how suitable the monomers are for the Hot Lithography. To compare the impact of the SOE- structure on the thermomechanical properties, two different systems were

54

investigated. Thereby, an aromatic monofunctional SOE, 2-(phenoxymethyl)-1,4,6-trioxaspiro[4.4]nonane (SOE-PGE) and an aliphatic monofunctional SOE ,2-(butoxymethyl)-1,4,6-trioxaspiro[4.4]nonane (5-SOE) were chosen to be polymerized with the bifunctional monomer. Three formulations containing the bifunctional SOE as the crosslinker and the monofunctional SOEs as reactive diluents were prepared. The content of the bifunctional monomer was set to 25, 50 and 65 wt% in each monomer system.
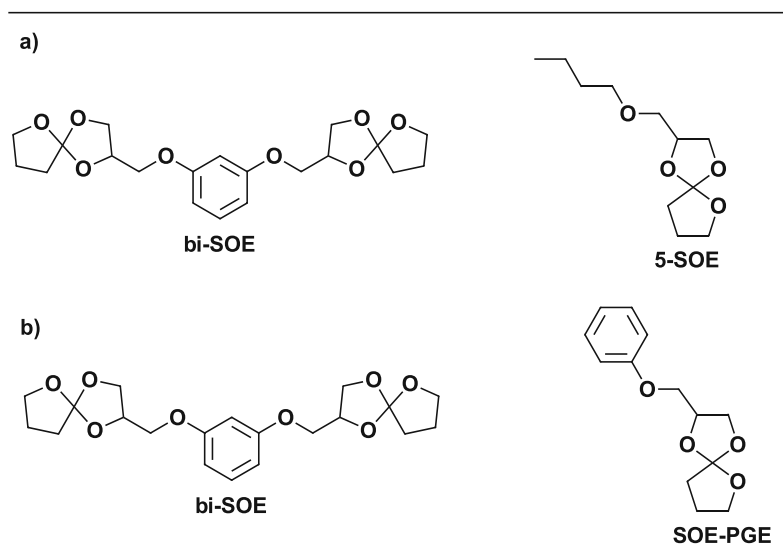
Figure 45: Investigated polymerization mixtures: a) mixed aromatic/aliphatic monomer system, b) aromatic monomer system

2.1 (Thermo-)mechanical Tests

Thermomechanical properties are of great importance for the application areas of polymers. Therefore, the materials were analyzed with dynamic mechanical thermal analysis (DMTA) and tensile testing. DMTA measurements are conducted in torsion mode in a temperature range from -100°C to 200°C. The material is exposed to oscillatory shear and storage and loss moduli are continuously recorded as a function of temperature. Additionally, the loss factor (tan δ) can be obtained from DMTA- analysis. The obtained storage modulus describes as an important parameter the stiffness and mechanical strength of the material. Furthermore, the glass-transition temperature T_g is obtained as the maximum value of the tan δ curve. The tensile strength is determined with tensile tests, where materials are subjected to axial tension

until failure. The tests provide important parameters such as strain and stress at break, as well as tensile toughness. The last parameter is obtained as the peak area under the tensile curves.

Before (thermo-)mechanical tests were performed, specimens for the respective measurement were prepared. Therefore, monomers were mixed together with 1 wt% photoinitiator. Since the mixtures needed to be heated up to 120 °C to obtain homogenous solutions, a photoinitiator with high thermal stability was needed. Irgacure 290 was chosen for this purpose (Figure 46). The concentration of the crosslinker bi-SOE was set to 25 , 50 and 65 wt%, since a homogenous solution could not be obtained with 75 wt% bi-SOE and the monofunctional monomers. As only viscous liquids were obtained during the photopolymerization of monofunctional monomers, the crosslinker content was chosen to be relatively high. The concentrations of the components were chosen in order to obtain a general overview of the material properties.
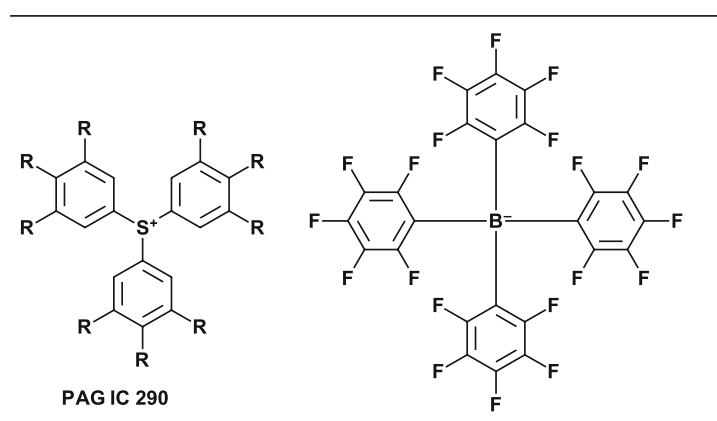
Figure 46: cationic PAG IC 290 used for the preparation of the specimens

The obtained formulations were poured into silicon molds an irradiated in a UV curing oven (320-580 nm) at 120 °C for 30 minutes. After the photopolymerization process, viscous liquids were obtained. The polymerization was complete after a post-curing process over night at 120 °C, whereafter form-stable specimens could be obtained.

2.1.1 Materials from a Mix of Aromatic and Aliphatic Spiro-Orthoesters

2.1.1.1 DMTA-Analysis

With the use of the aliphatic SOE (5-SOE) as monofunctional monomer in combination with the aromatic crosslinker bi-SOE, highly elastic materials were obtained. The stiffness of the materials, which was obtained as the storage modulus, as well as T_gs increased with crosslinker content (Figure 47). The polymerized material with 65 wt% bi-SOE was the stiffest, but still very stretchable.
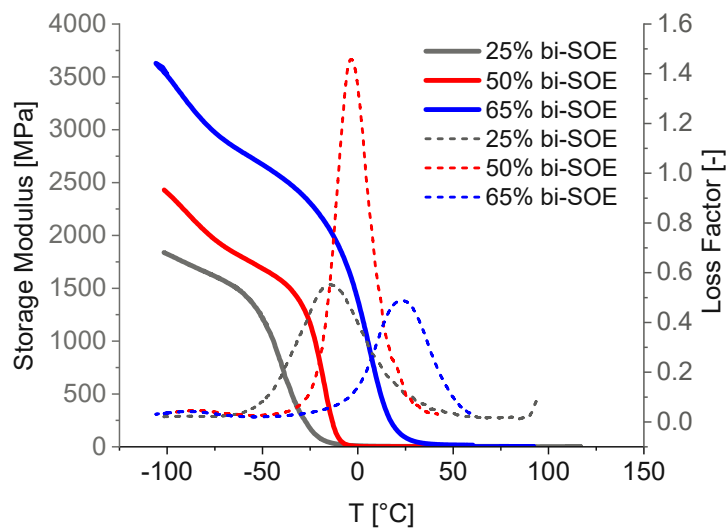
Figure 47: Storage moduli (G', solid lines) and loss factor (tan δ, dotted lines) of the specimens containing bi-SOE and 5-SOE as monomers in varying compositions with 1 wt % IC 290 as photoinitiator; 25 wt% bi- SOE (black lines); 50 wt% bi-SOE (red lines); 65 wt% bi-SOE (blue lines)

The glass transition temperatures (T_gs) of the materials were obtained as the maximum values of the loss factor (tan δ) and are listed together with the storage moduli (G') in Table 7.

Table 7: Results obtained from the DMTA-measurements of specimens containing bi-SOE and 5-SOE monomers in varying amounts and IC 290 as photoinitiator: weight percent of the compounds [wt%], glass transition temperature Tg, storage modulus at 20° C G'$_{20}$, storage modulus at glass-transition temperature G'$_{Tg}$

bi-SOE [wt%]	5-SOE [wt%]	PI [wt%]	T_g [°C]	G'$_{20}$ [Mpa]	G'$_{Tg}$ [Mpa]
25	75	1	-15	3.80	44.17
50	50	1	-4	0.964	11.67
65	35	1	23	161.79	117.98

As expected, elastic formulations with 25 and 50 wt% of bi-SOE have a negative T_g and therefore, their storage modulus decreases at 20 °C compared to the storage modulus at T_g. The T_g increases with the amount of bi-SOE, since the crosslinking density increases. The highest value, which is around room temperature, was obtained for the specimens with 65 wt% bi-SOE.

2.1.1.2 Tensile Testing

The tensile strength is defined as the maximum of stress that can be applied to the material before it breaks and was determined with tensile tests for the obtained materials. The test specimen containing 25 wt% of bi-SOE could not be measured, since extremely thin specimens were obtained. It is assumed that the monofunctional liquid monomer evaporated during the post-curing process.

Nevertheless, specimens comprised of 50 wt% and 65 wt% bi-SOE were investigated (Figure 48 and Figure 49). Relevant parameters such as stress at break (σ_B), strain at break (ε_B), and tensile toughness (U_T) are summarized in Table 8.
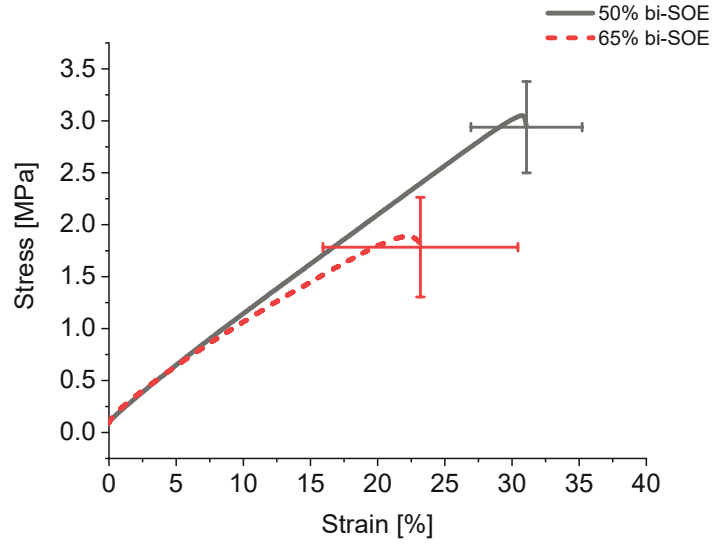
Figure 48: Representative tensile testing curves and mean values for stress and strain at break for the specimens containing 5-SOE and bi-SOE as momomers in varying compositions and 1 wt% IC 290 as photoinitiator: 50 wt% bi-SOE (black line); 65 wt% bi-SOE (red line)
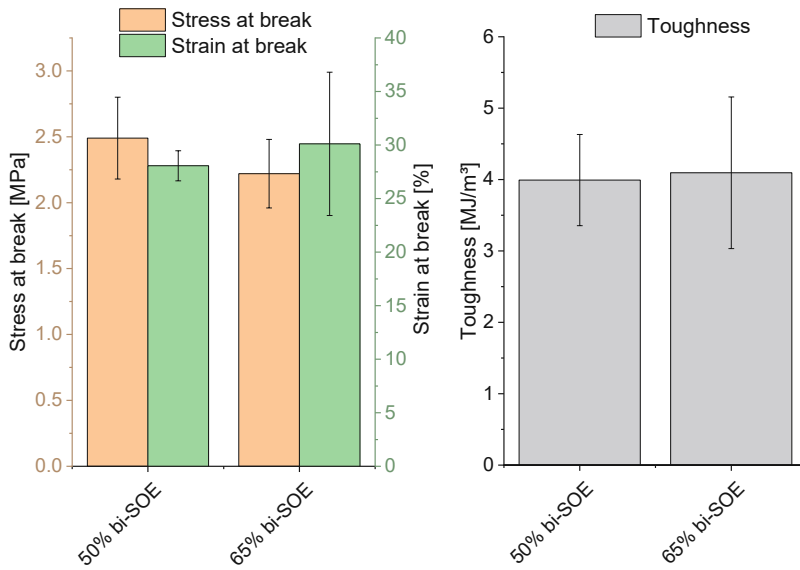
Figure 49: Left: mean stress and strain at break values; Right: toughness of the materials obtained from the monomers bi-SOE and 5-SOE in varying compositions and 1 wt% IC 290 as photoinitiator

Table 8: Results obtained from tensile testing for materials polymerized from bi-SOE and 5-SOE in varying concentrations with IC 290 as photoinitiator: weight percent of the compounds [wt%], stress at break σ_B, strain at break ε_B, tensile toughness U_T

bi-SOE [wt%]	5-SOE [wt%]	PI [wt%]	σ_B [MPa]	ε_B [%]	U_T [MJ/(m³)$^{-1}$]
50	50	1	2.49 ± 0.31	28.06 ± 1.41	3.993 ± 0.639
65	35	1	2.22 ± 0.26	30.11 ± 6.69	4.095 ± 1.062

As expected, the soft materials show a low tensile strength and are not resilient against mechanical stress. They break at low stress, whereby elongations of about 30% were reached. The toughness of the materials is similar for the analyzed specimens.

2.1.2 Materials with Exclusively Aromatic Spiro-Orthoester

2.1.2.1 DMTA-Analysis

(Thermo-)mechanical properties of the cured material were determined with DMTA- analysis, as it was done for the materials with the aliphatic spiro-orthoester. The storage modulus curve and the loss factor plot obtained from DMTA are shown in Figure 50.The combination of the aromatic monofunctional monomer SOE-PGE to the aromatic bi-SOE led to better and stiffer materials. Nevertheless, they were still rather soft and elastic. The curve progression in the transition region is more defined which is caused by the better homogeneity of the aromatic network. This is due to the similar reactivity of the aromatic monofunctional and the aromatic bifunctional monomer. Due to π-stacking of the aromatic substituents, the network can arrange itself better and more homogeneously (Figure 50).
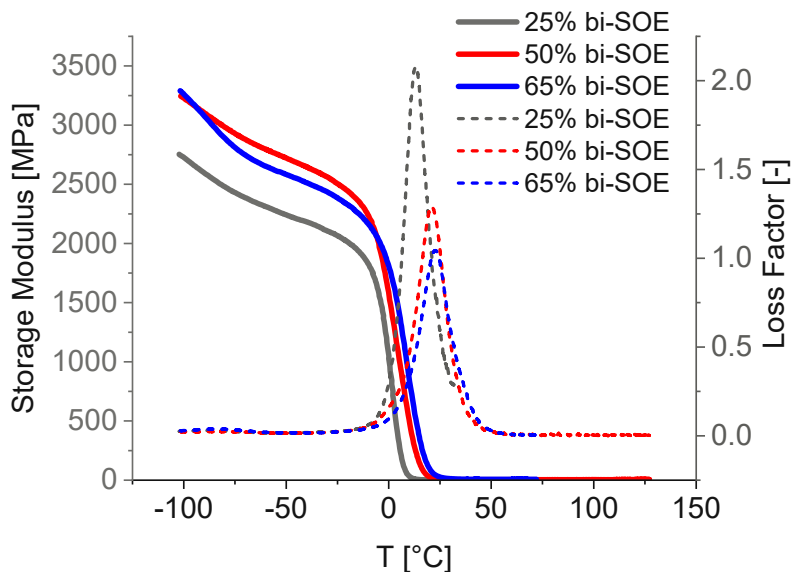
Figure 50: Storage moduli (G', solid lines) and loss factor (tan δ, dotted lines) of the specimens containing bi-SOE and SOE-PGE monomers in varying amounts with 1 wt % IC 290 as photoinitiator; 25 wt% bi-SOE (black lines); 50 wt% bi-SOE (red lines); 65 wt% bi-SOE (blue lines)

Table 9: Results obtained from the DMTA-analysis of specimens containing bi-SOE and SOE-PGE monomers in varying amounts and IC 290 as photoinitiator: weight percent of the compounds [wt%], glass transition temperature T_g, storage modulus at 20° C G'_{20}, storage modulus at glass-transition temperature G'_{T_g}

bi-SOE [wt%]	SOE-PGE [wt%]	PI [wt%]	T_g [°C]	G'_{20} [MPa]	G'_{T_g} [MPa]
25	75	1	14	1.65	5.48
50	50	1	21	21.11	17.03
65	35	1	23	88.32	38.25

The aromatic structure of the monomer leads to networks with higher T_g values, compared to materials obtained from the aliphatic monofunctional 5- SOE. Materials consisting of 50 wt% and 65 wt% of bi-SOE have T_gs in the range of room temperature. As expected, the T_g increases with the content of the bifunctional monomer. Furthermore, the storage moduli also increase with the content of the bifunctional monomer.

2.1.2.2 Tensile Testing

Tensile tests were performed with the aromatic specimens and the obtained results show the expected trend. With increasing crosslinker content the tensile strength increases (Figure 51). The specimen containing 65 wt% bi-SOE and 35 wt% SOE- PGE stands out with the obtained results. Hereby, a remarkable stress of 10 MPa was reached, whereby the strain at break remained quite high with 120 %.
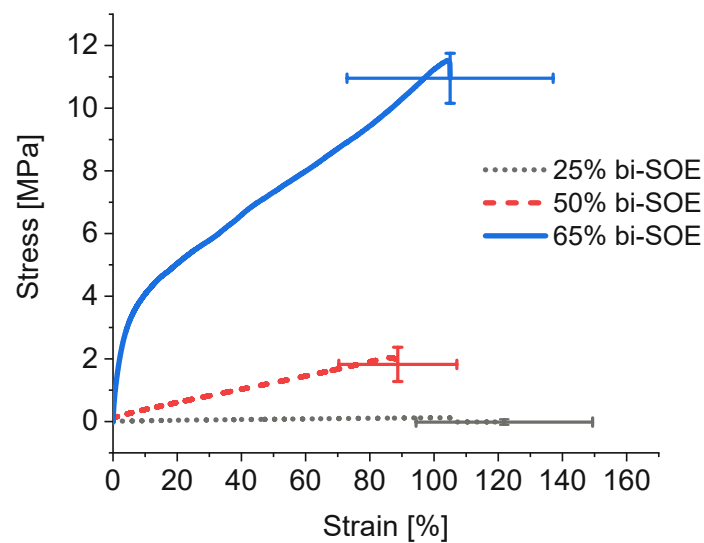
Figure 51: Tensile testing curves and mean stress and strain at break values of the specimens containing SOE-PGE and bi-SOE as momomers in varying amounts and 1 wt% IC 290 as photoinitiator: 25 wt% bi- SOE (black dotted line); 50 wt% bi-SOE (red dashed line); 65 wt% bi-SOE (blue solid line)
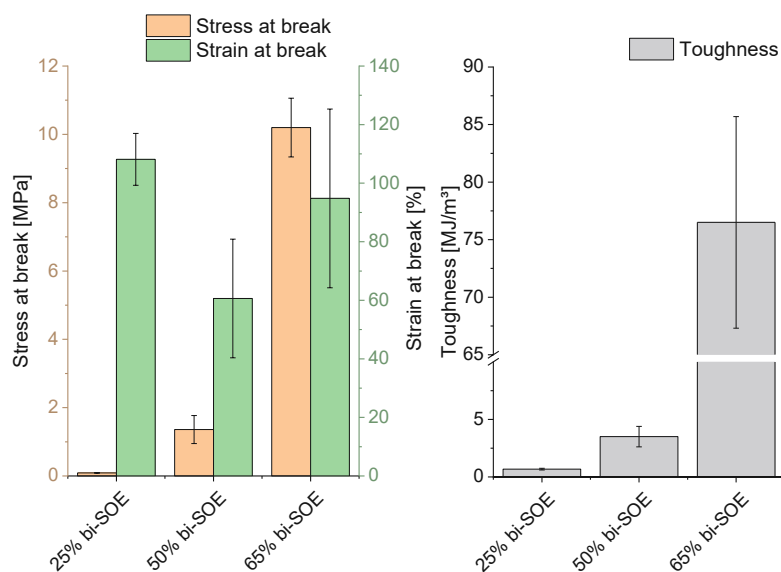
Figure 52: mean stress and strain at break values; Right: toughness of the materials obtained from the monomers bi-SOE and SOE-PGE in varying compositions and 1 wt% IC 290 as photoinitiator

Table 10: Results obtained from tensile testing for materials polymerized from bi-SOE and SOE-PGE in varying concentrations with IC 290 as photoinitiator: weight percent of the compounds [wt%], stress at break σ_B, strain at break ε_B, tensile toughness U_T

bi-SOE [wt%]	SOE-PGE [wt%]	PI [wt%]	σ_B [MPa]	ε_B [%]	U_T [MJ(m³)$^{-1}$]
25	75	1	0.09 ± 0.01	108.13 ± 8.88	0.679 ± 0.071
50	50	1	1.36 ± 0.41	60.62 ± 20.27	3.5 ± 0.889
65	35	1	10.20 ± 0.86	94.80 ± 30.50	76.5 ± 9.191

Strains at break vary within the formulations and thereby, high standard deviations were achieved for the specimens with 50 wt% and 65 wt% bi-SOE (Table 10). The specimens achieve higher strain at break than their aliphatic analogues. The incorporation of the aromatic monomer leads to slightly harder materials, and the formulation with 65 wt% bi-SOE and 35 wt% SOE-PGE withstands an impressive mechanical stress of approximately 10 MPa (Figure 52). The toughness of the specimens increases with bi-SOE content and reaches a high value for the specimen of 65 wt% bi-SOE, suggesting ductile behavior (Figure 52).

Summarizing the results from the specimens containing the aliphatic and aromatic monofunctional monomer in combination with varying amounts of aromatic bi-SOE, a

postive influence of the aromatic monomer structure on the thermomechanical properties can be seen. Higher T_g values, tensile strength, and toughness could be obtained. However, the glass transition temperatures at room temperature or below are not efficient for tough thermoset behavior of the materials. Therefore, further optimization of the material properties was conducted with the most promising, purely aromatic SOE monomer system.

3 Photopolymerization of Spiro-Orthoester with Epoxide CE

Additive manufacturing (AM) processes require fast printing of the sequential, form-stable layers to guarantee rapid prototype production. Since the pure spiro-orthoester systems always required a post-curing process to yield form-stable materials, the reactivity of the system had to be increased. Additionally, the spiro-orthoester systems led both to rather low T_gs of 23° C. To tackle this drawback and ensure the suitability for 3D- printing, the bifunctional SOE was exchanged against a more reactive bifunctional epoxide as crosslinker in combination with the aromatic monofunctional monomer (Figure 53). To compare the results with the epoxy-free materials, same crosslinker concentrations were chosen (25, 50 and 65 wt% CE).
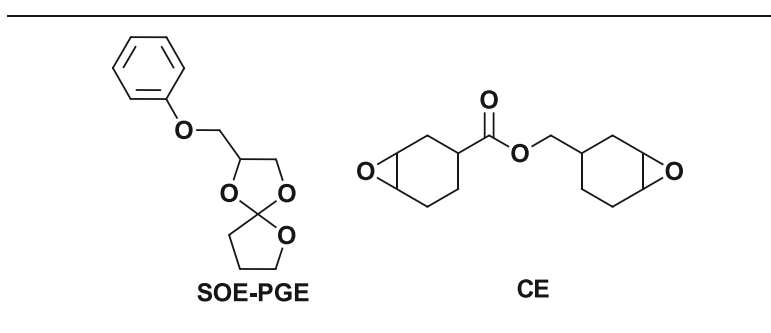
Figure 53: Investigated polymerization mixture containing the bifunctional epoxide as crosslinker and SOE- PGE in varying concentrations

By photopolymerization of the spiro-orthoester and the bifunctional epoxide, a poly(ether ester) is obtained (Figure 54). Herein, epoxides are an optimal choice, since poly(ether ester) structures are also obtained during the polymerization of pure spiro- orthoester systems.
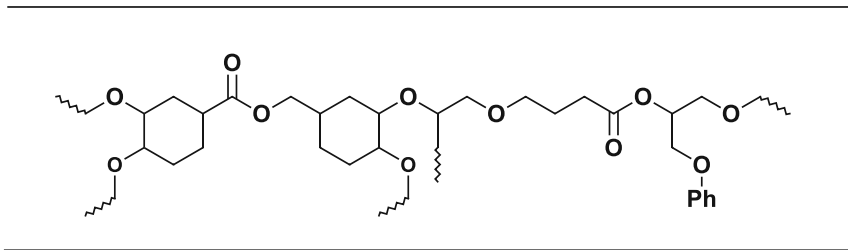
Figure 54: Polymer structure obtained from photopolymerization of SOE-PGE and CE

3.1 Reactivity Analysis via Photo-DSC

The reactivity towards photopolymerization of the new, epoxide containing system was tested with photo-DSC. The readily polymerizable epoxide increased the reactivity of the system whereby exothermic behavior was observed. Hereby, a clear trend between the epoxide content and the reactivity of the system is recognizable (Figure 55). The formulation with 25 wt% epoxide exhibits higher t_{max} and t_{95} values, and additionally a lower polymerization enthalpy was observed than with other formulations. The formulation with 65 wt% epoxide as crosslinker stands out with the best results.
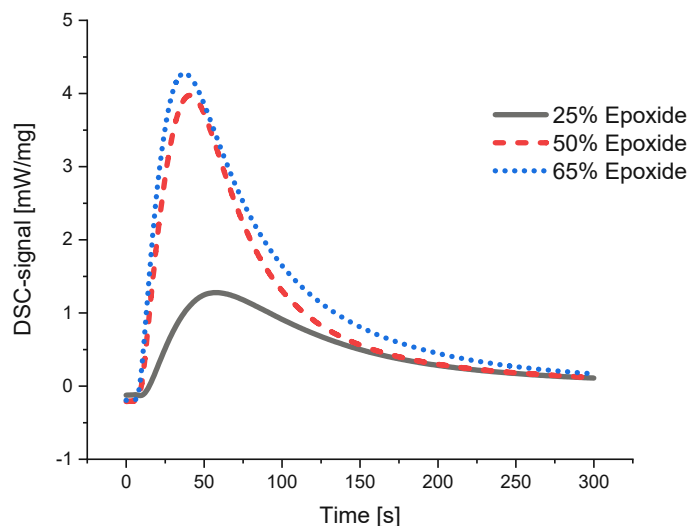
Figure 55: Photo-DSC plot of the formulation containing aromatic monofunctional SOE-PGE and bifunctional epoxide CE in varying concentrations with 1 wt% IC 290 as photoinitiator: 25 wt% epoxide (black solid line); 50 wt% epoxide (red dashed line); 65 wt% bi-SOE (blue dotted line)

65

The conversion of the epoxide monomer is related to the heat of polymerization obtained by the photo-DSC measurement (Equation II). It can be calculated with the theoretical heat of polymerization of epoxy groups, which is 80.6 kJ mol^{-1} per reactive group (determined with BADGE).[6] The calculation of the epoxide-conversion is possible since the exothermic heat of the spiro-orthoester tends to zero.

$$C = \frac{\Delta H * M}{\frac{m_i}{m_{tot}} * \Delta H_0} \quad (II)$$

C	Conversion after photo-DSC according to NMR [%]
ΔH	Experimental polymerization heat [J g^{-1}]
M	Molecular weight of the monomer [J mol^{-1}]
$\frac{m_i}{m_{tot}}$	Ratio of the monomer mass to total mass [-]
ΔH_0	Theoretical heat of polymerization of monomer [J mol^{-1}]

The conversion of the bifunctional epoxide was determined to be approximately 80% (Table 11).

Table 11: Results obtained from the photo-DSC measurement for the system containing the epoxide CE and SOE-PGE as monomers in varying amounts and 1 wt% IC 290 as photoinitiator: weight percent of the compounds [wt%]; time at maximum heat development t_{max}; peak maximum (height); time at 95% of heat development t_{95}: polymerization enthalphy (area); conversion C

CE [wt%]	$t_{max.}$ [s]	Height [mW mg^{-1}]	t_{95} [s]	Area [J g^{-1}]	C [%]
25	50 ± 12	1.508 ± 0.449	200 ± 12	140.7 ± 21.0	81
50	42 ± 1	3.826 ± 0.033	180 ±0	283.2 ± 4.1	88
65	38 ± 1	4.104 ± 0.021	187 ± 2	337.4 ± 4.6	82

3.2 (Thermo-)mechanical tests

3.2.1 DMTA-Analysis

To investigate the influence of the epoxy crosslinker on material properties, specimens with 25, 50, and 65 wt% of the rigid CE were prepared and tested thermomechanically. The selected CE concentrations allowed a direct comparison with the pure SOE-

specimens. Through the use of the bifunctional epoxide, stiffer and harder materials were obtained. One exception is the formulation consisting of 25 wt% epoxide and 65 wt% SOE-PGE. Due to the high content of the monofunctional monomer and the low crosslinking density, a soft material was obtained. Therefore, the DMTA-measurement of this specimen could not be accomplished. The analysis was executed several times but the material failed repeatedly before the T_g. Nonetheless, DMTA analysis was successfully performed with the obtained materials from the residual formulations containing 50 and 65 wt% epoxide CE (Figure 56).
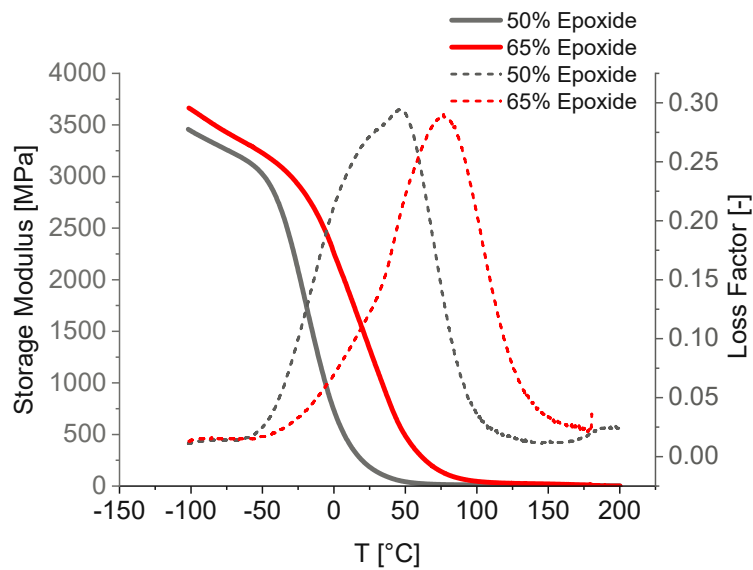
Figure 56: Storage moduli (G', solid line) and loss factors (tan δ, dotted line) of the specimens containing SOE-PGE and the bifunctional epoxide CE in varying amounts and 1 wt% IC 290 as photoinitiator: 50 wt% epoxide (black lines); 65 wt% epoxide (red lines)

Table 12: Results obtained from the DMTA-analysis of specimens containing CE and SOE-PGE as monomers in varying amounts and IC 290 as photoinitiator: weight percent of the compounds [wt%], glass transition temperature Tg, storage modulus at 20° C G'20, storage modulus at glass-transition temperature G'Tg

CE [wt%]	SOE-PGE [wt%]	PI [wt%]	T_g [°C]	G'_{20} [MPa]	G'_{Tg} [MPa]
50	50	1	48	242.13	50.39
65	35	1	77	1500.5	128.82

According to the results, thermomechanical properties could successfully be optimized by the use of the bifunctional epoxide CE. The T_g could be increased to 77 °C and a

significant increase in the storage moduli was achieved compared to the pure aromatic spiro-orthoester system (chapter 2.1). The content of the epoxide has a great impact on the mechanical properties, which can be seen in Table 12. At 20 °C, the formulation with 50 wt% epoxide reaches a storage modulus of 242 MPa, whereas the formulation with 65 wt% epoxide reaches 1500 MPa.

3.2.1.1 Tensile Testing

Tensile tests were performed with the prepared specimens to investigate the tensile strength of the mixed epoxide-SOE materials with varying composition. In Figure 57, a clear trend between stress (σ_B) and strain (ε_B) at break and the epoxide content can be observed.
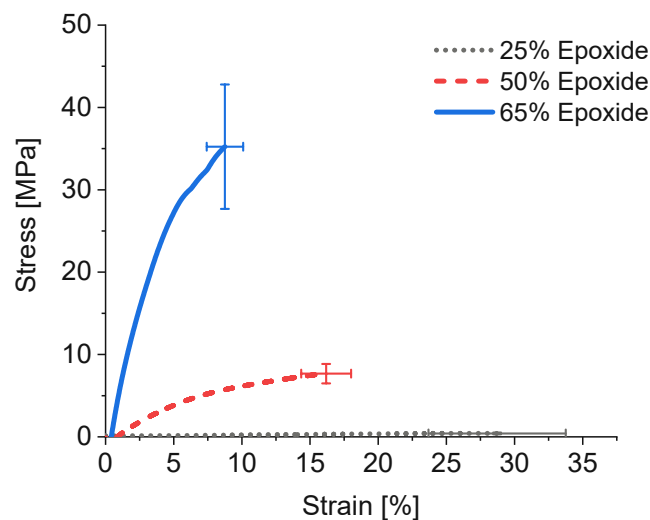
Figure 57: Tensile testing curves and mean stress and strain at break values of the specimens containing SOE-PGE and epoxide CE as momomers in varying amounts and 1 wt% IC 290 as photoinitiator: 25 wt% epoxide CE (black dotted line); 50 wt% epoxide CE (red dashed line); 65 wt% epoxide CE (blue solid line)
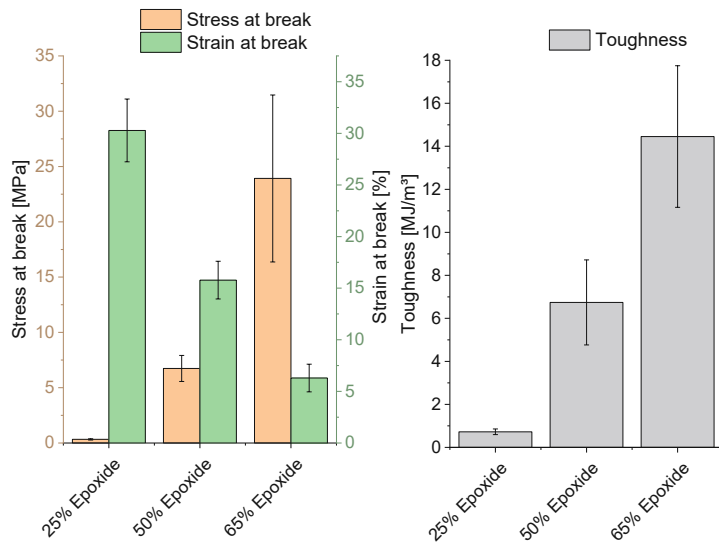
Figure 58: Mean stress and strain at break values; Right: toughness of the materials obtained from the epoxide CE and SOE-PGE in varying compositions and 1 wt% IC 290 as photoinitiator

Table 13: Results obtained from tensile testing for materials polymerized from CE and SOE-PGE in varying concentrations with IC 290 as photoinitiator: weight percent of the compounds [wt%], stress at break σ_B, strain at break ε_B, tensile toughness U_T

CE [wt%]	SOE-PGE [wt%]	PI [wt%]	σ_B [MPa]	ε_B [%]	$U_T[MJ/(m^3)^{-1}]$
25	75	1	0.33 ± 0.06	30.28 ± 3.04	0.726 ± 0.132
50	50	1	6.74 ± 1.18	15.78 ± 1.83	6.742 ± 1.977
65	35	1	23.92 ± 7.55	6.30 ± 1.34	14.454 ± 3.293

The tensile strength could be improved with the bifunctional epoxide: Materials could withstand higher mechanical stress before break set in. The material properties strongly depend on the epoxide content (Table 13). With lower amounts of epoxide, stretchable and soft materials were obtained, resulting in higher strains at break (Figure 58). Additionally, lower amount of stress could be applied to the material. With increasing amounts of the epoxide, stress at break and toughness increase and, as expected, strain at break decreases (Figure 58).

3.3 Laser-Exposure Tests for Hot Lithography

After increasing the reactivity and improving material properties with the bifunctional epoxides, laser-exposure tests were performed as a proof of concept for the suitability of the optimized formulation for Hot Lithography. The tests were conducted with a Hot Lithography prototype setup comprising of a laser (375 nm) and operating temperatures up to 100 °C. The laser-exposure tests should prove the printability of a formulation containing the aromatic spiro-orthoester and the bifunctional epoxide. Since the highest reactivity and the best thermomechanical properties were achieved with the formulation containing 65 wt% epoxide, this was also used for the laser-exposure tests.

In addition to the spiro-orthoester SOE-PGE (35 wt%) and the epoxide CE (65 wt%), the printing formulation contained the photoinitiator IC 290 (1 wt%) and the photosensitizer 9,10-dibutoxyanthracene (DBA, 0.1 wt%, Figure 59). Photosensitizers are common components in printing formulations, they absorb the light and transfer the energy to the photoinitiator IC 290.
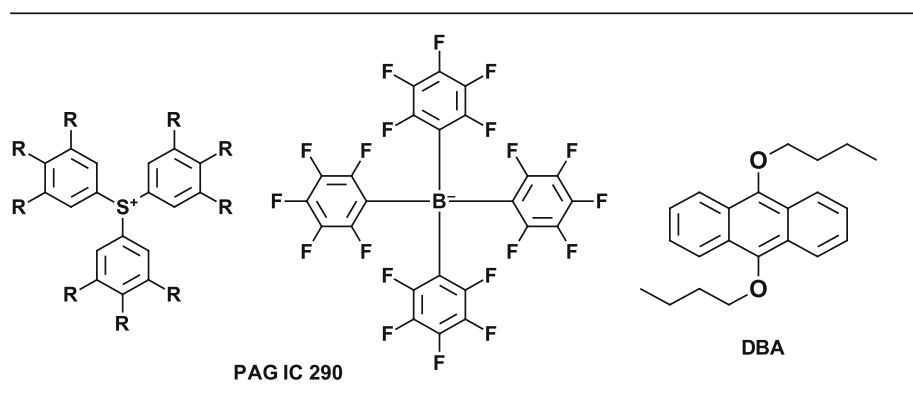
Figure 59: IC 290 used as photoinitiator and 9,10-Dibutoxyanthracene (DBA) used as photosensitizer for laser-exposure tests

After the irradiation of the formulation, the obtained polymerized material was removed from the device and unpolymerized material was removed with acetone. With the first laser-exposure test, diffusional overpolymerization was observed, a rather common phenomenon in cationic photopolymerization. It takes place when the formed superacid migrates from the irradiated area to the adjoining area of the formulation

(Figure 60). The printed part was washed with acetone to remove the soluble, unpolymerized material. A milder solvent, methyl *tert*-butyl ether (MTBE) was chosen for further tests, since acetone damaged the surface of the printed disc.

Figure 60: Printed part immediately after the exposure test with signs of overpolymerization

To reduce diffusional overpolymerization during laser-exposure tests, a base was added to the formulation. The base acts as an inhibitor and prevents polymerization in the unexposed area. To maintain the same reactivity of the system, low concentrations of the base were chosen and their influence on the photopolymerization was investigated. Ethyl 4-(dimethylamino)benzoate (EDAB, Figure 61) was selected as base and two further laser-exposure tests were performed. The content of the base was set to 0.01 and 0.03 wt%.
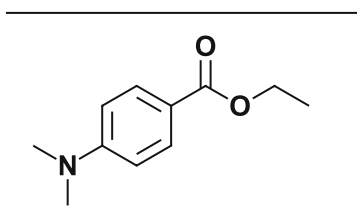
Figure 61: Ethyl 4-(dimethylamino)benzoate EDAB used as base against overpolymerization

Overpolymerization was still observed but could be reduced with the addition of 0.01 wt% EDAB (Figure 62). To remove unpolymerized material, methyl *tert*-butyl ether was used. By that, smoother surface could be observed.

Figure 62: Printed part immediately after the exposure test with overpolymerization.

The last laser-exposure test was performed with the formulation containing 0.03 % of the base EDAB. Unfortunately, the pipetted formulation did not cover the whole irradiation area. Therefore, a circular shape could not be obtained. Nevertheless, the impact of the base on the printing process could be examined. Overpolymerization is clearly decreasing with increasing content of EDAB (Figure 63), compared to the formulation without EDAB (Figure 60). The washing step with methyl *tert*-butyl ether MTBE was performed, as with other printed discs (Figure 63).
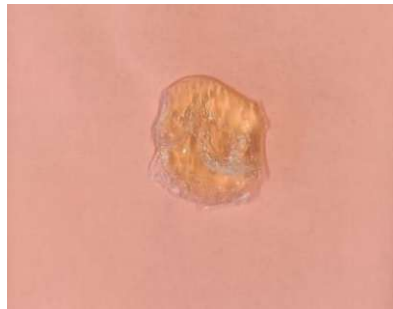
Figure 63: Printed part immediately after the exposure test with decreased overpolymerization.

Experimental Part

1 Evaluation of Spiro-Orthocarbonates and Spiro-Oprthoesters

1.1 Spiro-Orthocarbonates

1.1.1 Synthesis of Spiro-Orthocarbonates

1.1.1.1 Synthesis towards the unsymmetrical SOC

HO‾‾‾OH + (tetraethyl orthocarbonate) →(dry toluene, reflux, 3 h)→ mono-SOC

[76.09]   [192.25]   [176.21]
                                                                 mono-SOC
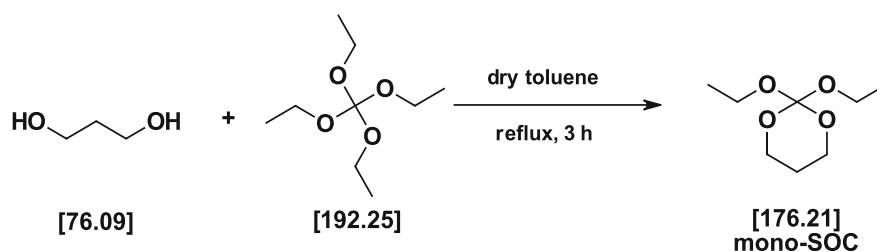
Compound	M [g mol^{-1}]	eq. [-]	n [mmol]	ρ [g mL^{-1}]	m [g]	V [mL]
Tetraethyl orthocarbonate	192.25	1	30	0.919	5.75	-
1,3-propanediol	76.1	1	30	1.05	2.3	-
p-TsOH monohydrate	190.2	0.015	0.45	-	0.086	-
Toluene (dry)						50

The synthesis of 2,2-diethoxy-1,3-dioxane was carried out in analogy to a literature procedure.[47] 1,3-propanediol (2.3 g, 30.0 mmol, 1 eq.) was added to a solution of 5.75 g tetraethyl orthocarbonate in 50 mL dry toluene. A catalytic amount of p-TsOH (0.086 g, 0.45 mmol, 0.015 eq.) was added carefully under inert conditions to the reaction mixture, which was afterwards stirred at room temperature until the solution turned clear. The reaction was refluxed and the formed ethanol was collected as an azeotropic mixture in a dean-stark trap. After three hours, the reaction was quenched with 0.08 mL triethylamine. The solvent was removed by evaporation in *vacuo*, whereby 4.3 g of a yellow crude material could be obtained. 2.56 g (48%) of a colorless

liquid were obtained after distillation in *vacuo* (76 °C, 8 mbar) as the targeted compound.

TLC: R_f = 0.62 (AlOx, PE:EE 4:1)

^{1}H-NMR (400 MHz, CDCl$_3$): δ 4.00 ppm (m, 4H, -O-C$\underline{H_2}$-), 3.67 ppm (m, 4H, O-C$\underline{H_2}$-CH$_2$-), 1.72 ppm (m, 2H, C$\underline{H_2}$-CH$_2$-O-), 1.21 ppm (t, 6H, C$\underline{H_3}$-).

1.1.1.2 Synthesis of 5-SOC

1.1.1.2.1 Synthesis of 3-Butoxy-1,2-propanediol

The ring-opening of the epoxide was carried out following a literature procedure.[48] A suspension of 2-(butoxymethyl)oxirane (6.49 g, 50.0 mmol, 1 eq.) in 300 mL distilled water was stirred over night at 100 °C. The solvent was removed *in vacuo* and the residual material was dissolved in 100 mL ethyl acetate. The solvent was concentrated to yield a yellow liquid as crude material (6.69 g, 90%), which was used as is for the next reaction step.

TLC: R_f = 0.33 (PE:EE 1:3)

^{1}H-NMR (400 MHz, CDCl$_3$): δ 3.86 ppm (d, J = 9.7 Hz, 1H, - C$\underline{H}$-OH), 3.66 ppm (d, J = 19.0 Hz, 2H, C$\underline{H_2}$OH-), 3.55 – 3.41 ppm (m, 4 H, -C$\underline{H_2}$-O-C$\underline{H_2}$-), 1.55 ppm (m, 2H, - C$\underline{H_2}$- CH$_2$-O-), 1.37 ppm (m, 2H, CH$_3$-C$\underline{H_2}$-), 0.91 ppm (t, 3H, C$\underline{H_3}$-).

^{13}C-NMR (100 MHz, CDCl$_3$): δ 72.90 ppm, 71.99 ppm, 71.03 ppm, 64.71 ppm, 32.09 ppm, 19.72 ppm, 14.35 ppm.

liquid were obtained after distillation in *vacuo* (76 °C, 8 mbar) as the targeted compound.

TLC: R_f = 0.62 (AlOx, PE:EE 4:1)

^{1}H-NMR (400 MHz, CDCl$_3$): δ 4.00 ppm (m, 4H, -O-C$\underline{H_2}$-), 3.67 ppm (m, 4H, O-C$\underline{H_2}$-CH$_2$-), 1.72 ppm (m, 2H, C$\underline{H_2}$-CH$_2$-O-), 1.21 ppm (t, 6H, C$\underline{H_3}$-).

1.1.1.2 Synthesis of 5-SOC

1.1.1.2.1 Synthesis of 3-Butoxy-1,2-propanediol

[130.18] → dist. H$_2$O, 100°C → [148.20]

Compound	M [g mol^{-1}]	eq. [-]	n [mmol]	ρ [g/ mL^{-1}]	m [g]	V [mL]
2-(butoxymethyl)oxirane	130.18	1	50.0	0.91	6.509	-
Dist. H$_2$O						300

1.1.1.2.2 Synthesis of 5-SOC

p-TsOH
dry toluene, 90°C

[192.25] + [148.20] → [304.28]
5-SOC
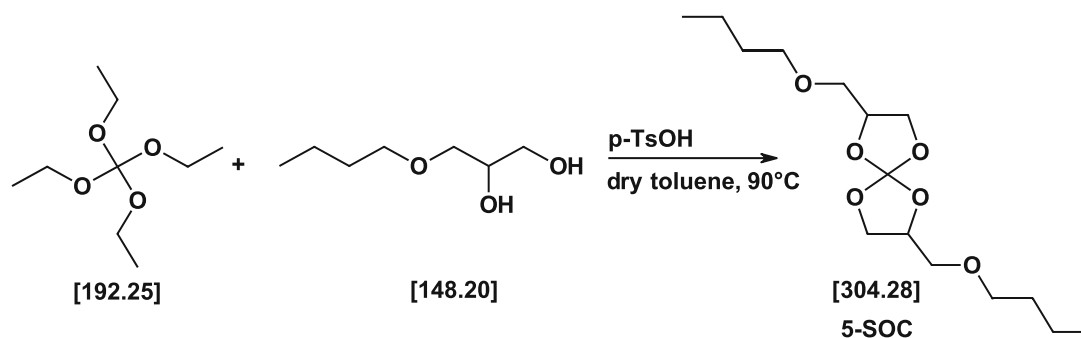
Compound	M [g mol^{-1}]	eq. [-]	n [mmol]	ρ [g mL^{-1}]	m [g]	V [mL]
Tetraethyl orthocarbonate	192.25	1	6.5	0.92	1.25	1.36
3-butoxy-1,2-propanediol	148.20	2	13	-	1.93	-
p-TsOH monohydrate	190.20	0.002	0.013	-	0.0025	-
Toluene (dry)						9.5

The aliphatic SOC, 2-butoxy-7-(butoxymethyl)-1,4,6,9-tetraoxaspiro[4.4]nonane (5- SOC) was synthesized following a literature procedure. [36] A solution of tetraethyl orthocarbonate (1.25 g, 6.5 mmol, 1 eq.) and 3-butoxy-1,2-propanediol (1.93 g, 0.013, 2 eq.) in 9.5 mL dry toluene was prepared under inert atmosphere in a three-necked flask equipped with a small distillation apparatus. After the addition of the catalyst p- toluenesulfonic acid (pTsOH) (2.5 mg, 0.013 mmol, 0.002 equiv.), the reaction temperature was increased to 90 °C and a vacuum of 800 mbar was applied. The generated ethanol was distilled off as an azeotropic mixture over night. The reaction mixture was washed with 15 mL cold saturated NaHCO$_3$ and two times with 15 mL distilled water. The aqueous phase was re-extracted three times with 50 mL dry toluene. Na$_2$SO$_4$ was used to dry the combined organic phases, which were afterwards concentrated *in vacuo*. Column chromatography on neutral aluminum-oxide was carried out to purify the obtained crude material (mobile phase: (PE:EE 8:1)), yielding 0.451 g (23%) of a colorless liquid as the desired compound.

TLC: R_f = 0.63 (PE:EE 8:1, AlOx)

¹H-NMR (400 MHz, CDCl₃): δ 4.51 – 4.36 ppm (m, 2H,-O-CH₂-C**H**-), 4.23 – 4.13 ppm (m, 2H, C-O-C**H₂**), 3.95 – 3.86 ppm (m, 2H, C-O-C**H₂**), 3.65 –3.42 ppm (m, 8H, - C**H₂**- O-C**H₂**), 1.60 – 1.49 ppm (m, 4H, CH₂-C**H₂**-CH₂) , 1.41 – 1.27 ppm (m, 4H, CH₃- C**H₂**-), 0.91 ppm (td, J = 7.4, 1.0 Hz, 6H; C**H₃**-)

¹³C-NMR (100 MHz, CDCl₃): δ 129.53 ppm, 75.47 ppm, 72.09 ppm, 67.77 ppm, 32.08 ppm, 19.69 ppm, 14.37 ppm.

1.1.1.3 Synthesis of 6-SOC
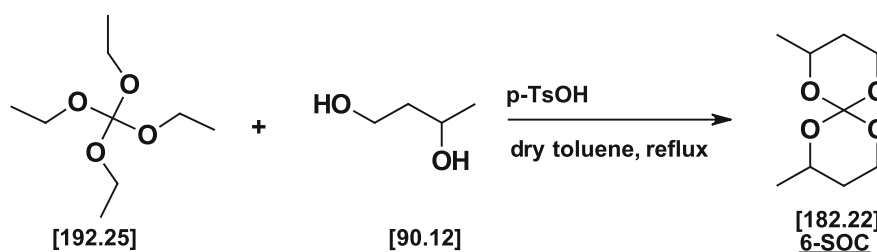
Compound	M [g mol⁻¹]	eq. [-]	n [mmol]	ρ [g mL⁻¹]	m [g]	V [mL]
Tetraethyl-orthocarbonate	192.25	1	15	0.919	2.86	-
1,3-butanediol	90.12	2	30	1.01	2.70	-
p-TsOH monohydrat	190.20	0.015	0.022	-	0.04	-
Toluene (dry)						48

The desired compound, 2,8-dimethyl-1,5,7,11-tetraoxaspiro[5.5]undecane (6-SOC) was synthesized in analogy to a literature procedure.[36] To a solution of 1,3-butanediol (2.70 g, 30 mmol, 2 eq.) in 48 mL dry toluene a catalytic amount of p-TsOH monohydrate (0.0426 g, 0.022 mmol, 0.015 eq.) was added under argon atmosphere. Subsequently, tetraethyl orthocarbonate (2.86 g, 15 mmol, 1 eq.) was added dropwise to the reaction mixture, which was stirred at room temperature until the solution became clear. The solution was refluxed over night while the formed ethanol was collected as an azeotropic mixture in a dean-stark trap. The reaction mixture was

quenched with 2.5 mL triethylamine and washed with 25 mL saturated NaHCO₃-solution and twice with 25 mL distilled water. The organic phase was concentrated in *vacuo* whereby 1.68 g of a yellow crude material were obtained. Flash column chromatography on neutral alumina was carried out to yield 1.2 g (44%) of a colorless liquid as the desired compound (mobile phase: (PE:EE 8:1)).

TLC: R_f =0.64 (PE:EE 7:1, AlOx)

¹H-NMR (400 MHz, CDCl₃): δ 4.49 – 4.18 ppm (m, 2H,CH₃-C**H**-O-), 4.12 – 3.82 ppm (m, 4H, C-O-C**H₂**-), 1.79 – 1.63 ppm (m, 2H, CH-C**H₂**-CH₂), 1.55 – 1.39 ppm (m, 2H, CH-C**H₂**-CH₂), 1.27 – 1.14 ppm (m, 6H, C**H₃**-).

¹³C-NMR (100 MHz, CDCl₃): δ 115.21 ppm, 69.36 ppm, 62.02 ppm, 31.88 ppm, 21.87 ppm.

1.1.1.4 Synthesis of 7-SOC

1.1.1.4.1 Synthesis of 1,4-Octanediol
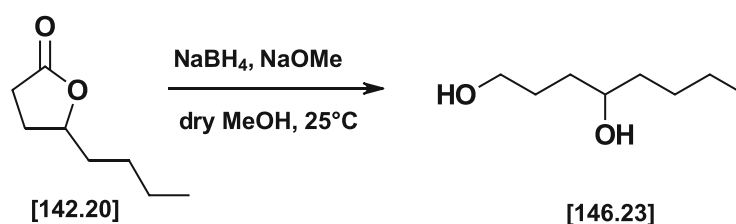
Compound	M [g mol⁻¹]	eq. [-]	n [mmol]	m [g]	V [mL]
γ-Octanolactone	142.2	1	35	4.98	-
Sodium borohydride	37.83	2	70	2.65	-
Sodium methoxide	54.02	0.05	1.75	0.09	-
Methanol, dry					35

The reduction to the desired diol was carried out according to a literature procedure.[49] γ-Octanolactone (4.98 g, 35 mmol, 1 eq.) was dissolved in 35 mL dry methanol under inert atmosphere in a three-necked round bottom flask. Following that, 0.31 mL of a 30% sodium methoxide (NaOMe 0.09 g, 1.75 mmol, 0.05 eq.) solution in methanol

were added to the solution. 2.65 g (70 mmol, 2 eq.) of $NaBH_4$ were added in portions under inert atmosphere at last. The reaction mixture was stirred at room temperature for four hours, while the formed hydrogen was led off into the fume hood through a tube. The reaction was quenched by the addition of excess methanol, which was afterwards removed *in vacuo*. The residue was dissolved in 150 mL dichloromethane and the organic phase was extracted with dist. H_2O and brine (100 mL) four times to remove the formed salt. The aqueous phase was re-extracted with 150 mL dichloromethane three times, the combined organic phase was dried over Na_2SO_4 and filtrated. The solvent was evaporated, yielding 4.57 g of a colorless liquid as crude material. The diol was used for the next reaction step without further purification.

TLC: R_f=0.23 (Silica, PE:EE 1:2)

^{1}H-NMR (400 MHz, D_2O): δ 3.59 ppm (tt, J = 7.3, 4.6 Hz, 1H, -C$\underline{H}$-OH), 3.53 ppm (t, J = 6.4 Hz, 2H, OH-C$\underline{H_2}$-), 1.63 – 1.14 ppm (m, 10H, -C$\underline{H_2}$-), 0.89 – 0.73 ppm (t, 3H, C$\underline{H_3}$-).

^{13}C-NMR (100 MHz, $CDCl_3$): δ 71.80 ppm, 62.98 ppm, 37.20 ppm, 34.21 ppm, 29.01 ppm, 27.77 ppm, 22.59 ppm, 13.93 ppm.

1.1.1.4.2 Synthesis of 7-SOC

p-TsOH

dry toluene, reflux

[192.25]   [146.23]   [300.43]
                                              7-SOC

78
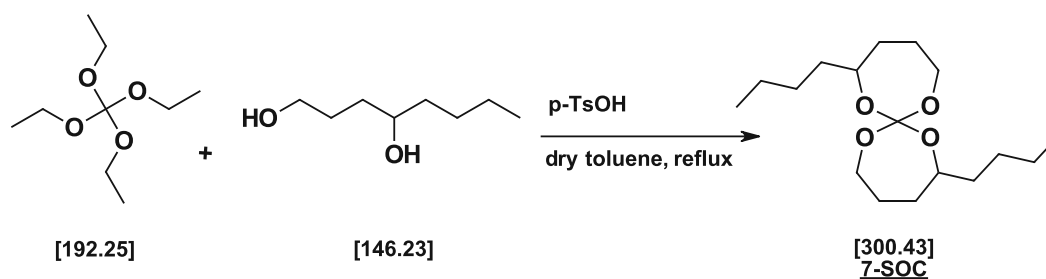
Compund	M [g mol^{-1}]	eq. [-]	n [mmol]	ρ [g mL^{-1}]	m [g]	V [mL]
Tetraethyl orthocarbonate	192.25	1	15	0.919	2.89	-
1,4-octanediol	146.23	2	30	-	4.36	-
p-TsOH monohydrate	190.20	0.015	0.022	-	0.045	-
Toluene (dry)						48

The desired compound, 2,9-dibutyl-1,6,8,13-tetraoxaspiro[6.6]tridecane (7-SOC) was synthesized in analogy to a literature procedure.[36] To a solution of 4.36 g (30 mmol, 2 eq.) 1,4-octanediol in 48 mL dry toluene, p-TsOH (0.045 g, 0.022 mmol, 1 eq.) was added under argon atmosphere. The addition of 2.89 g (15 mmol, 1 eq.) tetraethyl orthocarbonate followed and the reaction mixture was refluxed for seven hours. During the reaction, the formed ethanol was distilled off as an azeotropic mixture. At last, 0.3 mL triethylamine were added to quench the reaction. The reaction mixture was washed with 25 mL saturated $NaHCO_3$-solution and twice with 25 mL dist. H_2O. The organic phase was dried over $MgSO_4$, filtrated and the solvent was removed *in vacuo*. 2.38 g of a yellow liquid were obtained as crude material. In the first attempt of the crude purification, flash column chromatography on neutral alumina was carried out using 500 mg of the crude material and 5% Et_2O in PE as mobile phase. Unfortunately, the product was obtained as a mixed fraction. 2D-TLC confirmed the stability of the reaction products on silica gel, so the residual crude material was purified by flash column chromatography on silica gel using 5% EE in PE as mobile phase. Hereby, 0.53 g (11%) of a colorless liquid were obtained as desired product.

TLC: R_f =0.66 (PE:EE 9:1, silica)

^{1}H-NMR (400 MHz, CDCl$_3$): δ 3.80-3.60 ppm (m, 6H, C-O-C$\underline{H}_2$- , C-O-C$\underline{H}$-), 1.82-1.20 ppm (m, 20H, -C$\underline{H}_2$-), 0.88 ppm (t, 6H, C$\underline{H}_3$-)

^{13}C-NMR (100 MHz, CDCl$_3$): δ 122.05 ppm, 73.62 ppm, 63.57 ppm, 35.99 ppm, 34.17 ppm, 28.45 ppm, 27.99 ppm, 22.32 ppm, 13.88 ppm.

HR-MS: (ACN, ESI+, m/z) calcd.: 301.4404 [M+H]$^+$; found: 301.4404 [M+H]$^+$

1.1.2 Photoreactivity by Photo-DSC

Photoreactivity measurements were conducted on a Netzsch photo-DSC 204 F1 device with an autosampler. The preparation of the formulations, as well as the execution of the measurement itself is described in the section 2, chapter Materials and Methods. Tert.-Butyldiphenyliodonium tetrakis(perfluoro-t-butyloxy) aluminate (tBuI-Al) was used as photoinitiator.

1.1.3 Synthesis of Spiro-Orthoesters

1.1.3.1 Synthesis of 5-SOE
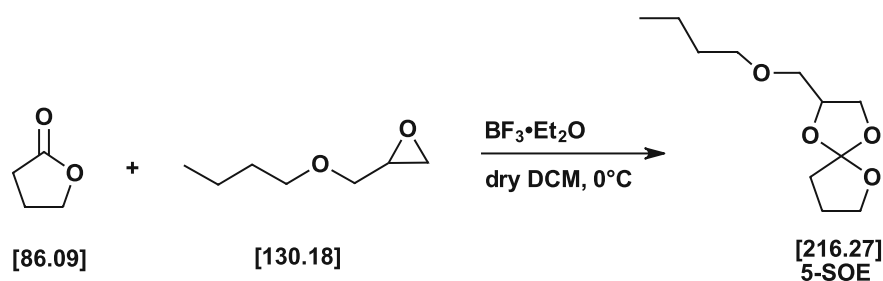
Compound	M [g mol^{-1}]	eq. [-]	n [mmol]	ρ [g mL^{-1}]	m [g]	V [mL]
Butyl-glycidyl ether	130.18	1.2	92.5	0.91	12.04	13.24
γ-butyrolactone	86.09	1	77.1	1.12	6.63	5.93
Boron trifluoride diethyl etherate	141.93	0.033	2.5	1.15	0.36	0.31
Triethylamine	101.19	0.036	2.7	0.726	0.28	0.39
DCM, dry						31

The synthesis of 2-(butoxymethyl)-1,4,6-trioxaspiro[4.4]nonane, (5-SOE) was carried out according to a literature procedure by Nishida *et al.*[53] A three-necked flask equipped with a dropping funnel was purged with argon. γ- Butyrolactone (6.63 g, 77.1 mol, 1 eq.) was dissolved in 19.5 mL dry dichloromethane under argon atmosphere and vigorous stirring at 0° C. 0.3 mL boron trifuoride diethyl etherate BF$_3$•Et$_2$O (2.5 mmol, 0.033 eq.) were added to the reaction mixture carefully. A solution

of 13.25 mL butyl-glycidyl ether BGE (92.5 mmol, 1.3 equiv.) in 11.5 mL dry dichloromethane was added dropwise to the reaction solution over a period of 30 min at 0° C. The reaction mixture was stirred for five hours at room temperature, whereupon the addition of 0.4 mL trimethylamine (2.7 mmol, 0.036 equiv.) followed. The organic phase was washed with 25 mL dist. H_2O three times and dried over sodium sulfate Na_2SO_4. The solvent was removed *in vacuo* and the obtained crude product was distilled fractionally to yield 29% of the desired compound (119-120° C, 10 mbar) as colorless liquid.

TLC: R_f =0.76 (PE:EE 9:1, AlOx)

^{1}H-NMR (400 MHz, CDCl$_3$): δ 4.31 ppm (d, *J* = 53.9 Hz, 1H, C-O-C**H**-), 4.16 – 3.29 ppm (m, 8H, O-C**H$_2$**,), 2.49 – 1.84 ppm (m, 4H, -C-C**H$_2$**-C**H$_2$**-), 1.51 ppm (m, 2H, C**H$_2$**-C**H$_2$**-CH$_2$O-), 1.32 ppm (m, 2H, CH$_3$-C**H$_2$**-), 0.86 ppm(s, 3H, C**H$_3$**-).

^{13}C-NMR (100 MHz, CDCl$_3$): δ 129.81 ppm, 74.65 ppm, 71.84 ppm, 67.53 ppm , 31.92 ppm, 24.57 ppm, 19.52 ppm,14.19 ppm

1.1.3.2 Synthesis of 6-SOE
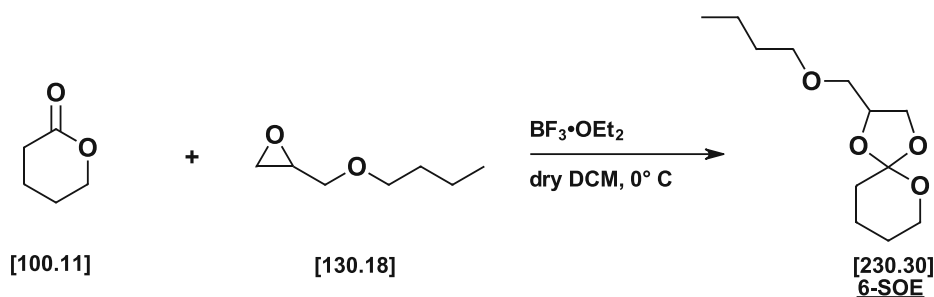
Compound	M [g mol^{-1}]	eq. [-]	n [mmol]	ρ [g mL^{-1}]	m [g]	V [mL]
δ-Valerolactone	100.11	1	17.5	1.079	1.74	-
Butyl-glycidyl ether	130.18	1.5	26.2	0.91	3.43	-
Boron trifluoride diethyl etherate	141.93	0.033	0.57	1.15	0.08	0.07
Triethylamine	101.19	0.036	0.63	0.726	0.06	0.07
DCM, dry						7.6

The six-membered spiro-orthoester, 2-(butoxymethyl)-1,4,6-trioxaspiro[4.5]decane (6-SOE), was synthesized in analogy to a typical procedure.[53] The starting material δ- valerolactone (1.74 g, 17.5 mmol, 1 eq.) was dissolved in 4.4 mL dry dichloromethane under inert atmosphere at 0 °C and 0.07 mL of the catalyst $BF_3 \cdot Et_2O$ (0.57 mmol, 0.033 eq.) were added thereto. A solution of butyl-glycidyl ether (3.43 g, 26.2 mmol, 1.5 eq.) in 3.2 mL dry dichloromethane was added dropwise to the reaction mixture, while inert conditions were ensured. After the addition was completed, the mixture was stirred for one hour at 0 °C and stirring continued over night at room temperature. The reaction was quenched with the addition of 0.07 mL of triethylamine whereupon it was poured onto 11 mL of 10% aqueous sodium-hydroxide solution (NaOH) and stirred for a while. The organic layer was washed with three portions of 15 mL dist. H_2O and dried over Na_2SO_4. After the evaporation of the solvent, the obtained crude material was distilled fractionally to yield the desired compound. The product was further purified by flash column chromatography on alumina oxide using PE:EE 8:1 as mobile phase, whereby 0.96 g (24%) of the product were obtained.

TLC: R_f =0.87 (PE:EE 8:1, AlOx)

^{1}H-NMR (400 MHz, CDCl$_3$): δ 4.56 – 4.23 ppm (m, 1H, C-O-C<u>H</u>), 4.20 –3.79 ppm (m, 4H, C-O-C<u>H$_2$</u>-), 3.71 – 3.29 ppm (m, 4H, -C<u>H$_2$</u>-O-C<u>H$_2$</u>-), 1.88 – 1.69 ppm (m, 4H, O- C- C<u>H$_2$</u>,C<u>H$_2$</u>-CH$_2$-O-), 1.54 ppm (m J = 7.2, 1.5 Hz, 4H, C-O-CH$_2$-C<u>H$_2$</u>-C<u>H$_2$</u>-), 1.44 – 1.28 ppm (m, 2H, CH$_3$-C<u>H$_2$</u>), 0.91 ppm (t, J = 7.4 Hz, 3H, C<u>H$_3$</u>-).

^{13}C-NMR (100 MHz, CDCl$_3$): δ 119.84 ppm, 74.66 ppm, 72.00 ppm, 66.86 ppm , 65.19 ppm, 32.71 ppm, 32.14 ppm, 25.09 ppm, 22.00 ppm, 19.73 ppm, 14.39 ppm.

HR-MS: (ACN, ESI+, m/z)   calcd.: 231.3077 [M+H]$^+$; found: 231.3077 [M+H]$^+$

1.1.3.3 Synthesis of 7-SOE

[114.14]   **[130.18]**   **[244.33]**
7-SOE
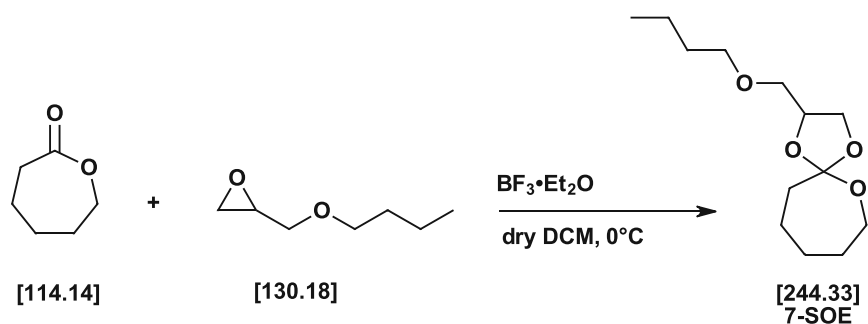
Compound	M [g/mol]	eq. [-]	n [mmol]	ρ [g/ml]	m [g]	V [mL]
ε-Caprolactone	114.14	1	20.0	1.08	2.28	-
Butyl-glycidyl ether	130.18	1.5	30.0	0.91	3.91	-
Boron trifluoride diethyl etherate	141.93	0.033	0.60	1.15	0.09	0.08
Triethylamine	101.19	0.036	0.70	0.73	0.07	0.10
DCM, dry						8.8

2-(butoxymethyl)-1,4,6-trioxaspiro[4.6]undecane (7-SOE) was synthesized in analogy to a literature procedure.[53] The starting material, ε- caprolactone (2.28 g, 20.0 mmol, 1 eq.) was dissolved in 5 mL dry DCM under argon atmosphere at 0° C. Afterwards, 0.08 mL (0.60 mmol, 0.033 eq.) of $BF_3 \cdot Et_2O$ were added to the solution. Finally, a solution of 3.91 g (30.0 mmol, 1.5 eq.) butyl-glycidyl ether in 3.8 mL dry DCM was added dropwise to the reaction mixture under inert conditions. The solution was stirred for one hour at 0° C, thereafter, stirring continued at room temperature overnight. Triethylamine (0.1 mL, 0.70 mmol, 0.036 eq.) was added to the reaction mixture, which was afterwards washed with 15 mL dist. H_2O three times. The aqueous phase was reextracted with 50 mL dry dichloromethane, whereafter the combined organic phase was dried over Na_2SO_4 and filtrated. The solvent was removed *in vacuo* and the crude material was distilled fractionally to separate the product from the lactone, whereby 1.03 g of crude material were obtained. The product was purified using flash column

chromatography on neutral alumina with 10% EE in PE as mobile phase, yielding 0.67 g (14%) of the desired compound.

TLC: Rf=0.85 (PE:EE 9:1, AlOx)

^{1}H-NMR (400 MHz, CDCl$_3$):δ 4.41 – 4.16 ppm (m, 1H, C-O-C**H**-), 4.11 – 3.25 ppm (m,8 H, C**H$_2$**-O), 2.04 ppm (dtd, J = 8.8, 4.2, 2.1 Hz, 2H, O-C-C**H$_2$**-), 1.68 – 1.42 ppm (m, 8H, O-CH$_2$-C**H$_2$**), 1.29 ppm (ddd, J = 9.6, 7.7, 6.1 Hz, 2H, CH$_3$-C**H$_2$**-), 0.84 ppm (t, J = 7.4 Hz, 3H, C**H$_3$**-).

^{13}C-NMR (100 MHz, CDCl$_3$):δ 124.76 ppm, 74.69 ppm, 71.80 ppm, 66.94 ppm, 64.71 ppm, 37.69 ppm, 32.11 ppm, 31.18 ppm, 29.74 ppm, 23.30 ppm,19.71 ppm, 14.38 ppm.

1.1.3.4 Synthesis of SOE- PGE
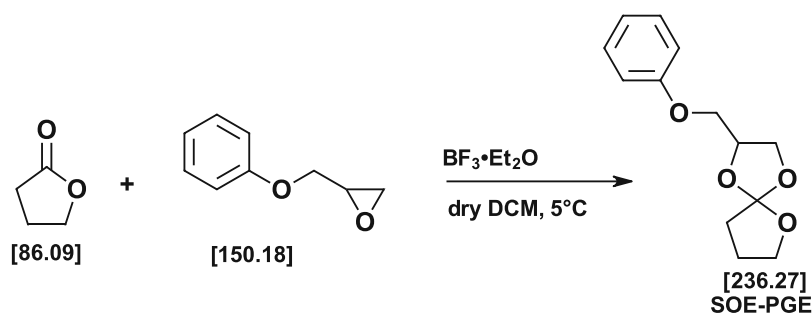
Reactant	M [g mol^{-1}]	eq. [-]	n [mmol]	ρ [g mL^{-1}]	m [g]	V [mL]
Phenylglycidylether	150.18	1	150	0.91	22.52	-
γ-butyrolactone	86.09	1	150	1.12	12.91	-
Boron trifluoride diethyl etherate	141.93	0.016	2.4	1.15	0.34	0.30
Triethylamine	101.19	0.036	5.4	0.726	0.54	0.75
DCM, dry						65

2-(Phenoxymethyl)-1,4,6-trioxaspiro[4.4]nonane (SOE-PGE) was synthesized in analogy to a literature procedure.[53] To a solution of 12.9 g (150 mmol, 1 eq.) γ- butyrolactone and 0.3 mL (2.4 mmol, 0.016 eq.) of boron trifluoride etherate in 50 mL dry dichloromethane, there was added a solution of 22.5 g (150 mmol, 1 eq.) of phenyl

glycidyl ether in 15 mL dry dichloromethane dropwise over a period of 30 min below 10° C under an argon atmosphere. After the addition was completed, the mixture was stirred for 3.5 hours at 5° C. The reaction was quenched with the addition of 0.75 mL triethylamine. The reaction mixture was washed with three portions of 50 mL 10% aqueous NaOH-solution, followed by a washing step with water and brine (150 mL). The combined organic phase was dried over sodium sulfate. After the solvent was removed under reduced pressure, the residue was kept in the freezer overnight. 12.49 g of colorless crystals were obtained as crude material. After recrystallization from methanol, 11.55 g (33%) of pure compound could be obtained.

MP: 72-73°°C (lit: 78-80°C[58])

TLC: R_f=0.23 (PE:EE 9:1, AlOx)

^{1}H-NMR (400 MHz, CDCl$_3$): δ=7.21 ppm (s, 2H, <u>H</u>C=CH-CH, aryl), 6.82 ppm (s, 3H, CH-C<u>H</u>=CH, aryl), 4.47 ppm (s, 1H, -O-C<u>H</u>-), 4.12 -3.90 ppm (m, 6H, -O-C<u>H</u>$_2$-), 2.09 ppm (s, 2H, C-C<u>H</u>$_2$-), 1.95 ppm (s, 2H, -C<u>H</u>$_2$-).

^{13}C-NMR (100 MHz, CDCl$_3$): δ= 158.77 ppm, 129.80 ppm, 121.52 ppm, 114.86 ppm, 74.02 ppm, 69.52 ppm, 68.30 ppm, 66.80 ppm, 33.06 ppm, 24.58 ppm.

1.1.4 Photoreactivity by Photo-DSC

The photoreactivity studies of spiro-orthoesters were carried out in analogy to the studies of spiro-orthocarbonates (section 2,Materials and Methods).

1.2 Synthesis and Reactivity Study of Bifunctional Spiro-Orthoester

1.2.1 Synthesis of bi-SOE

[222.24]   [86.09]   BF$_3$•OEt$_2$, dry DCM, 5°C   [394.41] bi-SOE
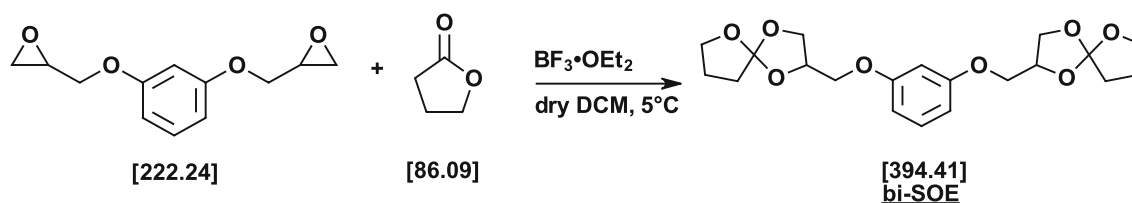
Reactant	M [g mol^{-1}]	eq. [-]	n [mmol]	ρ [g mL^{-1}]	m [g]	V [mL]
Resorcinol diglycidyl ether	222.24	1.0	90.0	-	20.00	-
γ-butyrolactone	86.09	6.5	585.0	-	50.00	-
Boron trifluoride diethyl etherate	141.93	0.087	7.8	1.15	1.11	1.00
Triethylamine	101.19	0.480	43.2	0.73	4.37	6.00
DCM, dry						250

The bifunctional 2-[(m-{(1,4,6-Trioxa-2-spiro[4.4]nonyl)methoxy}phenoxy)methyl]-1,4,6-trioxaspiro[4.4]nonane (bi-SOE) was synthesized following a literature procedure.[57] To a suspension of 20 g (90.0 mmol, 1 eq.) resorcinol diglycidyl ether in 250 mL dry dichloromethane and 30 g (350 mmol) butyrolactone, a solution of 1.0 mL boron trifluoride etherate (7.8 mmol, 0.087 equiv.) in 20 g butyrolactone (585.0 mol in total, 6.5 equiv.) was added dropwise at 5° C. After 90 minutes, 6 mL triethylamine were added to quench the reaction. The solvent was evaporated *in vacuo* and the residue was stored in the freezer overnight. The crystalline product was collected by filtration, then washed with cold methanol and recrystallized from methanol. 8.89 g (25%) of the desired compound were obtained as colorless solid.

MP: 103-105 °C (lit.: 108° C[59])

TLC: R_f=0.39 (PE:EE 4:1, AlOx)

^{1}H-NMR (400 MHz, DMSO-d$_6$): δ 7.30 – 7.11 ppm (m, 1H, O-C-C<u>H</u>=C-O, aryl), 6.66 – 6.40 ppm (m, 3, -C<u>H</u>=C<u>H</u>-, aryl), 4.60 – 4.38 ppm (m, 2H, -C-O-C<u>H</u>-), 4.12 – 3.67 ppm (m, 12H, - O- C<u>H</u>$_2$), 2.15 – 1.83 ppm (m, 8H,-C<u>H</u>$_2$-).

^{13}C-NMR (100 MHz, CDCl$_3$): δ 160.18 ppm, 130.23 ppm, 129.73 ppm, 107.83 ppm, 102.17 ppm, 74.14 ppm, 69.87 ppm, 68.62 ppm, 67.91 ppm, 33.27 ppm, 24.78 ppm.

1.2.2 Photoreactivity by Photo-DSC

Photo-DSC measurements were performed as described in the section 2, Materials and Methods. Since the synthesized monomer was a solid, it was mixed with the photoinitiator tBuI- Al and dissolved in a small amount dichloromethane. After the solution was well homogenized, dichloromethane was evaporated *in vacuo*. Finally, the formulation was placed in the crucibles and the measurements were performed.

2 Bulk-Photopolymerization of Spiro-Orthoesters

2.1 (Thermo-)mechanical Tests

For the (thermo-)mechanical tests, specimens were prepared as described in section 2 of the chapter Materials and Methods.

2.1.1 Materials from a Mix of Aromatic and Aliphatic Spiro-Orthoesters

2.1.1.1 DMTA-Analysis

The DMTA-measurements were performed with the Anton Paar MCR 301 device equipped with a CTC 450 oven. The cured specimens were tested as described in Materials and Methods. The composition of the formulations is listed in Table 14.

Table 14: Formulations for the DMTA-analysis containing bi-SOE and 5-SOE as monomers in varying compositions and IC 290 as photoinitiator

Formulation	bi-SOE		5-SOE		IC 209	
	m [mg]	[wt%]	m [mg]	[wt%]	m [mg]	[wt%]
aliph25	749.47	25	253.40	75	12.32	1
aliph50	523.21	50	502.74	50	16.21	1
aliph65	637.02	65	358.21	35	9.80	1

2.1.1.2 Tensile Testing

Tensile tests were performed with a tensile testing machine as described in the chapter Materials and Methods. The compositions of the formulations are given in Table 15.

Table 15: Formulations for tensile testing containing bi-SOE and 5-SOE as monomers in varying compositions and IC 290 as photoinitiator

Formulation	bi-SOE		5-SOE		IC 209	
	m [mg]	[wt%]	m [mg]	[wt%]	m [mg]	[wt%]
aliph25	2253.41	25	2259.38	75	31.48	1
aliph50	1500.86	50	1514.05	50	29.73	1
aliph65	2276.89	65	1231.92	35	34.95	1

2.1.2 Materials with Exclusively Aromatic Spiro-Orthoester

2.1.2.1 DMTA Analysis

DMTA analysis was performed as described in Materials and Methods, section 2. The test specimens were prepared from formulations listed in Table 16.

Table 16: Formulations for the DMTA-analysis containing bi-SOE and SOE-PGE as monomers in varying compositions and IC 290 as photoinitiator

Formulation	bi-SOE		SOE-PGE		IC 209	
	m [mg]	[wt%]	m [mg]	[wt%]	m [mg]	[wt%]
aro25	254.97	25	753.49	75	12.2	1
aro50	514.42	50	501.39	50	11.07	1
aro65	651.08	65	349.90	35	10.5	1

2.1.2.2 Tensile Testing

Tensile tests were performed as described in Materials and Methods, section 2. The compositions of the formulations are given in Table 17.

Table 17: Formulations for tensile testing containing bi-SOE and SOE-PGE as monomers in varying compositions and IC 290 as photoinitiator

Formulation	bi-SOE		SOE-PGE		IC 209	
	m [mg]	[wt%]	m [mg]	[wt%]	m [mg]	[wt%]
aro25	886.7	25	2623.3	75	36.50	1
aro50	1769.7	50	1749.4	50	39.95	1
aro65	2282.9	65	1227.4	35	37.07	1

3 Bulk-Photopolymerization of Spiro-Orthoester with Epoxide

3.1 Reactivity Analysis by Photo-DSC

The photoreactivity studies were carried out as described in Material and Methods, section 2. Thereby, 1 wt% IC 290 was used as photoinitiator.

3.2 (Thermo-)mechanical Tests

Formulations for the respective specimens were prepared according to the chapter 2, Materials and Methods.

3.2.1 DMTA-Analysis

DMTA analysis of the obtained materials was performed as described in the chapter Material and Methods. The test specimens were prepared from formulations listed in Table 18.

Table 18: Formulations for the DMTA-analysis containing CE and SOE-PGE as monomers in varying compositions and IC 290 as photoinitiator

Formulation	CE		SOE-PGE		IC 209	
	m [mg]	[wt%]	m [mg]	[wt%]	m [mg]	[wt%]
CE25	254.6	25	749.3	75	9.96	1
CE50	505.5	50	503.9	50	9.42	1
CE65	654.8	65	353.6	35	12.5	1

3.2.2 Tensile Testing

Tensile tests were executed as described in section 2 of the chapter Materials and Methods. The composition of the prepared formulations were given in Table 19.

Table 19: Formulations for tensile testing containing CE and SOE-PGE as monomers in varying compositions and IC 290 as photoinitiator

Formulation	CE		SOE-PGE		IC 209	
	m [mg]	[wt%]	m [mg]	[wt%]	m [mg]	[wt%]
CE25	880.7	25	2626.4	75	37.91	1
CE50	1756.3	50	1750.7	50	39	1
CE65	2280	65	1225	35	35.96	1

3.3 Laser-Exposure Tests for Hot Lithography

Laser-exposure tests were performed in a Hot Lithography device as described in the Materials and Methods section.

Formulations with different concentrations of the base ethyl 4-(dimethylamino)benzoate (EDAB) were printed (Table 20). Every formulation contained 65 wt% of the epoxide 3,4-(epoxycyclohexane)methyl-3,4-epoxycyclohexylcarboxylate (CE) and 35 wt% of the spiro- orthoester SOE-PGE. 1 wt% of Irgacure 290 was added as photoinitiator and 0.1 wt% 9,10- Dibutoxyanthracene (DBA) were used as photosentisizer. The thickness of the obtained disc was measured with a caliper.

Table 20: Different formulations for laser-exposure tests

Formulation	IC 290 [wt %]	DBA [wt %]	EDAB [wt %]	Thickness [mm]
A	1	0.1	0	1.46
B	1	0.1	0.01	1.63
C	1	0.1	0.03	1.30

Materials and Methods

1. Materials

Chemicals	Provider
1,2-Epoxy-3-phenoxypropane	Sigma Aldrich
1,3-butanediol	TCI Europe
2-(Butoxymethyl)oxirane	TCI Europe
Boron trifluoride diethyl etherate	TCI Europe
Chloroform-d	Eurisotop
Dichloromethane	Donau Chemie
DMSO-d_6	Eurisotop
Ethyl acetate	Donau Chemie
Irgacure 290	BASF
Methanol	Donau Chemie
Petroleum ether	Donau Chemie
p-toluene sulfonic acid	ABCR
Resorcinol diglycidyl ether DENACOL EX-201	Nagase ChemteX
Sodium borohydride (60% in wax)	TCI Europe
Sodium methanolate (30% solution)	Sigma Aldrich
Sodium sulfate	VWR
tBuIAl	Synthon
Tetraethyl orthocarbonate	ABCR
Triethylamine	Sigma Aldrich
γ-butyrolactone	Sigma Aldrich
γ-Octanolactone	TCI Europe
δ-Valerolactone	ABCR
ε-Caprolactone	TCI Europe

2. Methods

Thin-layer chromatography was conducted on aluminium TLC-plates from Merck Silicagel 60 F_{254}, and Aluminium oxide 60, F_{254}, neutral.

Column chromatography was performed on Carl Roth neutral aluminium oxide 90 (0.063-0.2 mm), and on Carl Roth silica gel (0.040-0.063 mm). Column chromatography was conducted with a Büchi MPLC device, with a control unit C-620, a Büchi UV-Photomerer C-635 and a Büchi fraction collector C-660.

Melting points were determined with an Optimelt devise from SRS Stanford Research Systems.

^{1}H-NMR and ^{13}C-NMR spectra were measured using the BRUKER Avance DRX-400 FT-NMR at and 400 and 100 MHz, respectively. Chemical shifts were obtained in ppm relative to tetramethylsilane (d= 0 ppm) and referenced on the used solvent. The multiplicity was reported as s = singlet, d= doublet, t = triplet, q = quartet and m = multiplet, quintet. Deuterated chloroform $CDCl_3$ or deuterated DMSO d_6-DMSO were used as NMR- solvents. All spectra were analyzed using the software MestreNova 12.0.4 by Mestrelab research. Reactions showing dark polymerization were quenched with pyridine (0.3 wt%) before the measurement.

Photo-DSC measurements were conducted with a DSC 204 F1 Phoenix device with an autosampler from the company Netzsch. The DSC-device was connected with Omnicure 2000 as light source in combination with a double core lightguide (3 mm fiber diatemer). The Omnicure was equipped with a broadband Hg-lamp and spectral range of 320 – 500 nm was set with a filter. Calibration of the Omnicure was performed with an Omnicure R2000 radiometer before every measurement. All measurements were conducted under N_2-flow of 20 mL min^{-1} and analyzed with Proteus-Thermal Analysis (version 5.2.1) from Netzsch.

The formulations for the measurements were prepared in the orange-light room. By that, 1 wt% of the respective photoinitiator (tBuIAl for SOE and SOC, IC 290 for the epoxide-SOE mix) was mixed with the monomer in a brown vial and vortexed vigorously. 10-14 mg of the prepared formulation were weighed into aluminum pans,

closed with a glass lid and inserted into the autosampler of the photo-DSC device. The measurements were carried out under nitrogen atmosphere (20 mL min^{-1}) at various temperatures (25, 70, 90, and 110 °C). The exposure unit, with UV-light (320- 500 nm) was connected to the photo-DSC device and irradiated the samples two times for 300 s. The light intensity was thereby set to 1.3 W cm^{-2}, which resulted in a light intensity of 45.5 mW cm^{-2} at the sample surface. Every measurement was performed three times at the same temperature for each formulation.

Before irradiation, every sample was conditioned during an isothermal phase of four minutes at the respective measurement temperature. Afterwards, the samples were irradiated for 300 s twice at the corresponding temperatures. The device recorded the heat evolution during polymerization over time. After the measurements, the heat flow from the second irradiation phase is subtracted from the heat flow during the first irradiation period to remove any background signals. The polymerization enthalpy ΔH [J g^{-1}] of the respective formulation is then obtained by integration as the peak area. Additionally, the time to maximum heat development t_{max} was obtained as peak maximum and the time until 95% of heat were developed was obtained as t_{95}. The evaluation of the measurements was conducted with Proteus-Thermal Analysis (version 5.2.1) from Netzsch.

Conversion analysis

After photo-DSC analysis, the samples were dissolved in CDCl$_3$ with 0.3 wt% pyridine and NMR-spectra were measured. The monomer conversion was calculated by the intensity decrease of the respecting monomer peaks in the spectra. All NMR-spectra were evaluated with the software MestreNova 12.0.4 by Mestrelab research.

Gel permeation analysis (GPC)

To perform GPC-analysis, the samples were dissolved with THF containing 0.5 mg mL^{-1} butylated hydroxytoluene (BHT) as flow marker. The concentrations of the sample solutions were in the range of 2 mg mL^{-1}. The solutions were filtered into GPC vials via a PTFE syringe filter and analyzed.

Gel permeation analysis **(GPC)** was performed with a Waters GPC, with three columns connected in series (Styragel HR 0.5, Styragel HR 3 and Styragel HR4) and three attached detectors (Waters 2410 RI, UV Detector Module 2550 for TDA 305, VISCOTEK SEC-MALS 9 for light scattering). Molecular weight of the polymers was examined using conventional calibration with polystyrene standards of 375 – 177 000 Da. OmniSEC 5.12 from Malvern was used for data analysis.

Preparation of the test specimens All formulations for test specimens were prepared in the orange light laboratory. Wavelengths below 480 nm were filtered with adhesive window foils. Curing of the specimens was performed in an Uvitron INTELLI- RAY 600 UV-oven with a 320-500 nm Hg broadband lamp (600 W; UV-A: 125 mW cm^{-2}; vis: 125 mW cm^{-2}).

Preparation of materials from a mix of aromatic and aliphatic spiro-orthoesters

Test specimens were prepared by mixing monofunctional monomers with the bifunctional SOE and 1 wt% of the photoinitiator IC 290. The formulations were vortexed well, then heated to 110 °C. After homogenization, the formulations were poured into silicon molds (5 x 2 x 40 mm). The silicon molds were placed on a heating plate (120°C). The molds were then irradiated in an Uvitron UV 1080 Flood Curing System with Uvitron Intelliray 600 halide lamps at 100% intensity (Hg broadband UV lamp, 600 W, 120 mW cm^{-2}, 320-580 nm) for 30 minutes. Afterwards, the molds were cured overnight in a drying oven at 120 °C to complete the polymerization process. The obtained specimens were carefully removed from the molds and polished to obtain a smooth surface.

Preparation of materials from a mix of epoxide CE and SOE-PGE

The formulations were prepared with the bifunctional epoxide CE as crosslinker, SOE-PGE as monomer and IC 290 as photoinitiator. The components were heated to 100 °C, homogenized, and the liquid formulation was poured into silicon molds. After the first irradiation phase of 300 s, the specimen was irradiated from the reversed side again for the same time.

Dynamic Mechanical Thermal Analysis DMTA was performed with an Anton Paar MCR 301 device, equipped with a CTD 450 oven. The data was processed with RheoCompass 1.24 software by Anton Paar. The cured specimens were tested in torsion mode, whereby the torsion strain was set to 0.1% and 1 Hz. During the measurement, the temperature range was scanned from -100° C to 200 °C, and the heating rate was set to 2°C min^{-1}. After execution of the measurement, the diagrams were processed with the Anton Paar Rheo Compass software. The glass transition temperature T_g was determined as the temperature at the maximum loss factor (tanδ). Additionally, storage moduli at T_g and at 20 °C were determined.

Tensile tests were conducted on a Zwick Z050 tensile machine with a maximum test force of 50 kN. The data was processed with TestXpert II software. The tests were conducted with a speed was 5 mm min^{-1} and a maximum force of 5 kN. The prepared specimens were polished and their dimensions were determined with a caliper. Their geometrical shape met the requirements of ISO 527 (2 x 2 x 12 mm parallel slided, overall length of 35 mm). The specimens were fixed in the machine and axial strain was applied. The stress-strain curve was recorded with TestXert II software. The material toughness was obtained by integration of the stress-strain curve in Origin2019, verison 9.6.0.172.

Laser-exposure tests were performed on a heated SLA prototype by TU Wien. The formulations were irradiated with a 375 nm laser and an optical output power of 70 mW. The plate was heated to 100 °C and the irradiated area was a circular disc of 1 x 3 cm². The laser speed was set to 25 mm s^{-1} and the hitching distance was 0.02. The formulations were irradiated twice, once in x- and afterwards in y-writing direction.

Summary

Stereolithography has gained much importance as an additive manufacturing process. Conventionally used monomers need optimization to enable the dificile production of low production number, complex three-dimensional objects from materials with good thermomechanical and surface properties. Additionally, the introduction of Hot Lithography optimizes the stereolithography process itself through high operating temperatures, which broadens the scope of potential monomers. This allows effective polymerization of cationic ring-opening monomers, which show low reactivity at room temperature. The aim of this thesis was to investigate the applicability of expanding monomers, spiro-orthocarbonates and spiro-orthoesters in Hot Lithography. These monomers should meet important requirements for this purpose: High reactivities, efficient polymerizations and good mechanical properties should be ensured. To investigate that, spiro-orthoesters and spiro-orthocarbonates were synthesized *via* appropriate procedures. Since the ring size of bicyclic monomers affects their polymerization and reactivity, monomers with different ring sizes were synthesized (Figure 64).
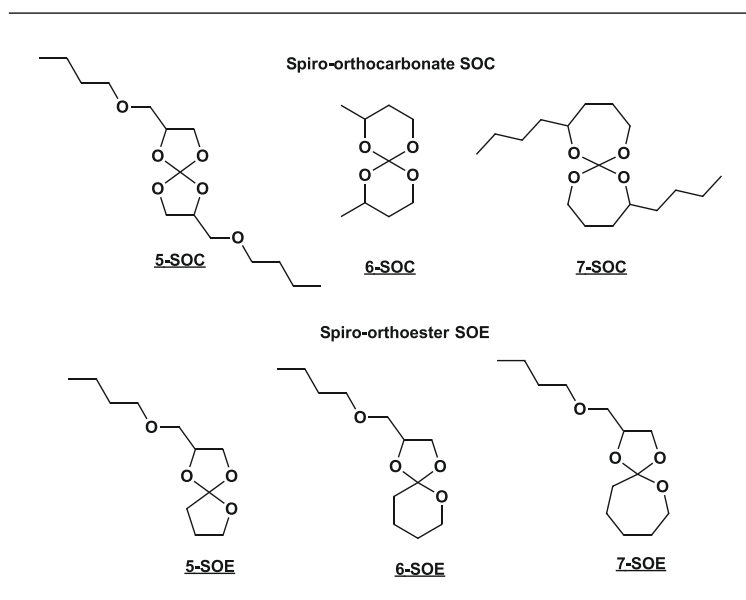
Figure 64: Analyzed spiro-orthocarbonates (SOC) and spiro-orthoesters (SOE)

To test the photoreactivity of these compounds, photo-DSC analysis was performed and gave information about the polymerization enthalpies. Additionally, the time when

96

the maximal amount of heat and 95% of heat were produced, could be determined. NMR-analysis of the polymerized compounds gave information about the monomer conversion and size exclusion chromatography provided the molecular weights. With these findings, good conclusions could already be drawn about the photoreactivity of both monomer classes. However, the polymerization mode of the monomers must be considered as another important factor. It was found that spiro-orthocarbonates were slightly more reactive than spiro-orthoesters, but their polymerization accompanies elimination of by-products. Since this is unfavorable, spiro-orthoesters proved to be the better monomer class due to their efficient double ring-opening polymerization. Among varying ring-sizes of SOEs, the five- and seven- membered spiro-orthoester led to good results, while the six-membered one was unreactive due to its lower ring strain.

To obtain a three-dimensional polymer network, a bifunctional monomer was necessary. Therefore, a bifunctional spiro-orthoester was synthesized in analogy to the most reactive monomer found for the monofunctional monomers. It was then polymerized with an aliphatic and an aromatic monofunctional SOE. As their resulting material properties were of interest, the influence of the monomer structure and ratio of mono- to difunctional monomer on the material properties was examined by integrating two different monofunctional spiro-orthoesters (Figure 65).
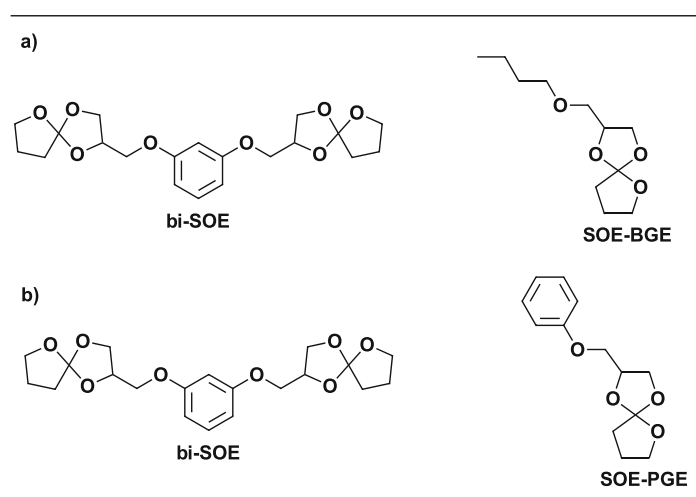
Figure 65: a) Polymerization system comprised of the monofucntional aliphatic 5-SOE and the bifunctional aromatic bi-SOE, b) polymerization system comprised of the monofunctional aromatic SOE-PGE and the bifunctional aromatic bi-SOE

To examine (thermo-)mechanical properties of the obtained materials, DMTA analysis and tensile test were performed. Relevant parameters such as the glass transition temperature T_g and the storage modulus G' could be determined. Additionally, strain at break, stress at break, and material toughness were obtained from tensile tests. These investigations established that materials comprised of the aromatic monofunctional SOE and the bifunctional SOE show better material properties. They are stiffer, have higher T_g values, higher toughness, and withstand higher stress before break. Nevertheless, the material properties still needed to be optimized since rather low T_gs (in the range of room temperature) were obtained. In addition, form-stable materials could not be obtained after the polymerization in the UV-oven. Viscous, liquid materials were obtained and needed a post-curing step at 120 °C overnight to solidify.

Epoxides, on the other hand, exhibit high reactivities towards cationic polymerizations and are used for 3D printing. Therefore, the polymerization of a bifunctional epoxide (CE) and the aromatic monofunctional monomer was investigated together with the material properties. To study the influence of the epoxide content, three formulations with 25 wt%, 50 wt%, and 65 wt% epoxide were analyzed.
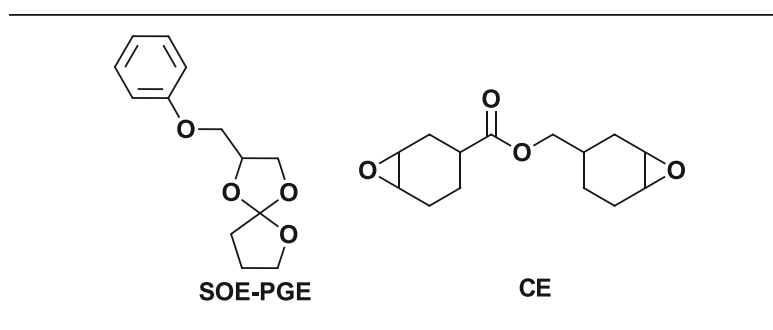
Figure 66: Polymerization system comprised of aromatic SOE-PGE and the bifunctional epoxide CE in varying concentrations

The photoreactivity could be indeed enhanced and material properties could be optimized. The formulation consisting of 65 wt% epoxide resulted in an increased T_g of 77 °C. Furthermore, solid and form-stable materials could be obtained subsequently after the polymerization of all formulations. By that, a post-cure step was not necessary.

Since the drawbacks of the pure spiro-orthoester systems could be tackled with the implementation of the epoxide as crosslinker, laser-exposure tests were performed for a proof of concept. Therefore, a printable formulation consisting of 35 wt% SOE-PGE, 65 wt% epoxide, 1 wt% of photoinitiator IC 290 and 0.1 wt% photosensitizer 9,10- dibutoxyanthracene (DBA) was exposed to a 375 nm laser at 100 °C in a Hot Lithography device. Arising from the nature of the cationic photoinitiator, overpolymerization was obtained in the first attempt. Cationic photoinitiators produce a super-acid upon irradiation, which migrates to the adjoining unexposed area and initiates the polymerization. To reduce overpolymerization, ethyl 4-(dimethylamino)benzoate (EDAB) was added as base in concentrations of 0.01 and 0.03 wt% in further attempts. With that, overpolymerization could be reduced successfully.

In summary, six monomers belonging to two different monomer classes were synthesized and investigated successfully. The impact of their ring size on the polymerization was examined in detail. Spiro-orthoesters were found to be printable and processable with Hot Lithography together with epoxides. Material properties as well as the reactivity of the system were improved. Thus, the first important conclusions for the application of these monomers in bulk-polymerization applications in general and Hot Lithography specifically were drawn. In the future, overpolymerization should be investigated further to obtain materials with good form precision. For this, the ideal content of the base in the formulation must be found.

Abbreviations

Abbreviation

2D-TLC	two dimensional thin-layer chromatography
3D	three dimensional
Al(acac)	aluminium acetylacetonate
AlOx	aluminium oxide
AM	Additive manufacturing
APT	attached proton test
AROP	anionic ring-opening polymerization
BADGE	bisphenol A diglycidyl ether
$BF_3 \bullet Et_2O$	boron trifluoride diethyl etherate
BGE	butyl glycidyl ether
BHT	butylated hydroxytoluene
CAD	computer-aided design
$CDCl_3$	deuterated chloroform
CDVE	1,4-cyclohexane dimethanol divinyl ether
CE	3,4-(epoxycyclohexane)methyl-3,4-epoxycyclohexylcarboxylate
CROP	cationic ring-opening polymerization
CS_2	carbon disulfide
DBA	9,10-Dibutoxyanthracene
DCM	dichloromethane
DDPI	Bis(4-dodecylphenyl)iodonium hexaflurorantimonate
DLP	Digital light processing
DMTA	Dynamic mechanical thermal analysis
DRO	double ring-opening
DSC	differential scanning calorimetry
DW	Direct-Writing
EDAB	Ethyl 4-(dimethylamino)benzoate
EE	ethyl acetate
Et_2O	Diethyl ether

FDM	Fused-deposition modeling
GPC	gel permeation chromatography
IC 290	Irgacure 290
MTBE	methyl tert-butyl ether
Na_2SO_4	sodium sulfate
$NaBH_3OMe$	monomethoxyborohydride
$NaBH_4$	sodium borohydride
$NaHCO_3$	sodium bicarbonate
NaOH	sodium hydroxide
NaOMe	sodium methoxide
NEt_3	triethylamine
PAG	Photoacid generator
PE	Petroleum ether
PGE	phenyl glycidyl ether
p-TsOH	p-toluenesulfonic acid
ROMP	ring-opening metathesis polymerization
ROP	ring-opening polymerization
RROP	radical ring-opening polymerization
SLA	Stereolithography
SLS	Selective laser sintering
SnCL4	tin(IV) chloride
SOC	spiro-orthocarbonate
SOE	spiro-orthoester
SRO	single ring-opening
tBuI-Al	tert.-Butyldiphenyliodonium tetrakis(perfluoro-t-butyloxy) aluminate
TEOC	tetraethyl orthocarbonate
T_g	glass transition temperature
THF	tetrahydrofuran
UV	ultra violet
UV-NIL	ultraviolet nanoimprint lithography

Literature

1.   Black, H. T.; Celina, M. C.; McElhanon, J. R. *Additive Manufacturing of Polymers: Materials Opportunities and Emerging Applications*; SAND2016-6644; Other: 644968 United States 10.2172/1561754 Other: 644968 SNL English; ; Sandia National Lab. (SNL-NM), Albuquerque, NM (United States): 2016; p Medium: ED; Size: 40 p.

2.   Huang, J.; Qin, Q.; Wang, J., A Review of Stereolithography: Processes and Systems. **2020,** *8* (9), 1138.

3.   Schmidleithner C, K. D., Stereolithography. In *3D Printing*, D, C., Ed. 2018; pp 1-22.

4.   Pfaffinger, M., Hot Lithography – New Possibilities in Polymer 3D Printing. **2018,** *15* (4), 45-47.

5.   Steyrer, B.; Busetti, B.; Harakály, G.; Liska, R.; Stampfl, J., Hot Lithography vs. room temperature DLP 3D-printing of a dimethacrylate. *Additive Manufacturing* **2018,** *21*, 209-214.

6.   Klikovits, N.; Knaack, P.; Bomze, D.; Krossing, I.; Liska, R., Novel photoacid generators for cationic photopolymerization. *Polymer Chemistry* **2017,** *8* (30), 4414-4421.

7.   Kaur, M.; Srivastava, A. K., PHOTOPOLYMERIZATION: A REVIEW. *Journal of Macromolecular Science, Part C* **2002,** *42* (4), 481-512.

8.   Sangermano, M.; Razza, N.; Crivello, J. V., Cationic UV-Curing: Technology and Applications. **2014,** *299* (7), 775-793.

9.   Fouassier, J.-P., *Photoinitiation, Photopolymerization, and Photocuring: Fundamentals and Applications.* Hanser: 1995.

10.   Crivello, J. V., 4.37 - Photopolymerization. In *Polymer Science: A Comprehensive Reference*, Matyjaszewski, K.; Möller, M., Eds. Elsevier: Amsterdam, 2012; pp 919-955.

11.   Fouassier, J. P.; Lalevée, J., Backgrounds in Photopolymerization Reactions: A Short Overview. 2021; pp 1-34.

12.   Zhang, J.; Xiao, P., 3D printing of photopolymers. *Polymer Chemistry* **2018,** *9* (13), 1530-1540.

13.   Bagheri, A.; Jin, J., Photopolymerization in 3D Printing. *ACS Applied Polymer Materials* **2019,** *1* (4), 593-611.

14.   Schricker, S. R., 9 - Composite resin polymerization and relevant parameters. In *Orthodontic Applications of Biomaterials*, Eliades, T.; Brantley, W. A., Eds. Woodhead Publishing: 2017; pp 153-170.

15.   RK Sadhir, M. L., *Expanding monomers: Synthesis, characterization, and applications*. 1992.

16.   Ligon, S. C.; Liska, R.; Stampfl, J.; Gurr, M.; Mülhaupt, R., Polymers for 3D Printing and Customized Additive Manufacturing. *Chemical Reviews* **2017,** *117* (15), 10212-10290.

17.   Ligon-Auer, S. C.; Schwentenwein, M.; Gorsche, C.; Stampfl, J.; Liska, R., Toughening of photo-curable polymer networks: a review. *Polymer Chemistry* **2016,** *7* (2), 257-286.

18.   Sangermano, M., Advances in cationic photopolymerization. *Pure and Applied Chemistry* **2012,** *84*.

19.   Peer, G.; Dorfinger, P.; Koch, T.; Stampfl, J.; Gorsche, C.; Liska, R., Photopolymerization of Cyclopolymerizable Monomers and Their Application in Hot Lithography. *Macromolecules* **2018,** *51* (22), 9344-9353.

20.   Sangermano, M.; Roppolo, I.; Chiappone, A., New Horizons in Cationic Photopolymerization. *Polymers* **2018,** *10* (2), 136.

21.   Aoshima, S.; Kanaoka, S., A Renaissance in Living Cationic Polymerization. *Chemical Reviews* **2009,** *109* (11), 5245-5287.

22.   Vitale, A.; Sangermano, M.; Bongiovanni, R.; Burtscher, P.; Moszner, N., Visible Light Curable Restorative Composites for Dental Applications Based on Epoxy Monomer. *Materials* **2013,** *7*.

23.   Jenkins, A. D., Photoinitiators for free radical cationic and anionic photopolymerisation, 2nd edition J V Crivello and K Dietliker Edited by G Bradley John Wiley & Sons, Chichester 1998. pp ix + 586, £ 90.00 ISBN 0-471-97892-2. *Polymer International* **2000,** *49* (12), 1729-1729.

24.   Nuyken, O.; Pask, S., Ring-Opening Polymerization—An Introductory Review. *Polymers* **2013,** *5*, 361-403.

25.   Su, W.-F., Ring-Opening Polymerization. In *Principles of Polymer Design and Synthesis*, Springer Berlin Heidelberg: Berlin, Heidelberg, 2013; pp 267-299.

26.   De, P.; Faust, R., Carbocationic Polymerization. In *Controlled and Living Polymerizations*, 2009; pp 57-102.

27.   Nuyken, O.; Pask, S. D., Ring-Opening Polymerization—An Introductory Review. **2013,** *5* (2), 361-403.

28.   Endo, T., General Mechanisms in Ring-Opening Polymerization. In *Handbook of Ring-Opening Polymerization*, 2009; pp 53-63.

29.   Takata, T.; Endo, T., Recent advances in the development of expanding monomers: Synthesis, polymerization and volume change. *Progress in Polymer Science* **1993,** *18* (5), 839-870.

30.   Marx, P.; Wiesbrock, F., Expanding Monomers as Anti-Shrinkage Additives. **2021,** *13* (5), 806.

31.   Chikaoka, S.;   Takata, T.; Endo, T., Cationic ring-opening polymerization of spiroorthoester: polymer structure, polymerization mechanism, and volume change on polymerization. *Macromolecules* **1992,** *25* (2), 625.

32.   Sadhir, R. K. L., R.M., *Expanding Monomers - Synthesis, Characterization, and Applications*. CRC Press: 1992.

33.   Bailey, W. J., Synthesis of Monomers That Expand on Polymerization. **1973,** *5* (3), 142-152.

34.   Mues, P.; Buysch, H.-J., Ein neuer Zugang zu Spiroorthocarbonaten und neuen Orthokohlensäure-Derivaten. *Synthesis* **1990,** *1990* (03), 249-252.

35.   Bodenbenner, K., Über spirocyclische Orthoester. **1959,** *623* (1), 183-190.

36.   Endo, T.;   Sato, H.; Takata, T., Synthesis and cationic polymerization of 3,9-dibenzyl-1,5,7,11-tetraoxaspiro[5.5]undecane. *Macromolecules* **1987,** *20* (6), 1416-19.

37.   Acosta Ortiz, R.;   Duarte, M. L. B.;   Gómez, A. G. S.;   Sangermano, M.; García Valdez, A. E., Novel diol spiro orthocarbonates derived from glycerol as anti-shrinkage additives for the cationic photopolymerization of epoxy monomers. *Polymer International* **2010,** *59* (5), 680-685.

38.   Ortiz, R. A.;   Berlanga Duarte, M. L.;   Gómez, A. G. S.;   Sangermano, M.;   García Valdez, A. E.; Ramírez, M. P., Novel Tetraspiroorthocarbonates as Successful Anti-shrinking Agents for the Photopolymerization of Epoxy Monomers. *Journal of Macromolecular Science, Part A* **2012,** *49* (4), 361-368.

39.   Acosta Ortiz, R.;   Berlanga Duarte, M. L.;   Robles Olivares, J. L.; Sangermano, M., Synthesis of the fluorene spiroorthocarbonate and the evaluation of its antishrinking activity in the cationic photopolymerization of an epoxy resin. *Designed Monomers and Polymers* **2013,** *16* (4), 323-329.

40.   Min, H.;   Zheng, N.;   Fan, Z.;   Jiang, Y.; Cheng, X., UV-curable nanoimprint resist with liquid volume-expanding monomers. *Microelectronic Engineering* **2019,** *205*, 32-36.

41.   Klemm, E., Photoinduced spiro ortho ester-epoxide copolymerization. *Zeitschrift für Chemie* **1984,** *24(11)*, p.412.

42.   Haase Ludwig, K. E. Homopolymers with spiroorthoester groups. 1986.

43.   Gorski Detlef, H. L., Klemm Elisabeth, Doms Ilona Preparation of photocurable composites containing spiro ortho esters. DD275062, 1990.

44.   Hsu, Y.-G.; Wan, Y.-S., Cationic Photopolymerization of cis-2,3-Tetramethylene-1,4,6-trioxaspiro[4,4]nonane. *Journal of Polymer Science Part A-polymer Chemistry - J POLYM SCI A-POLYM CHEM* **2009,** *47*, 3680-3690.

45.   Marx, P.; Romano, A.; Fischer, R.; Roppolo, I.; Sangermano, M.; Wiesbrock, F., Dual-Cure Coatings: Spiroorthoesters as Volume-Controlling Additives in Thiol–Ene Reactions. **2019,** *304* (4), 1800627.

46.   Marx, P.; Romano, A.; Roppolo, I.; Chemelli, A.; Mühlbacher, I.; Kern, W.; Chaudhary, S.; Andritsch, T.; Sangermano, M.; Wiesbrock, F., 3D-Printing of High-κ Thiol-Ene Resins with Spiro-Orthoesters as Anti-Shrinkage Additive. **2019,** *304* (12), 1900515.

47.   Endo, T.; Okawara, M., A Facile Synthesis of Spiro Orthocarbonates. *Synthesis* **1984,** *1984* (10), 837-837.

48.   Wang, Z.; Cui, Y.-T.; Xu, Z.-B.; Qu, J., Hot Water-Promoted Ring-Opening of Epoxides and Aziridines by Water and Other Nucleopliles. *The Journal of Organic Chemistry* **2008,** *73* (6), 2270-2274.

49.   C. P, P.; Joseph, E.; A, A.; D. S, N.; Ibnusaud, I.; Raskatov, J.; Singaram, B., Stabilization of NaBH4 in Methanol Using a Catalytic Amount of NaOMe. Reduction of Esters and Lactones at Room Temperature without Solvent-Induced Loss of Hydride. *The Journal of Organic Chemistry* **2018,** *83* (3), 1431-1440.

50.   Okada, M., Ring-opening polymerization of bicyclic and spiro compounds. Reactivities and polymerization mechanisms. In *Polymer Synthesis Oxidation Processes*, Springer Berlin Heidelberg: Berlin, Heidelberg, 1992; pp 1-46.

51.   Takata, T.; Endo, T., New aspect of cationic ring-opening polymerization of seven-membered spiroorthocarbonates: synthesis and polymerization of substituted 1,6,8,13-tetraoxaspiro[6.6]tridecanes. *Macromolecules* **1988,** *21* (4), 900-904.

52.   Spegazzini, N.; Ruisánchez, I.; Larrechi, M.; Cadiz, V.; Canadell, J., Spectroscopic and quantitative analysis of spiroorthoester synthesis by two-dimensional correlation and multivariate curve resolution methods of NIR data. *The Analyst* **2008,** *133*, 1028-35.

53.   Nishida, H.; Sanda, F.; Endo, T.; Nakahara, T.; Ogata, T.; Kusumoto, K., Addition reaction of spiro orthoesters with electrophiles: A model reaction for the development of novel polyaddition accompanying ring-opening isomerization. **1999,** *37* (24), 4502-4509.

54.   Penczek, S.; Pretula, J.; Slomkowski, S., Ring-opening polymerization. *Chemistry Teacher International* **2021**.

55.   Duda, A.; Kowalski, A., Thermodynamics and Kinetics of Ring-Opening Polymerization. In *Handbook of Ring-Opening Polymerization*, 2009; pp 1-51.

56.   Chikaoka, S.; Takata, T.; Endo, T., New aspects of cationic polymerization of spiroorthoester: cationic single ring-opening polymerization and equilibrium polymerization. *Macromolecules* **1991,** *24* (25), 6557-6562.

57.   Bailey, W.; Iwama, H.; Tsushima, R., Synthesis of elastomers by cationic polymerization with expansion in volume. *Journal of Polymer Science: Polymer Symposia* **2007,** *56*, 117-127.

58.   Klemm, E. H., *Journal für praktische Chemie* **1981,** *323*, 585-588.

59.   Zhidkova, N. V. K., V.M Method of producing spiro ortho esters. 1988.

Appendix

Below, the data obtained from the photoreactivity study is shown. Additionally, evaluated NMR spectra for the determination of polymerization modes can be found.
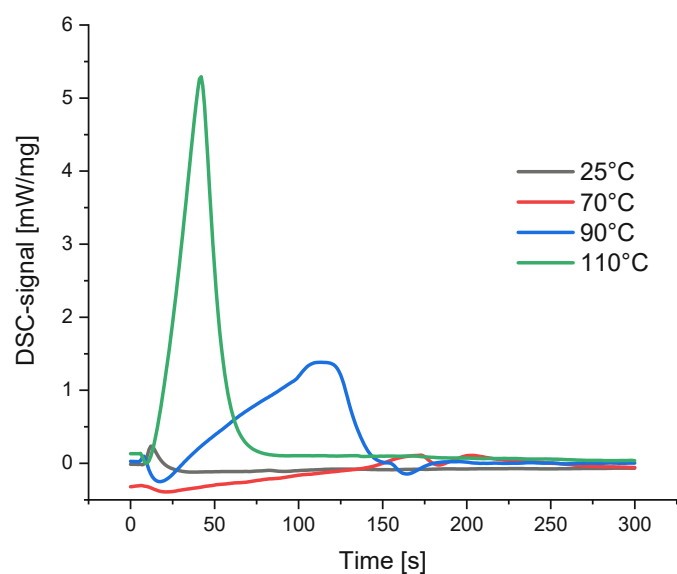
Spiro-orthocarbonates:

5-SOC:

Figure 67: Photo-DSc plot of 5-SOC at different temperatures

Table 21: results obrained from the photoreactivity study for 5-SOC

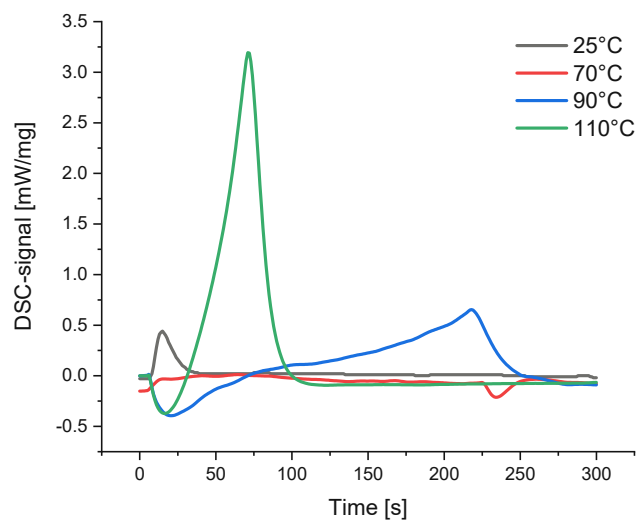| T [°C]	Area [J g^{-1}]	t$_{max}$ [s]	t$_{95}$ [s]	M$_n$ [Da]	C [%]
25	-1.698	13	270	492	12
70	13.165	169	266.3	884	86
90	85.81 ± 1.03	127 ± 10	141 ± 9	1127	88
110	129.57± 4.41	42 ± 0.2	98 ± 29	1313	95

6-SOC:

Figure 68: Photo-DSC plot of 6-SOC

Table 22: Data obtained from the photoreactivity study of 6-SOC

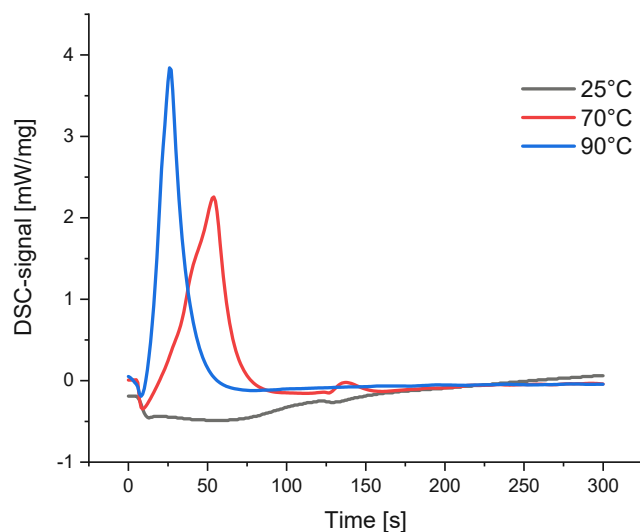| T [°C]	Area [J g^{-1}]	t_{max} [s]	t_{95} [s]	M_n [Da]	C [%]
25	14.03 ± 0.65	15 ± 0.2	224 ± 20	787	4
70	11.00 ± 2.14	128 ± 8	187 ± 14	2 940	48
90	66.31 ±2.26	216 ± 5	234 ±8	2 238	88
110	86.69 ± 0.95	73 ± 1	84 ± 0.6	2 056	88

7-SOC:

Figure 69: Photo-DSC plot of 7-SOC

Table 23: results obtained from the photoreactivity study of 7-SOC

T [°C]	Area [J g^{-1}]	t_{max} [s]	t_{95} [s]	M_n [Da]	C [%]
25	-83.63 ±4.55	47 ± 14.	229 ± 4	4333	>99
70	49.91 ± 1.57	55 ± 1	60 ± 1	1845	>99
90	53.57 ± 6.07	26 ± 0.1	34 ± 2	1176	>99

Spiro-orthoester:

Below, the obtained data after photopolymerization of spiro-orthoesters is shown. They polymerized without elimination of by-products *via* clean ring-opening polymerization. Therefore, NMR-spectra are not depicted.
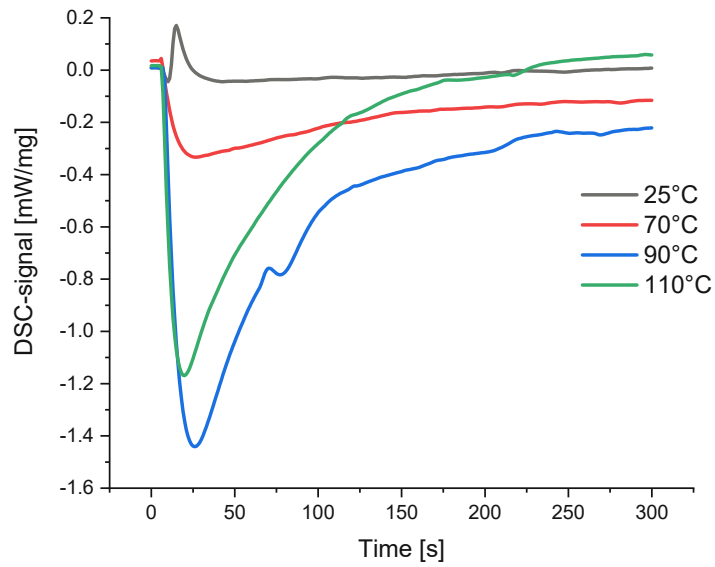
5-SOE:

Figure 70: Photo-DSC plot of 5-SOE

Table 24: results obtained from the photoreactivity study of 5-SOE

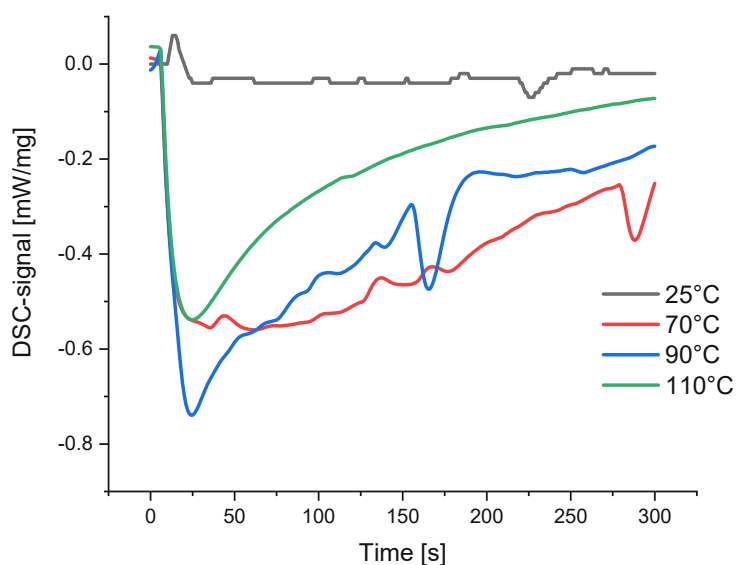| T [°C]	Area [J g^{-1}]	t_{max} [s]	t_{95} [s]	M_n [Da]	C [%]
25	-3.94 ± 1.86	15 ±0.4	235 ± 11	688	12
70	-43.15 ±15.49	14 ± 9	190 ± 15	703	48
90	-87.79 ± 2.97	25 ± 1	210 ± 12	557	56
110	-80.50 ± 11.97	20 ±0.1	161 ± 29	564	61

6-SOE:

Figure 71: Photo-DSC plot of 6-SOE

Table 25: results obtained from the photoreactivity study of 6-SOE

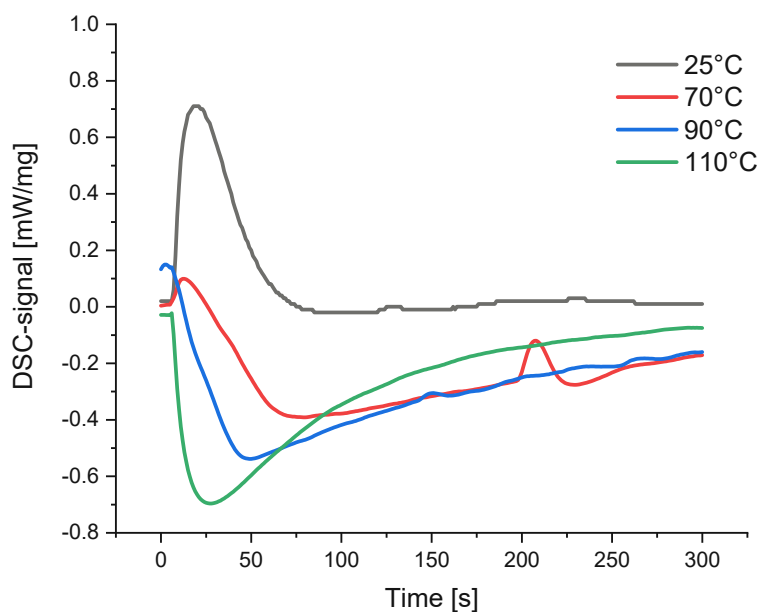| T [°C]	Area [J g^{-1}]	t_{max} [s]	t_{95} [s]	M_n [Da]	C [%]
25	-2.25 ± 0.62	14 ± 0.3	253 ± 20	403	3
70	-53.86 ± 1.32	56 ± 7	236 ± 20	857	10
90	-58.95 ± 6.45	28 ± 3	213 ± 19	908	9
110	-49.37 ± 3.49	23 ± 1	215 ± 4	2385	15

7-SOE:

Figure 72: Photo-DSc plot of 7-SOE

Table 26: results obtained from the photoreactivity study of 7-SOE

T [°C]	Area [J g^{-1}]	t_{max} [s]	t_{95} [s]	M_n [Da]	C [%]
25	20.68 ± 4.63	19.0 ± 0.9	41	832	34
70	-29.11 ± 5.29	82 ± 19	254 ± 8	1091	44
90	-41.04 ± 2.57	56 ± 5	224 ± 12	1202	51
110	-61.08 ± 2.89	26.2 ± 0.7	197 ± 5	1506	65

112